Exp Fluids (2008) 45:371–422
DOI 10.1007/s00348-008-0526-0

REVIEW ARTICLE

On the experimental investigation on primary atomization of liquid streams

Christophe Dumouchel

Received: 7 September 2007 / Revised: 3 June 2008 / Accepted: 3 June 2008 / Published online: 22 June 2008

Abstract The production of a liquid spray can be summarized as the succession of the following three steps; the liquid flow ejection, the primary breakup mechanism and the secondary breakup mechanism. The intermediate step—the primary breakup mechanism—covers the early liquid flow deformation down to the production of the first isolated liquid fragments. This step is very important and requires to be fully understood since it constitutes the link between the flow issuing from the atomizer and the final spray. This paper reviews the experimental investigations dedicated to this early atomization step. Several situations are considered: cylindrical liquid jets, flat liquid sheets, air-assisted cylindrical liquid jets and air-assisted flat liquid sheets. Each fluid stream adopts several atomization regimes according to the operating conditions. These regimes as well as the significant parameters they depend on are listed. The main instability mechanisms, which control primary breakup processes, are rather well described. This review points out the internal geometrical nozzle characteristics and internal flow details that influence the atomization mechanisms. The contributions of these characteristics, which require further investigations to be fully identified and quantified, are believed to be the main reason of experimental discrepancies and explain a lack of universal primary breakup regime categorizations.

List of symbols

a	liquid jet radius (mm)
A	spray angle parameter
A_L, A_G	fluid flow exit section area (mm^2)
d	nozzle diameter (mm)
D	drop diameter (μm)
D_{32}	Sauter mean diameter (μm)
D_{43}	arithmetic mean diameter of the volume-based drop-size distribution (μm)
f	undulation frequency (Hz)
g	gravitational acceleration (m/s^2)
k	wave number (m^{-1})
K	liquid sheet thickness parameter (cm^2)
L	nozzle length (mm)
L_{BU}	breakup length (mm)
L_C	liquid jet core length (mm)
L_p	boundary-layer length (mm)
L_{PC}	liquid jet potential core length (mm)
LPP	liquid presence probability
m	mass flux ratio
M	momentum flux ratio
Oh	Ohnesorge number
P_{amb}	gas ambient pressure (MPa)
r	radial coordinate (mm)
r_b	radial position of a flat sheet breakup (mm)
Re	Reynolds number
T	Taylor number
t	time (s)
t_{BU}	breakup time (s)
t_L, t_G	liquid and gas flow thickness (mm)
U	average velocity (m/s)
U_{LC}	critical liquid jet velocity (m/s)
U_{L0}	minimum liquid jet velocity (m/s)
We	Weber number
We_{Gc}	critical gaseous Weber number
We_R	relative gaseous Weber number
x	axial distance from nozzle (mm)

C. Dumouchel (✉)
CNRS UMR 6614–CORIA, Université de Rouen, BP 12,
76801 Saint Etienne du Rouvray, France
e-mail: dumouchel@coria.fr

Greek symbols

δ	air vorticity thickness (mm)
ΔP_i	injection pressure (MPa)
ρ	fluid density (kg/m^3)
λ	wavelength (cm)
Λ	radial spatial integral length of turbulence (μm)
μ	fluid dynamic viscosity (kg/ms)
σ	surface tension (N/m)
η	interface displacement (mm)
η_0	initial interface displacement (μm)
ω	pulsation (s^{-1})

Subscripts

L	related to the liquid flow
G	related to the gas flow
max	maximum
opt	optimum

1 Introduction

Many industrial processes and domestic applications involve liquids as dispersed phases or sprays, rather than as continuous flows (Lefebvre 1989; Bayvel and Orzechowski 1993). This is the case of field treatment in agriculture, drug delivery in medical therapy, mixture preparation for combustion purposes, coatings at small scale (pills fabrication, etc.) or large scale (industrial paintings, etc.), fire extinction, atmosphere cleaning, powder fabrication to quote just a few examples. Whatever the process or application involving a liquid spray, its efficiency depends on the spray characteristics and its optimization requires the spray formation to be controlled.

A spray is defined as a flow of individual liquid droplets evolving in a surrounding gaseous medium. Each droplet has its own diameter and velocity and may collide and coalesce with other droplets. The important spray characteristics are the drop-size distribution, the drop-velocity distribution, the density (number of droplets per unit volume), the spatial distribution (local volume fraction), and drop temperature. Specific diagnostics have been developed to determine these characteristics by experiment. Descriptions of such diagnostics are available in Bachalo (2000), Frohn and Roth (2000) and Tropea et al. (2007). The spray characteristics depend on the atomization process.

Liquid atomization processes are mechanisms during which the ratio of surface to mass in the liquid is increased (Mansour and Chigier 1991). The most widely encountered liquid spray formation process consists in ejecting a liquid flow into a gaseous environment. The interaction between the liquid flow and the gas leads to a rapid disintegration of the liquid flow into a flow of droplets. The spray production results in three main steps, namely, the ejection of a liquid flow, the primary breakup mechanism and the secondary breakup mechanism. As soon as the liquid flow issues from the nozzle, deformations appear on the liquid interface. These deformations grow in space and time and eventually result in the ejection of liquid fragments from the main liquid flow. The initial flow deformation and the subsequent production of liquid fragments constitute the primary atomization mechanism. Then, these liquid fragments may also distort and disintegrate into smaller elements, this process being repeated until these elements are stable drops. Stable drops are obtained when surface tension forces are strong enough to ensure the cohesion of the liquid fragment. This step constitutes the secondary atomization process. The relative importance of each step depends on the initial energy of the liquid flow. For low initial energy, the primary atomization may produce stable drops as well as greater liquid fragments that may undergo secondary breakup. For high initial energy, the secondary atomization might be dominant in the production of the final spray.

From a general point of view, two major factors control the primary atomization mechanism, namely, the presence of initial disturbances on the liquid–gas interface and a mechanism that allows some of these disturbances to grow leading to the breakup of the liquid flow. The characteristics of the resulting spray depend on both factors.

Theoretical analyses have been carried out on the initial distortion and disintegration of liquid streams (Lin and Reitz 1998; Sirignano and Mehring 2000). These approaches are based on the determination of unstable waves that grow on the liquid–gas interface and therefore dominate its breakup. These approaches have a limited domain of application so far. High-energy atomization processes are still untouched and little theoretical analysis exists on the coupling of the wave phenomenon with behavior upstream in the nozzle.

From an experimental point of view, the primary atomization step has been often ignored and atomization analyses have consisted in developing correlations between spray characteristics (such as cone angle, breakup length or mean drop diameter) and selected parameters (such as liquid properties, selected nozzle dimensions, injection pressure, etc.). This was due to the fact that experimental approaches have suffered from a lack of specific and powerful diagnostics. Things have been changing for the past two decades with the emergence of new experimental techniques and now efforts should be done to study the crucial primary atomization step, which is the vital link between the liquid emerging from the nozzle and the fully developed spray (Chigier 2005).

This paper intends to shed more light on the current knowledge of primary breakup mechanisms by reviewing experimental investigations dedicated to this

early atomization step. Several situations are considered. Section 2 reports studies on cylindrical liquid jets. This section is divided into two subsections dedicated to low and high-velocity jets, respectively. Section 3 presents investigations carried out on flat liquid sheets. Section 4 considers the case of air-assisted cylindrical liquid jets, and the final section is dedicated to air-assisted liquid sheets. All the studies reported in this paper were conducted with Newtonian fluids and the atomization processes were free of any external forcing (except otherwise mentioned). For the cases of air-assisted atomization, external mixing with co-flowing gas and liquid streams has been only considered. The experimental techniques are summarized and details can be found in the respective references.

2 Cylindrical liquid jets

2.1 General considerations

The behavior of cylindrical liquid jets discharging into a quiescent gaseous atmosphere has received a continuous attention from the scientific community over the past years. The first experimental investigation dated on the first half of the nineteenth century (Savart 1833). Cylindrical jets are produced by forcing the liquid to pass through a cylindrical tube of diameter d and length L. Several disintegration mechanisms are observed as a function of the liquid flow rate. A commonly used way of categorizing the cylindrical jet disintegration mechanisms is to plot the breakup length L_{BU} of the jet versus the average issuing velocity U_{L}. This plot is called the jet stability curve (Mc Carthy and Molloy 1974; Lefebvre 1989; Chigier and Reitz 1996; Lin and Reitz 1998). The breakup length is the coherent portion of the jet, i.e., the length of the continuous jet attached to the nozzle. The average issuing velocity is defined as the volume flow rate divided by the exit section of the nozzle. A typical jet stability curve is schematized in Fig. 1. Five breakup regimes are identified. Following the traditional nomenclature, these regimes are called the dripping regime (region A), the Rayleigh (region B), the first wind-induced (region C), the second wind-induced (region D) and the atomization (region E) regimes.

The dripping regime (region A) corresponds to the situation where drops are directly emitted from the nozzle exit without the formation of a continuous liquid column. The velocity U_{L0} under which this regime is observed is a function of the nozzle diameter and the liquid surface tension.

In the Rayleigh regime (region B, Fig. 1) one assumes the liquid column to be disturbed by a single axisymmetric perturbation with a wavelength of the same order of magnitude of the jet diameter. When the amplitude of the perturbation becomes equal to the jet radius, a drop detaches from the jet. Drops issued from the Rayleigh mechanism have similar diameter and the breakup length is easily identifiable. Rayleigh (1878) demonstrated that the behavior observed in this regime is a capillary instability.

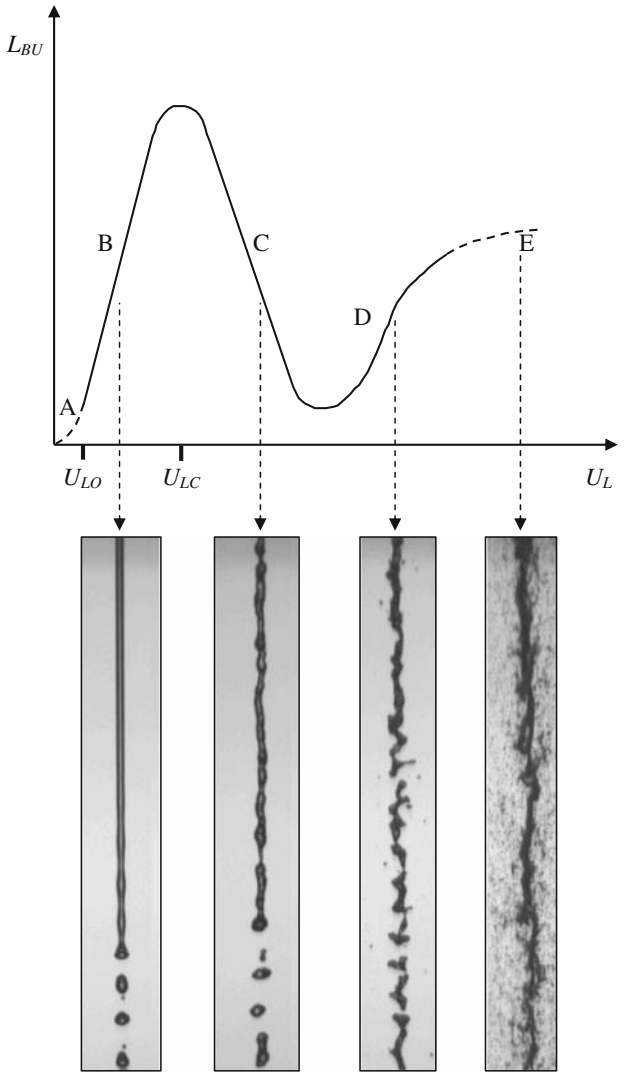

Fig. 1 Cylindrical jet behavior. *Top* stability curve, *bottom* example of visualizations (from *left* to *right*): Rayleigh regime (region B) $Re_{\mathrm{L}} = 790$, $We_{\mathrm{G}} = 0.06$; first wind-induced regime (region C) $Re_{\mathrm{L}} = 5{,}500$, $We_{\mathrm{G}} = 2.7$; second wind-induced regime (region D) $Re_{\mathrm{L}} = 16{,}500$, $We_{\mathrm{G}} = 24$; atomization regime (region E) $Re_{\mathrm{L}} = 28{,}000$, $We_{\mathrm{G}} = 70$ (images from Leroux 1996)

In the first wind-induced regime (region C, Fig. 1), a dominant perturbation evolving on the jet interface is still visible. Although it is still rather axisymmetric, the drop production is not as organized as in the Rayleigh regime. For instance the production of satellite droplets between the main drops may be enhanced and the whole drop-size distribution may become wider. Although the main drops are slightly smaller than the Rayleigh regime drops, their

diameters are still of the order of magnitude of the jet diameter. This regime owes its name to the fact that, as theoretically demonstrated by Weber (1931), the growth perturbation process is assisted by the presence of the gaseous environment.

In the second wind-induced regime (region D, Fig. 1), the liquid jet column is perturbed right at the nozzle exit and shows a very chaotic shape as the perturbations grow. The characteristic length-scales of these perturbations cover a large range and increase the width of the drop-size distribution. Two primary breakup mechanisms can be observed. Near the nozzle exit, small droplets are peeled off the interface. Farther downstream, the remaining liquid flow breaks up as a whole into large liquid fragments. These latter are subject to secondary atomization. The second wind-induced regime is due to the joint contribution of the liquid flow turbulence and the effect of the aerodynamic forces.

Lefebvre (1989) defined the atomization regime (region E, Fig. 1) as a complete jet disruption at the nozzle exit producing average drop diameters much less than the jet diameter. Faeth et al. (1995) pointed out that, in the atomization regime, spray properties including criteria for the onset of breakup are strongly influenced by the degree of flow development and the presence of turbulence at the jet exit. Chigier and Reitz (1996) emphasized the importance of liquid cavitation in the atomization regime: cavitating flows produce small breakup length jets whereas fully detached flows produce high breakup length jets. In the latter case, the issuing liquid jet has a diameter less than the nozzle diameter and shows a perfectly smooth interface. Lin and Reitz (1998) noted confusion about the breakup length trend in this region and associated apparent anomalies between several experimental investigations with changes in the nozzle internal flow patterns caused by separation and cavitation phenomena.

Lefebvre (1989) associated each atomization regime to a typical flow structure, namely, laminar flow region, transition region and turbulent flow region for the regions B, C and D, respectively. Attempts of delimiting the regimes on the basis of non-dimensional numbers can be found in the literature (see Lefebvre 1989). Chigier and Reitz (1996) and Lin and Reitz (1998) reviewed the criteria for the jet breakup regimes found in the literature. Table 1 summarizes this review and shows that regimes B and C are associated to typical values of liquid Weber number We_L, gaseous Weber number We_G and Ohnesorge number Oh whereas regimes D and E involve the gaseous Weber number, the Taylor parameter T and the liquid to gas density ratio. These numbers are defined by

$$\begin{cases} We_L = \dfrac{\rho_L U_L^2 d}{\sigma} & We_G = \dfrac{\rho_G U_L^2 d}{\sigma} \quad Re_L = \dfrac{\rho_L U_L d}{\mu_L} \\ Oh = \dfrac{\mu_L}{\sqrt{\rho_L d \sigma}} & T = \dfrac{\rho_L}{\rho_G}\left(\dfrac{Re_L}{We_L}\right)^2 \end{cases} \quad (1)$$

where ρ_L and ρ_G are the liquid and gas densities, respectively, μ_L is the liquid dynamic viscosity and σ is the surface tension coefficient.

Ranz (1956) derived criteria from force balance considerations. The dripping from the nozzle exit no longer occurs if the liquid inertia force becomes greater than the surface tension force, leading to a limit in terms of We_L for the region A. Furthermore, Ranz (1956) argued that the first wind-induced regime is reached when the surrounding gas inertia force reached 10% of the surface tension force, and that these two forces become of the same order of magnitude when the second wind-induced regime is approached. The limits for these two regimes were therefore associated to specific value of the gaseous Weber number (see Table 1).

The criterion due to Sterling and Sleicher (1975) to delimitate the Rayleigh and first wind-induced regimes comes from linear stability theoretical considerations. The Rayleigh and first wind-induced regimes have been widely investigated by linear stability theories (Rayleigh 1878; Weber 1931; Sterling and Sleicher 1975; Leib and Goldstein 1986a, b, etc.). A complete review of these approaches is available in Sirignano and Mehring (2000) and a summary of linear theories applied to cylindrical jets can be found in Lin and Reitz (1998). The linear stability theory bases are the following.

The temporal linear stability theory assumes that the interface of a cylindrical jet of radius a is perturbed by an axisymmetric wave with a Fourier component of the form:

Table 1 Criteria of cylindrical liquid jet disintegration regimes

Disintegration regime		Comment
Region A: dripping regime	$We_L < 8$[a]	
Region B: Rayleigh regime	$We_L > 8$[a]	
	$We_G < 0.4$[a] or $1.2 + 3.41Oh^{0.9}$[b]	
Region C: first wind-induced regime	$1.2 + 3.41Oh^{0.9}$[b] $< We_G < 13$[a]	
Region D: second wind-induced regime	13[a] $< We_G < 40.3$[c]	
Region E: atomization regime	40.3[c] $< We_G$	$f(T) = \frac{\sqrt{3}}{6}[1 - \exp(-10T)]$[e]
	$\frac{\rho_G}{\rho_L} > \frac{(\sqrt{A}-1.15)}{744} f(T)^{-2}$[d]	

[a] Ranz (1956), [b] Sterling and Sleicher (1975), [c] Miesse (1955), [d] Reitz (1978), [e] Dan et al. (1997)

$$\eta(x,t) = \eta_0 \exp(\omega t + ikx) \quad (2)$$

in the cylindrical coordinate system (r, θ, x) that follows the liquid and whose origin $x = 0$ is at the nozzle exit at time $t = 0$. $\eta(x, t)$ represents the displacement of the interface from the position $r = a$, η_0 is the initial amplitude of the perturbation, k is the wave number of the disturbance. The temporal linear stability theory assumes that the frequency ω is complex and that its real part ω_r is the temporal growth rate of the perturbation. The combination of the fluid dynamics equations (continuity and momentum) with kinematic and dynamic conditions that owe to be satisfied at the liquid–gas interface leads to the dispersion equation. The resolution of this equation, which gives the growth rate ω_r for a given perturbation wave number k, shows that the growth rate reaches a maximum $\omega_{r\max}$ for a given wave number k_{opt}. This perturbation is called the dominant or optimum perturbation and is supposed to be responsible for the disruption of the liquid column that occurs at the location where the perturbation amplitude is equal to the jet radius. This breakup criterion is written as

$$a = \eta_0 \exp(\omega_{r\max} t_{\text{BU}}) \quad (3)$$

where t_{BU} is the breakup time. The breakup length L_{BU} is then obtained by multiplying the breakup time by the jet velocity:

$$L_{\text{BU}} = \frac{U_{\text{L}}}{\omega_{r\max}} \ln\left(\frac{a}{\eta_0}\right) \quad (4)$$

Rayleigh (1878) considered the case of an infinite column of non-viscous liquid at rest and in vacuum. He found that only the perturbations such that $k(2a) < 1$ can grow and that the characteristics of the dominant perturbations are

$$\lambda_{\text{opt}} = 4.51(2a) \quad k_{\text{opt}} = \frac{0.7}{2a} \quad \omega_{r\max} = 0.393\sqrt{\frac{\sigma}{\rho_{\text{L}} a^3}} \quad (5)$$

where λ_{opt} is the wavelength of the optimum perturbation. This solution shows that a liquid column is unstable and reorganizes as droplets under the action of the surface tension forces only. Considering that one single drop is produced per wavelength, a mass conservation at the breakup reports a drop diameter D proportional to the jet diameter d ($D = 1.89d$). Although the capillary instability theory due to Rayleigh was developed for liquid column at rest, it is assumed that it is applicable to liquid jet with sufficiently low velocity. In this case Eqs. (4) and (5) shows that the jet breakup length evolves linearly with the liquid jet velocity as observed in region B of the stability curve (Fig. 1). Therefore, region B is recognized as being the manifestation of this capillary instability. Sirignano and Mehring (2000) analyzed the energy transfer in the Rayleigh mechanism and concluded that, during the oscillation, surface energy is transferred to viscous dissipation via kinetic energy and that the viscous dissipation slightly increases the liquid temperature.

Weber (1931) extended the Rayleigh theory by taking into account the liquid viscosity, the jet velocity and the surrounding gas that introduces aerodynamic forces. He found that, as the liquid jet velocity increases, the aerodynamic forces increase the growth rate of the dominant wave in such a way that the breakup length (Eq. 4) decreases when the jet velocity increases as observed in the region C of the jet stability curve. (At the same time, the dominant wavelength decreases suggesting a decrease of the droplet sizes.) Thus, according to Weber development, the critical point of the stability curve (first maximum) characterized by the critical jet velocity U_{LC} (Fig. 1) is the manifestation of the action of aerodynamic forces. Weber's theory associates a critical gaseous Weber number We_{Gc} to the critical point of the stability curve. (We_{Gc} varies from 1.8 to 3 when the jet Ohnesorge number Oh ranges from 10^{-3} to 10.) The result of Weber's theory pleads for a criterion based on the gaseous Weber number to delimitate the Rayleigh and the first wind-induced.

Weber's theory often failed in predicting critical velocities in agreements with measurements (see Grant and Middleman 1966; Fenn and Middleman 1969, for instance) and some investigators discounted this theory entirely (Lefebvre 1989). Sterling and Sleicher (1975) argued that one of the drawbacks of Weber's analysis is to disregard the effect of gaseous viscosity whose expected contribution is to reduce the aerodynamic effects. They subsequently proposed a correction of the dispersion equation by multiplying the aerodynamic force term by a constant that they found to be equal to 0.175. Consequently, the critical velocity was associated to a critical gaseous Weber number 1/0.175 greater than the one reported by Weber. The modified theory developed by Sterling and Sleicher (1975) reported the criteria given in Table 1 that corresponds the gaseous Weber number at which the aerodynamic term is 10% of the surface tension term.

As far as the linear stability theory is concerned, one should mention the more recent spatio-temporal stability analyses (Keller et al. 1973; Leib and Goldstein 1986a, b; Lin and Lian 1990; Lin 2003). Contrary to the purely temporal stability analysis, the spatio-temporal stability analysis considers that the perturbation may grow in time as well as in space allowing the wave number k in Eq. (2) to be complex, its imaginary part k_{i} being the spatial growth rate of the perturbation. Keller et al. (1973) demonstrated that temporal and spatial analyses converge when $We_{\text{L}} > 6$. The analysis due to Leib and Goldstein (1986a, b) pointed out the existence of unstable disturbances that must propagate in both downstream and upstream directions. These instabilities are absolute instabilities. They

differ from convective instabilities that are characterized by a downstream propagation only. Leib and Goldstein (1986a) found that an inviscid jet evolving in vacuum is subject to an absolute instability if $We_L < 2\pi$, otherwise the instability is convective. This limit is slightly reduced when the gas density and the liquid velocity are taken into account (Leib and Goldstein 1986b; Lin and Lian 1989; Funada et al. 2004). According to Lin and Reitz (1998), the theoretical prediction that the unstable distance must propagate in both downstream and upstream directions when the jet velocity is smaller than that corresponding to $We_L = 2\pi$ signifies that absolute instability occurs when the inertia is not sufficiently large to carry downstream all the unstable disturbances that derive their energy from the surface tension. Thus, surface tension remains the source of instability and transition from absolute to convective instability corresponds to the beginning of the formability of the liquid jet. (Let us note that the theoretical delineation between absolute and convective instabilities is similar to the criterion for the dripping regime reported by Ranz (1956).) Lin and Reitz (1998) concluded that the dripping regime ($U_L < U_{L0}$, region A in Fig. 1) is an illustration of absolute instabilities whereas Rayleigh, first wind-induced, second wind-induced and atomization regimes are all the manifestations of convective instability. Considering Keller et al.'s criterion, it appears therefore that temporal stability analyses are acceptable approaches in the Rayleigh and the first wind-induced regimes.

The criterion provided by Miesse (1955) to delimit the second wind-induced to the atomization regimes (Table 1) comes from empirical considerations. Chigier and Reitz (1996) mentioned that nozzle internal flow effects are known to be important for high-speed jets and that this criterion must be regarded as indicative of the regime boundary, since nozzle design details are not represented in this criterion. An alternative criterion to account for nozzle effects was established by Reitz (1978) using results from the surface wave growth theory developed by Taylor (1940). This theoretical development corresponds to the temporal linear stability theory in the limiting case of $ka \rightarrow \infty$. In Reitz's criterion for the onset of the atomization regime, A is the spray angle parameter that accounts for nozzle internal flow effects. This parameter must be determined from experiments (Reitz and Bracco 1982).

Lin and Creighton (1990) calculated an energy budget of an atomizing liquid jet based on a spatial linear stability theory. This budget revealed that in the Rayleigh and the first wind-induced regimes, capillary pinching remains the mechanism of breakup and that the term associated to surface tension is always dominant (even in the first wind-induced regime). Based on this observation Lin and Reitz (1998) concluded that a best denomination of the first wind-induced breakup regime would be wind-assisted breakup regime. However, the second wind-induced and atomization regimes are genuinely wind-induced. In these regimes, surface tension acts against the formation of small droplets generated by the interfacial pressure fluctuations.

The following subsections present a review of experimental studies on cylindrical liquid jet primary atomization processes. This review will help to appreciate the relevance and completeness of the criteria presented in Table 1. The presentation is divided into two parts: low-Weber cylindrical liquid jets (regions B and C in Fig. 1) and high-Weber cylindrical liquid jets (regions D and E in Fig. 1).

2.2 Low-Weber cylindrical liquid jets

The low-Weber cylindrical liquid jets considered in this section are those showing a breakup mechanism identified as being in the Rayleigh or the first wind-induced regimes. These jets show several common features such as an organized atomization process, drops pinched off the end of the jet, drop diameter of the order of the jet diameter and the absence of secondary atomization. First, experimental investigations based on the measurement of jet breakup length are presented. Second, experimental investigations conducted on the characterization of the deformation that conducts to the breakup are reviewed.

Grant and Middleman (1966) and Fenn and Middleman (1969) took liquid jets shadowgraph images with a high-speed electronic flash unit (0.5 μs flash duration). The breakup length measurements were made directly from negatives with an accuracy that ranged from 0.01 to 1 mm according to the order of magnitude of the dimensions. The number of negatives analyzed for each operating condition was not specified. Grant and Middleman (1966) worked with several nozzles with a diameter ranging from 0.3 to 1.4 mm and a L/d ratio comprised between 7 and 150. Furthermore, several liquids were tested ($\mu_L \in [10^{-3}$, 0.16 kg/ms]; $\sigma \in [23,\ 71$ mN/m]; $\rho_L \in [800,\ 1{,}230$ kg/m^3]). The corresponding jet Ohnesorge number ranged from 4×10^{-3} to 0.9. Grant and Middleman (1966) returned poor agreement between the measured critical jet velocity and Weber's prediction. It was found that Weber's theory underestimated the critical velocity for high-Ohnesorge jets and overestimated it otherwise. From this observation Grant and Middleman (1966) suggested a correction of Weber's theory. This correction was made in two steps. First, a correction function was introduced in the aerodynamic force term in Weber's dispersion equation in order to force the equation to report the measured critical velocity. Second, for each situation, the term $\ln(a/\eta_0)$ was calculated in order that the breakup length calculated by Eq. (4) returned the measured value. Grant and Middleman (1966) found that both the correcting function introduced in the dispersion equation and the term $\ln(a/\eta_0)$ depended

on the jet Ohnesorge number. Although this modified theory reported good predictions for jets under atmospheric condition, it failed to predict the critical jet velocity under subatmospheric pressure. They also noticed that the modified theory did not account properly of the influence of the nozzle L/d ratio. They suggested that these disagreements were caused by the influence of the relaxation of the jet velocity-profile, which is not taken into account in the theory.

Fenn and Middleman (1969) measured the stability curve in the Rayleigh and first wind-induced regimes as a function of the ambient pressure, which was decreased from 0.1 MPa to 670 Pa. They observed that the effect of ambient pressure depends upon the viscosity of the liquid. For high-Ohnesorge number jets, the critical velocity increases as the ambient pressure decreases. This trend agrees with the one reported by Weber's theory. However, Fenn and Middleman (1969) obtained a critical gaseous Weber equal to 5.3, which is greater than Weber's prediction. For low-Ohnesorge number jets (<0.04 in their experiments) the critical velocity was found independent of the ambient pressure and the associated Weber number always <5.3. Thus, the passage from the Rayleigh to the first wind-induced regimes cannot be attributed to aerodynamic force effects. For these jets, Fenn and Middleman (1969) reported a correlation between the Reynolds number calculated with the critical velocity and the liquid–gas dynamic viscosity ratio. Despite the ambient viscosity was not varied in their experiments, they suggested that the appearance of the maximum is due to the effect of the shear stresses generated by the motion of the interface.

Sterling and Sleicher (1975) argued that the independence between the stability curve and the ambient conditions reported by Fenn and Middleman (1969) was due to jet velocity-profile relaxation effects that they demonstrated to become paramount when the jet Ohnesorge is small. Furthermore, as said in the previous section, they noted that Weber's theory overestimated the aerodynamic effects and introduced a constant in the dispersion equation to correct this drawback. They tested their modified theory by measuring breakup length on jets produced by nozzles especially designed to produce nearly uniform velocity-profile jets at the nozzle exit when the L/d ratio is small (≈ 0.25). They also used extended nozzles ($L/d = 49$ and 96). The experiments were performed with three liquids ($\mu_L \in [10^{-3}, 30 \times 10^{-3}$ kg/ms]; $\sigma \in [30, 72$ mN/m]; $\rho_L \in [868, 1{,}000$ kg/m^3]). At low liquid velocity, the breakup lengths were measured from stroboscopic visualizations of the jets. For higher velocities, 50–100 shadowgraph images taken by a 24 frames/s camera were analyzed at each velocity. They found that their modified theory agreed well with their measurements when the velocity-profile relaxation effects were small, i.e., for small L/d ratio nozzles or large Ohnesorge jets. This agreement was lost when relaxation effects became paramount, i.e., for large L/d nozzles and small Ohnesorge jets. In these cases, the critical velocities were always overestimated. They concluded that in the absence of velocity-relaxation effects, the passage from the Rayleigh to the first wind-induced is a manifestation of aerodynamic forces.

The exact role of velocity-relaxation on the jet behavior has not been established so far as well as a criterion for determining when these effects can be ignored. Some authors argued that for jets whose stability curve is independent of the ambient condition, the maximum of the stability curve and the change of the slope sign are likely to be due to an increase of the initial amplitude of the perturbation (Phinney 1972; Mansour and Chigier 1994). However, the correlation between velocity-profile relaxation and increase of initial amplitude of the perturbations has not been demonstrated so far. On the other hand, a temporal linear stability theory accounting for the jet velocity-profile but neglecting its relaxation showed that the characteristics of the dominant waves are functions of the velocity-profile (Ibrahim and Marshall 2000). Thus, a modification of the wave growth due to velocity-profile relaxation cannot be excluded.

Leroux et al. (1996, 1997) conducted an experimental investigation on the influence of the ambient pressure on the stability curve of Newtonian cylindrical liquid jets. The measurements were based on an image processing technique. Backlight visualizations (shadowgraph images) of liquid jets were taken with a CCD camera and a 2 μs flash duration stroboscope. The gray-level histograms of the images were analyzed in order to determine a threshold to dissociate liquid pixel (low levels) from background pixels (high levels). Pixels whose gray level was equal to this threshold were assumed to reproduce the contour of the liquid jet. Then, the position of the farthest contour pixel from the nozzle gave the liquid jet breakup length. One of the main advantages of this technique is that it required <4 min to acquire and analyze 1,000 images. Thus, breakup length distributions could be plotted and analyzed as a function of the working conditions. Results showed that the breakup length distributions were well represented by Gaussian distributions and that the distribution width roughly followed the evolution of the breakup length when the liquid velocity increased. In their analysis, Leroux et al. (1996, 1997) used the maximum reported by the Gaussian distribution as representative breakup length.

Stability curves were measured for a wide range of operating conditions ($d \in [0.28, 1$ mm]; $L/d \in [10, 100]$; $\sigma \in [0.027, 0.075$ N/m]; $\mu_L \in [10^{-3}, 7 \times 10^{-3}$ kg/ms]; $P_{amb} \in [0.1, 8$ MPa]). It was found that the evolution of the critical velocity with the ambient gas density depends on the operating conditions including the nature of the fluid,

the nozzle characteristics and the gas density. From a general point of view, the variation of the critical velocity with the gas density can be schematized as shown in Fig. 2. The predictions due to Weber (1931) and Sterling and Sleicher (1975) are also indicated in this figure. Since both stability theories attribute a constant gaseous Weber number at the critical point, their predictions appear as straight lines with a slope equal to −1/2 on the log–log representation given in Fig. 2. The results found by Leroux et al. (1996, 1997) show three jet regimes according to the ratio ρ_G^*/ρ_G, the characteristic value ρ_G^* being defined as the gas density for which Weber's prediction is correct (see Fig. 2).

When $\rho_G^*/\rho_G > 1$ (regime 1 in Fig. 2), the critical velocity is independent of the gas density and therefore the transition from the Rayleigh to the first wind-induced regimes in this condition is not due to aerodynamic force effects. This is emphasized by the fact that, as seen in Fig. 2, the regime 1 jet critical velocity is far less than the velocity required to expect an action of aerodynamic forces, this later velocity being at least the one given by Weber's analysis. When $\rho_G^*/\rho_G \ll 1$ (regime 3 in Fig. 2), the jet critical velocity decreases when the gas density is increased and are well predicted by Sterling and Sleicher's (1975) modified theory giving credit to the value of the correcting constant they introduced in Weber's dispersion equation. Thus, as concluded by Sterling and Sleicher (1975) the transition from the Rayleigh to the first wind-induced regimes for regime 3 jets is the manifestation of aerodynamic force effects. Regime 2 in Fig. 2 is a transitional regime.

Leroux et al. (1997) suggested a modification of the Weber theory in order to correctly predict the critical velocity for all regime jets. Following Sterling and Sleicher's approach, they multiplied the aerodynamic term in Weber's dispersion equation by a correcting function $f(\rho_G^*/\rho_G)$. This function eliminated the gas density effect when $\rho_G^*/\rho_G > 1$ and was equal to Sleicher and Sleicher's correcting constant in the opposite situation. The application of this modified Weber theory reported critical velocities in agreement with measurements for all regime jets. However, whereas for regime 3 jets, the experimental and calculated stability curves were in perfect agreement over the Rayleigh and the first wind-induced regimes, sharp disagreements were obtained in the first wind-induced regime of regime 1 jets, the measured breakup lengths being always less than the calculated ones in this region. Thus, the increase of the optimum wave growth rate returned by the linear theory in the first wind-induced regime is not appropriate to describe regime 1 jet behavior.

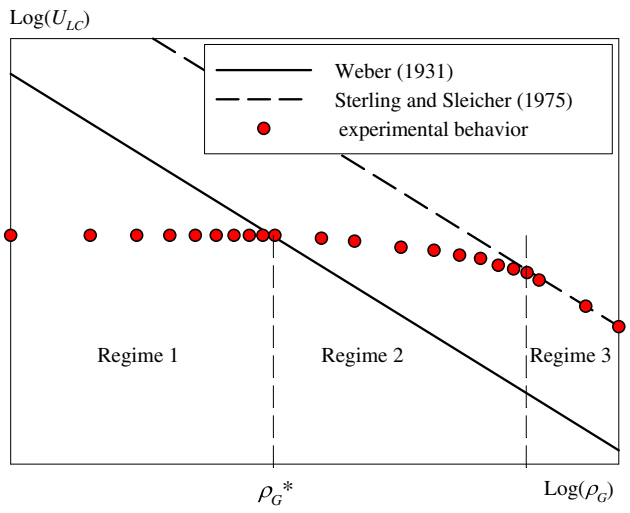

Fig. 2 Schematic presentation of Leroux et al. (1996, 1997) experimental results (from Malot and Dumouchel 2001)

Malot et al. (2000) and Malot and Dumouchel (2001) pointed out another disagreement between the linear theory and the behavior of regime 1 jets by measuring the drop-size distribution of the spray produced in the Rayleigh and first wind-induced regimes. The measurements were performed by an image analysis technique paying attention to disregard liquid elements that were highly non-spherical. The results showed that the arithmetic mean diameter of the volume-based drop-size distribution D_{43} (see Sowa 1992) was constant in the Rayleigh and the first wind-induced regimes. As mentioned in the previous section, this behavior is not in agreement with the decrease of the optimum wavelength (and thus of the drop diameter) reported by the linear theory. Malot and Dumouchel (2001) suggested that the behavior of regime 1 jets in the Rayleigh and first wind-induced regimes is the manifestation of capillary instability but with a modification of the nature of this instability that evolves from a supercritical type in the Rayleigh regime to a sub-critical type in the first wind-induced regime. One of the illustrations of this modification can be found in Dumouchel (2001), who investigated the evolution of the breakup time as a function of the jet velocity ratio U_L/U_{LC} for regime 1 jets. As expected, in the Rayleigh regime ($U_L/U_{LC} < 1$), the breakup time was found constant with the liquid velocity and its value was imposed by the liquid surface tension regardless the nozzle internal geometry. However, for $U_L/U_{LC} > 1$, the breakup time decreased with the jet velocity ratio U_L/U_{LC} and was found dependent on the nozzle only, regardless the surface tension while its effects are known to control the destabilization process.

Malot and Dumouchel (2001) found that the jet parameter ρ_G^* correlates with the Ohnesorge number (Fig. 3: $\rho_G^* \propto Oh^{-1.5}$). This correlation unifies many experimental results including those of Grant and Middleman (1966), Fenn and Middleman (1969) and Sterling and Sleicher (1975) described above. This result shows that

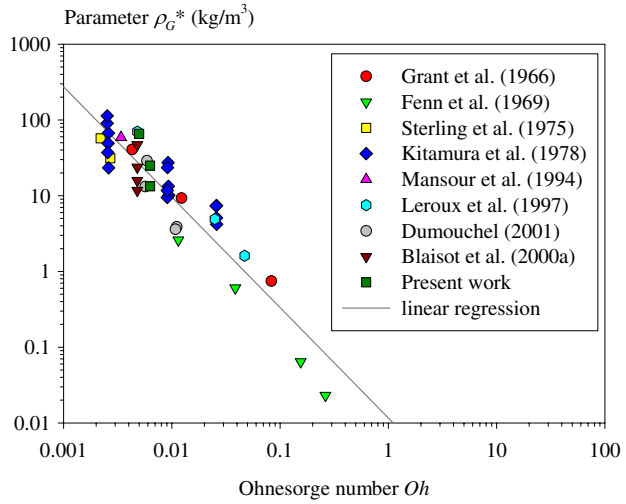

Fig. 3 Correlation between ρ_G* and the jet Ohnesorge number *Oh* (from Malot and Dumouchel 2001)

under atmospheric condition ($\rho_G \approx 1.3$ kg/m^3) regime 3 jets defined by $\rho_G^*/\rho_G \ll 1$ have an Ohnesorge number greater than 0.1. In agreement with Sterling and Sleicher's conclusions, the velocity-profile relaxation effects should be small for these jets and the aerodynamic forces should determine the critical velocity. On the other hand, regime 1 jets have small Ohnesorge numbers and the velocity-profile relaxation becomes paramount and renders the stability curve independent of the ambient conditions. A criterion to segregate regime 1 and regime 3 jets should be based on the parameter ρ_G*. Such a criterion has not been established so far.

The series of investigations presented above are based on the analysis of an average 'macroscopic' characteristic of the liquid jet, namely, the breakup length. As explained above, the breakup mechanisms in the Rayleigh and first wind-induced regimes have in common a rather axisymmetric shape with the development of a clearly visible disturbance whose characteristics, such as the frequency, the wavelength, the amplitude and the propagation speed, can be referred as 'microscopic' characteristics of the disintegrating jets. Recent experimental investigations were dedicated to the determination of these characteristics to provide a better description of low-Weber jet behavior. The experimental protocols of these investigations could be categorized in two groups, namely, the temporal sampling and the spatial sampling of the jet diameter. Temporal sampling of the jet diameter consists in recording the temporal evolution of the jet at a given distance from the nozzle, whereas spatial sampling consists in recording the spatial evolution of the jet diameter at a given time.

Amagai and Arai (1997), Arai and Amagai (1999), Godelle et al. (2000a, b) and Godelle and Letellier (2000) used a temporal jet diameter sampling technique. This technique is based on laser extinction. A laser sheet with a thickness smaller than the liquid jet diameter intercepts the jet perpendicularly to its axis and the intensity is collected in the forward direction, using a method of ombroscopy, by a photomultiplier with a sufficiently high sampling rate. It was demonstrated that the collected intensity is linearly related to the jet diameter (Amagai and Arai 1997; Godelle 1999). A FFT is applied on each temporal diameter series to calculate the power spectra. Arai and Amagai (1999) duplicated this system in order to simultaneously measure two diameter series at different locations and calculated the cross-correlation of the signals.

Amagai and Arai investigated the behavior of water jets produced by long nozzles in order to have fully developed velocity-profile at the nozzle exit. The experiments were conducted under atmospheric pressure. The nozzle diameter varied from 2 to 6 mm corresponding to jet Ohnesorge numbers ranging from 0.015 to 0.02. According to Fig. 3 these working conditions correspond to a ratio ρ_G*/$\rho_G > 3.1$: the jets were therefore of the regime 1 type. The laser sheet thickness was of the order of 1.2 mm giving laser sheet thickness/jet diameter ratio ranging from 0.2 to 0.6. In the Rayleigh regime, no frequency was detected down to a distance from the nozzle exit equal to $L_{BU}/2$. At $L_{BU}/2$, three frequencies emerged. These frequencies did not report an harmonic relationship with each other indicating that the surface wave is constituted of several wave components of various modes. Furthermore, these frequencies were of the order of the half of Rayleigh frequency calculated with the local jet diameter and velocity, which vary because of jet contraction. Using a cross-correlation method Amagai and Arai measured the wave velocity and found it always equal to the local jet velocity. With this wave velocity, Amagai and Arai calculated the wavelengths associated to the three detected frequencies. They found that all of them were less than the optimum Rayleigh wavelength based on the nozzle diameter (Eq. 5) but were greater than that of this optimum wavelength when using the local jet diameter. Furthermore, since no relative velocity was measured between the liquid and the wave, the jet contraction induced an elongation of the wavelengths with the downstream distance. This wave deformation was illustrated by very low cross-correlation coefficients between the breakup position and any position upstream. In the breakup region, the frequency spectrum became considerably broader than upstream, revealing a very irregular behavior of the disintegration. Furthermore at this point, the main frequency was of the order of a third of the local Rayleigh frequency.

Godelle et al. (2000a) investigated the behavior of a 600 μm diameter water jet of regime 1 type at three velocities; two velocities in the Rayleigh regime and one in the first wind-induced regime. The thickness of the laser

sheet was of the order of 30 μm and corresponded to a laser sheet thickness/jet diameter ratio equal to 0.05. On the continuous liquid column the power spectra reported the emergence of three frequencies: a fundamental mode and its two first harmonics. The analysis of the power spectra density reported an exponential growth of these modes as assumed by Rayleigh theory. (In the Rayleigh regime, the fundamental mode corresponded to the Rayleigh frequency.) While the fundamental mode was dominant during the perturbation growth along the jet, it was noticed that the three modes had equivalent amplitude in the breakup region. The important result of this investigation concerned the fundamental mode growth along the jet. In the Rayleigh regime, the growth of the fundamental mode started at some distance from the nozzle (of the order of $L_{BU}/2$ in agreement with Amagai and Arai's observations) and whatever the velocity, the breakup time was found constant in the regime (of the order of 28 ms). However, in the first wind-induced regime the growth of the fundamental mode started as soon as the jet issued from the nozzle leading to reduced breakup time and length. Furthermore, it was noticed that the growth rate of the fundamental mode slightly decreased from the Rayleigh regime to the first wind-induced regime.

In a subsequent investigation, Godelle and Letellier (2000) analyzed the dynamics of these liquid jets by using concepts introduced in the theory of nonlinear dynamical systems. This original study investigated the nature of the dynamics of the jet according to its breakup regime by analyzing the temporal diameter series using tools such as phase portraits, first returned map to Poincaré sections, angular first return map as well as symbolic sequence statistics. This approach revealed a fundamental difference of jet dynamics between the Rayleigh and the first wind-induced regimes for regime 1 jets. When $U_L/U_{LC} < 1$, the atomization processes are clearly governed by a deterministic dynamics characterized by intermittencies. This means that jet diameter temporal evolution can be modelized and that such atomization process could be controlled by external constraints. In the opposite, when $U_L/U_{LC} > 1$, the dynamics underlying the liquid jet was found to be 'white noise'. This means that the jet dynamics is stochastic: it is not absolutely deterministic and requires to be statistically studied.

Ruiz (2002) presented a slightly different technique that consisted of intercepting the jet by two laser beams positioned at different distances from the nozzle and in analyzing the temporal deformation of the light pattern detected on a screen positioned in the forward direction. Ruiz examined the behavior of water jets ejected from a 6.25 mm diameter nozzle with L/d ratio equal to 1. The issuing liquid jet mean velocity was not greater than 4 m/s. For these operating conditions, the gaseous Weber number does not exceed 1.8. Thus the jets belong to the Rayleigh regime of atomization. Contrary to the previous experimental works, the jet is mechanically excited by the recoil of a large speaker with an independent control of the frequency and of the amplitude of the exciting signal. Ruiz (2002) measured the response of the jets as a function of the exciting frequency and deduced from these measurements the jet response in terms of wave number. This wave number was calculated by assuming that the wave propagation speed was equal to the local jet velocity, this latter being greater than the issuing jet average velocity because of jet contraction. In agreement with Rayleigh's theory, Ruiz (2002) found that only perturbations with a non-dimensional wave number $k(2a)$ less than 1 could grow on the jet. However, contrary to Rayleigh's results, he reported a $k_{opt}(2a)$ of the order of 0.3–0.5 instead of 0.7 (see Eq. 5). Furthermore, beside the maximum of amplification reported for $k_{opt}(2a)$, one or two secondary maxima could be detected for wave numbers that appeared to be harmonics of $k_{opt}(2a)$. Ruiz (2002) suggested that the disagreement between his results and Rayleigh's theory led to the fact that the examined liquid jets were subject to acceleration by gravity. First, this acceleration continuously increases the liquid jet velocity and therefore continuously elongates the wavelength. Second, the jet is subject to a constant stretch, which will tend to smooth out smaller disturbances by itself.

Spatial jet diameter sampling consists in performing visualizations of the jet. However, considering the large aspect ratio L_{BU}/d of liquid jets in the Rayleigh and first wind-induced regimes, it is difficult to visualize the whole jet with a sufficient spatial resolution to study the spatial diameter variations. To overcome this difficulty, Blaisot and Adeline (2000a, b, 2003) used a shadowgraph imaging system composed of two cylindrical lenses in order to create asymmetric magnification that dilates the jet in the radial direction (magnification = 5.9) and contracts it in the axial direction (magnification = 0.17). An example of their images is presented in Fig. 4. They studied the behavior of regime 1 water jets produced by 600 μm diameter nozzles with L/d ratio ranging from 10 to 200 ($Oh = 0.005$). Two cameras were used: a high framing rate (1,000 images/s) drumming camera that provided spatio-temporal evolution of the jet behavior and a CCD camera to perform a statistical analysis.

In the Rayleigh regime, the spatio-temporal analysis revealed that each individual wave experienced an exponential growth in time as well as in space but that each of them reported its own initial amplitude η_0. Furthermore, this initial perturbation amplitude reported temporal oscillations. However, considering the extremely small values of η_0 (between 10^{-3} and 1 nm), Blaisot and Adeline emitted the idea of the existence of a delay length

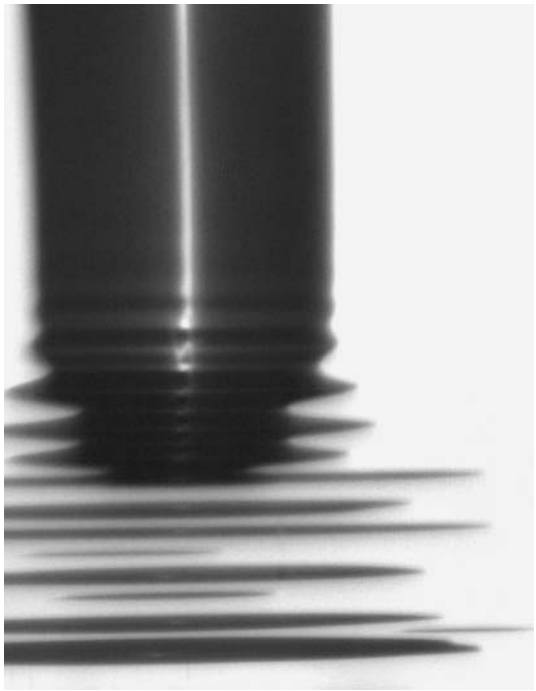

Fig. 4 Asymmetric magnification imaging of a Rayleigh jet (from Blaisot and Adeline 2003)

corresponding to the distance under which no significant wave growth occurs. Near the breakup point, the wave propagation velocity was reported almost equal to the local liquid velocity, which was slightly greater than the exit mean velocity because of profile relaxation.

The statistical analysis performed with the CCD camera visualizations concentrated on the measurements of the wavelength and of the spatial growth rate of the perturbation. It must be emphasized here that the image analysis process developed to identify the wave crests on the jet interface and their characteristics (position, amplitude, width) made use of the wavelet transform. Although it was rather tedious and time consuming, this sophisticated procedure was free of any experimenter decision and reported reliable measurements. In a subsequent investigation, Yon et al. (2004) proposed a different analysis of the same images by conducting a morphological analysis. This analysis consisted in applying morphological operators on binary images of the jet. The morphological analysis measures the distribution of the characteristic length-scales that define the shape of the object. It is similar to a multifractal approach. The characteristic length-scale distributions allow the wavelength and the growth rate to be calculated. The morphological analysis is far less time consuming than the wavelet transform developed by Blaisot and Adeline. Both analyses reported similar results. It was found that the measured spatial growth rate and wave number agreed well with the linear theory predictions in the Rayleigh regime and that the first wind-induced regime was characterized by a sharp increase of both the spatial growth rate and the initial perturbation amplitude as well as by a decrease of the wavelength of the dominant wave.

Several conclusions can be drawn from these experimental investigations dedicated to low-Weber cylindrical jets. In the Rayleigh regime, several investigations agree to say that the capillary instability growth does not begin right at the nozzle exit but starts at a distance of the order of $L_{BU}/2$ (Amagai and Arai 1997; Arai and Amagai 1999; Godelle 1999; Godelle et al. 2000a, b; Godelle and Letellier 2000; Blaisot and Adeline 2000a, b, 2003). The absence of detection of growing wave in the first part of the jet could be attributed to a lack of accuracy of the experimental diagnostics. However, the perturbation initial amplitudes calculated at the nozzle exit by Blaisot and Adeline (2003) appeared not physically reliable in terms of interface displacement since they could reach values of the order of 10^{-2} times the inter-molecular length in water. This pleads for the existence of a neutral region during which the perturbation growth is not effective. Blaisot and Adeline (2003) argued that this neutral region length should increase with the jet velocity and estimated it to be of the order of 50 jet diameter when the jet critical velocity is approached.

Temporal analyses of the jet diameter evolution agree on another point, that is, that more than one perturbation grows along the jet in the Rayleigh regime (Amagai and Arai 1997; Arai and Amagai 1999; Godelle 1999; Godelle et al. 2000a, b; Ruiz 2002). This behavior is not described by the linear theory since this approach considers the evolution of one wave at the time. Amagai and Arai found that these waves did not show an harmonic relationship with each other. However, Godelle et al. found that the three detected waves corresponded to a fundamental mode and the two first harmonics. Furthermore, contrary to Amagai and Arai, they found that the fundamental mode corresponded quite well to the Rayleigh prediction. These differences might come from the fact that the jets examined by Amagai and Arai were ten times larger than those studied by Godelle et al. and were therefore subject to contraction due to gravitational effects, these effects being limited in Godelle et al. experiments. This indicates that the Rayleigh theory appears more appropriate to describe the behavior of small diameter jets: for such jets the capillary wave characteristic time is small and gravitational effects are negligible.

From the works reported by Grant and Middleman (1966), Fenn and Middleman (1969), Sterling and Sleicher (1975) and Leroux et al. (1996, 1997) it can be concluded that the onset of the first wind-induced regime has a different origin according to the working conditions. For high-Ohnesorge jets, the critical velocity and the onset of the first wind-induced regime are the manifestation of

aerodynamic force effects. For these jets, Sterling and Sleicher's (1975) modified theory reports a good prediction of the jet breakup length evolution. For low-Ohnesorge jets, the onset of the first wind-induced regime is independent of the ambient conditions and arises at a lower velocity than the one reported by Sterling and Sleicher's modified theory. A criterion to segregate these two jet categories has not been fully established yet. Furthermore, the behavior of low-Ohnesorge jets is not completely understood so far. Grant and Middleman (1966) and Phinney (1972) suggested that the increase of the perturbation initial amplitude was at the origin of this behavior. Sterling and Sleicher (1975) argued that velocity-profile relaxation effects influence the behavior of these jets. Godelle et al. (2000a, b) noticed the disappearance of the neutral region for these jets with an exponentially growing disturbance right at the nozzle exit. This observation pleads in favor of the increase of the perturbation initial amplitude. One point can be ascertained: details of the internal flow influence the behavior of these jets. Further experimental works addressing this point should be conducted.

The studies reported in this section show the emergence of new experimental diagnostics and protocols. One should especially emphasize recent image analyzing techniques that allow reliable and quantitative information to be obtained.

2.3 High-Weber cylindrical liquid jets

This section reports experimental investigations performed on cylindrical jets belonging to regions D and E of the stability curve (see Fig. 1). According to Ranz (1956), the gaseous Weber number of these jets is >13 (see Table 1). As described above, one of the characteristic features of the primary atomization of these jets is the peeling off the interface of small droplets near the nozzle exit. Two parts constitute this section: the first one considers the behavior of large jets ($d > 1$ mm) and the second one is dedicated to small jets ($d < 1$ mm).

Faeth published a series of experimental investigations on the primary breakup of liquid jets in the second wind-induced and atomization regimes (Wu et al. 1992, 1995; Wu and Faeth 1993, 1995; Faeth et al. 1995). These investigations focused on the primary breakup along the liquid round jets as opposed to breakup of the entire liquid column. High-Weber and Reynolds numbers were achieved by combination of high nozzle diameter (in the millimeter range) and high liquid velocities (up to 140 m/s). Their operating conditions covered wide ranges of non-dimensional numbers thanks to the use of several nozzle diameters, liquids, surrounding gas and ambient pressures, namely, $Re_L \in [5{,}600;\ 780{,}000]$, $We_G \in [12;\ 3{,}790]$, $Oh \in [0.001;\ 0.02]$ and $\rho_L/\rho_G \in [104;\ 6{,}230]$. A particular attention was paid to the nozzle internal design. It was profiled in order to minimize any internal flow instability and to provide a uniform velocity-profile across the exit section aside from boundary layers along the wall passages. A sharp leading edge cutter of constant diameter (less than the nozzle orifice diameter) was positioned under the nozzle. The role of this cutter was to remove the boundary layers formed along the nozzle walls and to provide a well-defined slug flow inlet condition for the constant-diameter section with flow properties at the exit of this section controlled by its length (Wu et al. 1995). Thanks to this arrangement, they could produce nonturbulent and turbulent flows according to the length of the constant diameter sections. The experimental techniques of investigation involved pulsed shadowgraph photography to visualize the primary breakup mechanisms and double-pulsed holography images to measure the size and the velocity of the droplets produced by these mechanisms.

For nonturbulent slug flows they identified two different behaviors. When the boundary layers were removed (thanks to the use of a short-length cutter) the primary breakup along the jet interface was entirely suppressed (Fig. 5a). In the presence of boundary layers, ligaments formed very close to the nozzle exit shortly followed by breakup of their tips (Fig. 5b). Furthermore, this behavior was found weakly dependent on the liquid/gas ratio when it was >500 showing the small influence of the aerodynamic forces. This result shows that vorticity generated in the injector passage dominates the primary breakup process. By assuming that the Sauter mean diameter D_{32} of the primary droplets is proportional to the boundary-layer thickness at the nozzle exit and that this thickness scales in the same manner as a laminar flat-plate boundary layer for an ambient velocity U_L and a length L_p, the latter being the length of the nozzle wall along which the boundary layer develops, Wu et al. (1995) derived a correlation that agreed satisfactorily with the experimental results; namely:

$$\frac{D_{32}}{d} = \frac{7}{We_G}\left[\left(\frac{L_p}{d}\right)^{1/2}\frac{We_G}{Re_L^{1/2}}\right]^{0.87} \tag{6}$$

Note that this correlation reports a weak dependence of the Sauter mean diameter with the ambient gas density ($D_{32} \propto \rho_G^{-0.13}$). Wu et al. (1995) pointed out that the condition for the onset of laminar breakup regime has not been established so far.

The turbulent primary breakup regime appeared along the jet surface provided that sufficient energy was available to initiate the mechanism. An example of the turbulent primary breakup is shown in Fig. 5c. Wu et al. (1995) established a criterion for the onset of turbulent primary breakup, namely, $L/d > 4$–6 and $Re_L > 1$–4×10^4, and

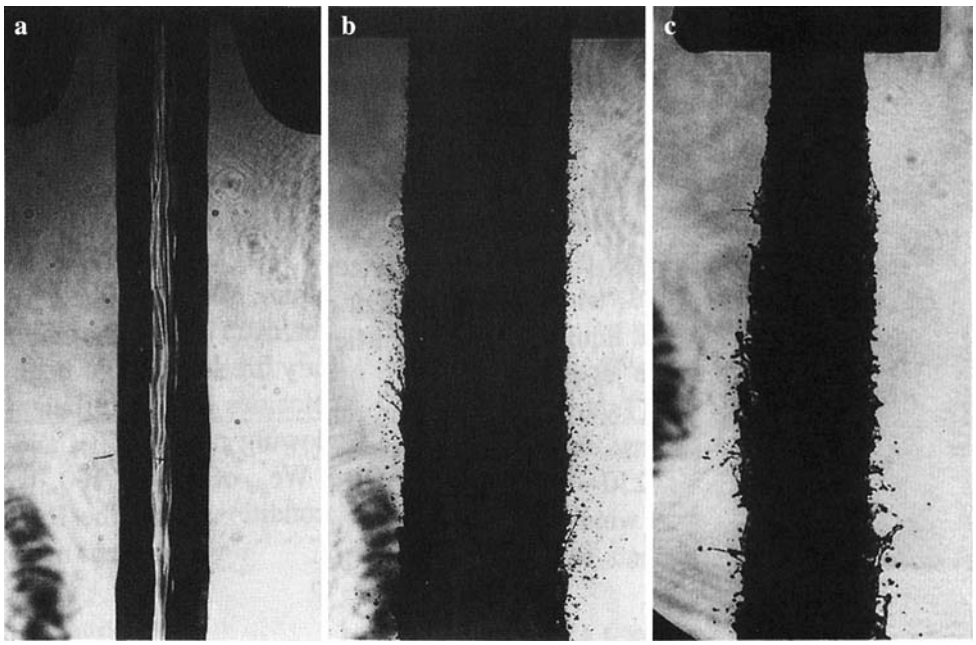

Fig. 5 Behavior of water jets with controlled characteristics at the nozzle exit. **a** Laminar jet without boundary layer ($d = 4$ mm, $U_L = 50$ m/s, $We_G = 185$); **b** laminar jet with boundary layers ($d = 6$ mm, $U_L = 50$ m/s, $We_G = 277$); **c** fully developed turbulent jet ($d = 3.6$ mm, $U_L = 35$ m/s, $We_G = 82$) (from Wu et al. 1995)

observed no effect of liquid/gas density ratio on transition to the turbulent primary breakup regime. However, the liquid/gas density ratio influences the primary breakup regime as follows.

When $\rho_L/\rho_G > 500$, Wu et al. (1992) noticed that the direction of the ligaments was not particularly correlated with the relative velocity of the gas. The motion of the ligament resulted largely of randomly directed liquid velocity fluctuation with aerodynamic drag forces playing a secondary role. This regime is called the non-aerodynamic turbulent primary breakup. In a subsequent study, Wu and Faeth (1995) demonstrated that for fully developed turbulent jets obtained with sufficiently long nozzles ($L/d > 40$), the liquid Weber number conditioned this breakup regime. When $We_L < 5{,}200$, the primary breakup along the jet surface did not appear; when $5{,}200 < We_L < 17{,}000$, the primary breakup was observed but stopped at some distance from the nozzle; and when $17{,}000 < We_L$ the turbulent breakup on the jet lasted over the atomization of the whole jet. Furthermore, the primary breakup of fully developed turbulent jets did not appeared right at the nozzle exit. Wu et al. (1992) and Wu and Faeth (1993, 1995) involved use of phenomenological analysis in order to develop a mean of estimating the drop sizes and the location at the onset of turbulent primary breakup. They assumed that drops at the onset condition were formed from the smallest turbulent eddy whose kinetic energy, relative to the surrounding fluid, was sufficient to provide the required surface energy of a comparable-sized drop and that the location of the onset of primary breakup was the distance required for this critical eddy to move from the jet exit in order to form a drop as a result of Rayleigh breakup of the corresponding protruding eddy-sized ligaments. These considerations yielded the following correlations:

$$\begin{cases} \frac{D_{32i}}{\Lambda} = 133\left(We_L \frac{\Lambda}{d}\right)^{-0.74} \\ \frac{x_i}{\Lambda} = 3,980\left(We_L \frac{\Lambda}{d}\right)^{-0.67} \end{cases} \quad (7)$$

where D_{32i} is the Sauter mean diameter at point of breakup initiation, x_i the distance from the nozzle where the breakup is initiated and Λ the radial spatial integral scale of turbulence. Then, by assuming that drop sizes at a given location correspond to the size of the ligaments completing Rayleigh breakup to form drops from their tips at the same position yielded the following correlation for the Sauter mean diameter D_{32} as a function of the distance x from the nozzle:

$$\frac{D_{32}}{\Lambda} = 0.69\left(\frac{x/\Lambda}{\left(We_L \frac{\Lambda}{d}\right)^{0.54}}\right)^{0.57} \quad (8)$$

In agreement with the observations, this correlation reports an increase of the primary drops as the distance from the nozzle increases. Sallam et al. (1999) obtained similar correlations with different constants and exponents for the primary breakup of plane turbulent liquid jets in still gases.

For lower liquid/gas ratio ($\rho_L/\rho_G < 500$), Wu et al. (1992) and Wu and Faeth (1993) observed two regimes of turbulent primary breakup according to the ratio of the characteristic Rayleigh breakup time to the aerodynamic secondary breakup time. For this ratio is <4, the aerodynamically enhanced turbulent primary breakup is observed at onset conditions. As the distance from the nozzle is increased, the time ratio becomes >4 and aerodynamic turbulent primary breakup is observed. This breakup

regime involves merging of turbulent primary and secondary breakup.

The main conclusion to be drawn from these investigations is that the presence of vorticity due to turbulence or to variations of mean velocities from viscous effects in the boundary layer plays a dominant role in primary breakup along the surfaces of liquid jets in gases. Furthermore, when $\rho_L/\rho_G > 500$, which corresponds to most of the situations where a liquid is ejected into air under atmospheric condition, aerodynamic forces have a reduced influence on the primary atomization onset and droplets. Therefore, a criterion as the one suggested by Ranz (1956) for the second wind-induced regime and based on the gaseous Weber number (see Table 1) is not suitable for the prediction of primary interfacial breakup of large jets.

The investigations described above concentrated on the onset of primary breakup along the surface of the liquid jets. Sallam et al. (2002) completed these works and examined the breakup of the entire liquid column for turbulent liquid flows ($Re_L \in [5{,}000; 200{,}000]$, $We_L \in [235; 270{,}000]$, $L/d > 40$). Three breakup modes of the liquid column were reported: weakly turbulent Rayleigh-like breakup mode (small Re_L and We_L), turbulent breakup mode (moderate Re_L and We_L) and aerodynamic bag/shear breakup mode (large Re_L and We_L). In the first mode the turbulence at the jet exit is only weakly developed and the liquid column is not significantly distorted by the turbulence and is perturbed and disintegrates in a rather axisymmetric and regular way. In the second mode, turbulence at the jet exit is reasonably well developed and yields to irregular distorted liquid jet. Furthermore, liquid jet breakup at these conditions appears to involve the turbulent primary breakup mechanism described above. This mechanism is similar to the one described in region D of the stability curve (Fig. 1). In the third mode, the turbulence distorts the liquid jet to a much greater degree than the jet diameter and places most liquid column elements in cross flow inducing significant aerodynamic effects. Two types of breakup are reported; bag-type liquid jet breakup, which involves the formation of bag-like structures in the liquid jet and their subsequent atomization; and the shear-type liquid breakup, which involves the formation of ligaments along the sides of the liquid jet and their subsequent breakup. As noticed by Sallam et al. (2002) these two breakup-types have been reported on laminar jet evolving in a cross-gas flow and are clearly associated to aerodynamic effects. However, Sallam et al.'s work shows that in the case of high-Weber cylindrical jets, the onset of this third breakup regime is controlled by the jet turbulence whose intensity may or may not orientate the jet perpendicular to its displacement. In conclusion, the primary breakup of an entire liquid column characterized by a large Weber number is very much dominated by the degree of development of the turbulence in the liquid flow issuing from the nozzle.

High-Weber jets that have received a permanent attention from the scientific community are those produced from a small diameter orifice at a very high injection pressure as typically encountered in diesel fuel injection. Reviews on diesel injection are available in Smallwood and Gülder (2000) and Dumont et al. (2000). Although typical diesel injector orifice diameters can be as small as 130 μm, the Weber numbers of these jets are very high due to the use of injection pressures that goes up to 250 MPa. In these conditions, the liquid velocity inside the nozzle hole reaches several hundreds of meters per second and as soon as the jet issues from the nozzle, a vivid atomization takes place characterized by a dense core region near the nozzle surrounded by a very high optical density spray. Experimental determination of characteristic features of the primary breakup is difficult as classical shadowgraph images as those used in the previous situations become ineffective to detail the mechanism. One of the common procedures has been to measure the spray angle at the nozzle exit.

Reitz and Bracco (1982) reported an experimental investigation where spray angle was measured on shadowgraph images for 67 operating conditions including several nozzle internal designs ($d \approx 0.36$ mm, $L/d \in [0.5; 85]$, constant diameter tube with sharp or round inlet, and convergent nozzles), injection pressures (from 3.3 to 14 MPa), ambient pressures (from 0.1 to 4 MPa), gaseous densities (from 1.3 to 50 kg/m^3) and liquid viscosity (from 10^{-3} to 1 kg/ms). They found that the spray angle increased when the ambient pressure increased up to 2 MPa and demonstrated that the parameter controlling the spray angle was the gas density and not the ambient pressure. Reitz and Bracco (1982) emphasized the influence of the nozzle internal design on the characteristics of the jet primary breakup. For instance, rounding the inlet of a short nozzle had a stabilizing effect similar to that of lengthening the nozzle. A detailed analysis of all the experimental results led them to conclude that aerodynamic effects, liquid turbulence, liquid supply pressure oscillations and jet velocity-profile rearrangement effects each could not explain the primary breakup in the atomization regime. Reitz and Bracco (1982) considered the possible influence of liquid cavitation. The phenomenon of cavitation is a rupture in liquid continuum due to excessive stress and that appears as soon as the pressure decreases below the liquid vapor pressure. It is characterized by a change of phase of the liquid. Although cavitation was always present in Reitz and Bracco's experiments, it did not guarantee the jet to disintegrate in the atomization regime. Therefore, cavitation cannot be the sole agency of atomization. Finally, they suggested that the effects of changes in nozzle

geometry could be to supply different initial disturbance levels to the flow but that the physical mechanism by which this could occur is unknown.

Hiroyasu and co-workers published a series of experimental investigations that underlined the importance of cavitation in diesel jet atomization (Arai et al. 1985, 1988; Hiroyasu et al. 1991). These investigations are summarized in Hiroyasu (2000). Arai et al. (1985) measured the breakup length of water jets. The internal flow was visualized by shadowgraph images thanks to the use of transparent nozzles. The issuing liquid jets were also visualized by shadowgraph images. The jet breakup lengths were determined by an electrical resistance method, which consists in measuring the electrical impedance between the nozzle and a fine wire net detector located downstream in the spray. Their working conditions covered several injector characteristics ($d \in [0.1; 3\ \text{mm}]$, $L/d \in [1; 50]$), an injection pressure that ranged from 0.1 to 50 MPa and an ambient pressure up to 10 MPa. Arai et al. (1988) and Hiroyasu et al. (1991) completed these measurements by two different nozzle inlet geometries, namely, round and sharp. One of the interesting results reported by these measurements is that, whatever the operating conditions, the second wind-induced regime (region D in Fig. 1) was reached for a rather constant liquid Reynolds number of the order of 3×10^3. Furthermore, they succeeded in detecting and measuring a breakup length for all working conditions and concluded that a continuous liquid jet always exists at the nozzle exit. Based on these measurements, Hiroyasu and co-workers proposed an extended jet stability curve in the atomization regime (region E). This curve is presented in Fig. 6. It shows a possible hysteresis either in the second wind-induced or in the atomization regimes. The condition to see this hysteresis is a function of the nozzle geometry and of the operating conditions. Jets produced by a smooth inlet nozzle never show the hysteresis and stability curves are continuous following the branch ABCDEF at high ambient pressure or the branch ABCDH at small ambient pressure. Note that for these jets, an influence of the ambient pressure could be observed in the second wind-induced regime (for instance for the condition $d = 0.3$ mm, $L/d = 4$ and $P_{amb} = 3$ MPa). The hysteresis in the stability curve was observed for jets produced by sharp-edge inlet nozzle provided that the L/d ratio was not too high ($L/d < 10$ when $P_{amb} = 0.1$ MPa and $d = 0.3$ mm), the ambient pressure was not too high ($P_{amb} < 1$ MPa when $L/d = 4$ and $d = 0.3$ mm) and the diameter was not too small ($d > 0.1$ mm when $L/d = 4$ and $P_{amb} = 0.1$ MPa). In these cases the stability curve follows the branch ABCDSF at high ambient pressure or the branch ABCDSH at small ambient pressure. When the jet velocity increases, the jump in breakup length is observed in the second wind-induced region for small jet diameter (point 1 in Fig. 6) and in the atomization regime for larger jet diameter (point 2 in Fig. 6). When the jet velocity decreases from the atomization regime, breakup length jump is observed at smaller velocity than when the velocity increases. Hiroyasu and co-workers attributed the hysteresis to the development of cavitation in the nozzle hole as summarized in Fig. 7. For short ($L/d = 0$) or smooth inlet nozzle orifice (Fig. 7a, b), no cavitation is observed. However, for sharp-inlet and sufficiently long nozzle, cavitation appears at the nozzle entrance (Fig. 7c) and extends along a distance that increases with U_L (Fig. 7d). Arai et al. (1985) noticed that the appearance of liquid cavitation at the nozzle entrance coincided with an increase of the jet angle at the nozzle exit and concluded therefore to an influence of the cavitation phenomena on the primary breakup mechanism. For sufficiently high liquid velocity, the cavitating region does not reattach on the nozzle wall and extends down to the nozzle exit (Fig. 7e). Free of any wall friction, no turbulence develops

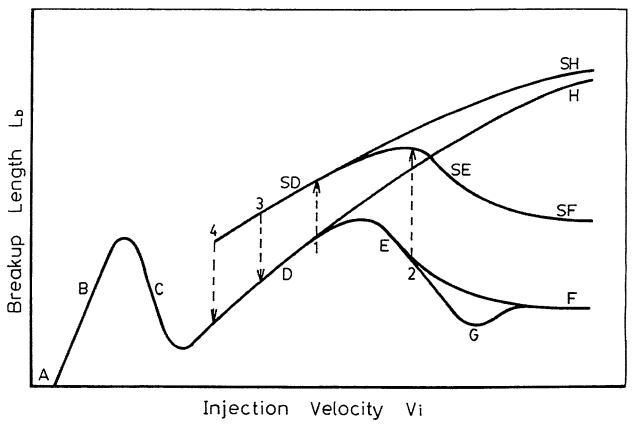

Fig. 6 Extended cylindrical jet stability curve (from Arai et al. 1998). Branches *F* and *H*: non-cavitating flow under high and low ambient pressure, respectively. Branches *SF* and *SH*: cavitating flow under high and low ambient pressure, respectively

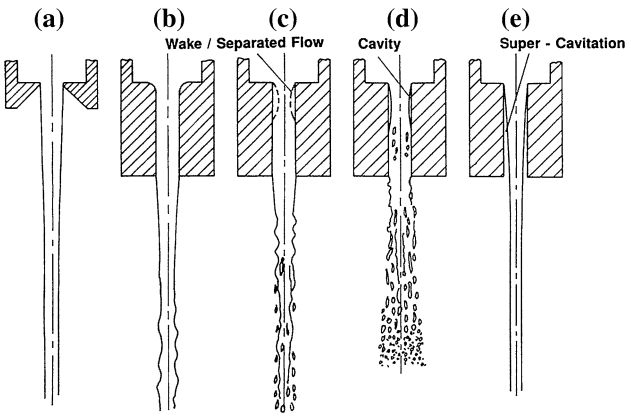

Fig. 7 Schematic appearance of a cylindrical jet as a function of cavitation (from Hiroyasu et al. 1991)

in the nozzle and the issuing jet shows a smooth interface and a sudden increase of the breakup length. Such jets are similar to the nonturbulent jet without boundary layers reported by Faeth and co-workers (see Fig. 5a). Hiroyasu et al. (1991) called this behavior super-cavitation. When the jet velocity decreases from a high value, the velocity at which re-attachment occurs is smaller than the one at which detachment appears when the velocity is increased. All these results evidenced the importance of liquid cavitation and therefore of internal flow details on the atomization mechanism.

Ohrn et al. (1991a, b) conducted a series of experiments on jets produced by nozzles of constant diameter ($d = 0.254$ mm) but with different L/d ratios (from 2 to 5) and different inlet conditions. They worked with sharp-edged and chamfered edge inlet nozzles as well as with rounded-inlet nozzles with controlled radius of the rounded-inlet profile. The measurements consisted in measuring the discharge coefficient (defined as the ratio of the average issuing liquid velocity to the Bernoulli's velocity) and the spray angle at the nozzle exit, the latter being measured on visualizations performed with a rather long exposure time (1/60 s) in order to visualize average spray angle. These measurements were performed for varying injection pressure (from 3 to 109 MPa) and with two fluids; a calibration fluid with physical properties close to diesel and water. The results demonstrated that the shape and condition of the nozzle inlet have a stronger effect on discharge coefficient than do L/d ratio and Reynolds number. Sharp-edged inlet nozzles are the more sensitive to small perturbations of the inlet edge. These nozzles reported smaller discharge coefficients compared to other nozzles. Ohrn et al. (1991a) argued that this behavior was due to the fact that the discharge coefficients of sharp-edged inlet nozzles are controlled by cavitation. Similarly, the discharge coefficients of the rounded-inlet nozzles increased with the radius of the rounded-inlet profile. This is due to the fact when this radius is increased, the flow becomes less restricted and cavitation is reduced or eliminated resulting in a higher discharge coefficient. Ohrn et al. (1991b) reported also that the shape and condition of the nozzle inlet have an important effect on spray angle. However, this effect is a function of the ratio L/d. More generally, they concluded that the effects of injection pressure, inlet radius and L/d ratio on cone angle are highly coupled and should not be viewed as separate phenomena.

Karasawa et al. (1992) performed an experimental investigation on water sprays produced by constant diameter nozzles ($d = 0.3$ mm) but with different L/d ratio (from 1 to 50) and a varying average issuing velocity U_L (from 90 to 220 m/s). These conditions correspond to a gaseous Weber number ranging from 45 to 270 and place the jets in the atomization regime. Furthermore two sets of nozzles with sharp-edge and round inlet were used. Their experiments consisted in measuring the discharge coefficient as well as the drop size of the spray. Drop sizes were measured by a PDPA, which reports information on the size and on the velocity of the droplets. One of the drawbacks of this technique is that it can be used in dilute spray region only to ensure that the measuring volume composed of the intersection of two laser beams contains one drop at the time. To achieve high validation rate measurements, Karasawa et al. (1992) positioned the measuring volume between 1,000 and 1,500 mm from the diesel injector. For all tested velocities, sharp-edge inlet nozzles reported almost constant Sauter mean diameters (D_{32}) for a L/d ratio <10 and then increased with this ratio. In the contrary, no specific variation of D_{32} with L/d was reported for nozzle with a round inlet. Furthermore, they noticed that drops produced by sharp-edge inlet nozzles were always less than those obtained with rounded-inlet nozzles. These two groups of nozzles also showed differences in terms of discharge coefficient. The discharge coefficients of sharp-edge nozzles were independent of the L/d nozzle ratio and less than those of round-inlet nozzles that decreased with L/d following the evolution of turbulent pipe flow discharge coefficients. This difference of behavior was attributed to the presence of flow separation that, as found by Hiroyasu et al. and Ohrn et al. (1991a), is not expected in round-inlet nozzle. When flow separation occurs (sharp-inlet nozzles), the effective liquid velocity at the nozzle exit is equal to the Bernoulli's velocity and the discharge coefficient is controlled by a reduction of the effective area of the nozzle exit section because of the presence of vapor pockets. On the other hand, when no flow separation occurs (round-inlet nozzle), the effective velocity is less than the Bernoulli's velocity and the discharge coefficient is controlled by this reduction of velocity. For all operating conditions, Karasawa et al. (1992) established a single correlation between the Sauter mean diameter and the effective jet velocity at the nozzle exit. Based on this correlation they concluded that the effective jet velocity was the primary factor for atomization. Furthermore, they attributed the independence between D_{32} and L/D for round-inlet nozzle to be representative of a weak influence of the liquid turbulence on atomization.

Kim et al. (1997) performed visualizations of the internal flow in diesel injection nozzles. They used transparent model nozzles ten times greater than real diesel injectors. The model nozzles reproduced two cylindrical holes, the sac volume above these holes and the presence of the needle. Several models were tested with different discharging-hole positions and sac volume capacities. Water instead of diesel fuel was used as the injection liquid. The injection pressure for the model nozzle were carefully scaled up in order to achieve a Reynolds number at the

discharge hole corresponding to diesel injection, namely, 40,000. Particles of polystyrene (0.25 mm in diameter) with used as tracers and 2D photographs of the steady flow pattern in the sac volume were taken using a 1 mm thick laser sheet. Furthermore, photographs of the spray plume were also taken at the nozzle exit. These visualizations showed complex flow structures in the sac volume including large-scale vortex, cavitation and turbulence that were functions of the needle position and the sac volume geometry. These characteristics influenced the internal flows in the discharge holes and consequently the discharge coefficient and the spray angle at the nozzle exit. For instance, small-needle lifts caused high turbulence in the sac volume and increased the spray angle. For high-needle lift, super-cavitation occurred in the discharge holes and reduced the spray angle. For small sac volume, column type of cavitation appeared in the sac volume and modified the spray plume structure as a hollow cone with fine droplets. Furthermore, it was also noticed than even in steady state conditions, cavitation in the sac volume was unstable causing fluctuation of the spray plume.

In order to clarify the respective influence of the liquid/gas interfacial forces and the internal flow effects (turbulence and cavitation) on jet behavior in the atomization regime, Tamaki et al. (1998) conducted an experimental work on water jets produced by transparent nozzles of different geometrical characteristics ($d \in [0.3;\ 0.5$ mm]; $L/d \in [2.5; 20]$; sharp-edged and round-inlet nozzles) under various injection conditions ($\Delta P_i \in [0.1;\ 200$ MPa]; $P_{amb} \in [0.008;\ 3.1$ MPa]). Internal flows were visualized using a micro-flash spark light and jet images were taken by a scattering light technique using a pulsed ruby laser. The jet breakup lengths were measured by the resistance method used by Arai et al. (1985, 1988). Furthermore, the disturbance magnitude of the internal flow was evaluated by measuring the vibration acceleration in the nozzle hole with a piezoelectric acceleration transducer. They observed that in the absence of cavitation in the nozzle hole, the jet did not atomize greatly even if the injection pressure is extremely high. In this case, breakup length elongates. However, when the occurrence of cavitation caused an increase of the disturbance level of the internal liquid flow, the jet atomization was considerably promoted. For round-inlet nozzle, in which cavitation never occurs, the increase of the injection pressure or of the ambient pressure did not help atomization. In the contrary, in the presence of cavitation (sharp-edge inlet nozzles) an increase of the ambient pressure promoted the disturbance level of the internal flow and helps atomization. Whatever the operating conditions, it was found that atomization was promoted when cavitation increased the internal flow disturbance level. Tamaki et al. (1998) concluded that the increase of internal liquid flow disturbance level caused by cavitation was the dominating factor in the onset of primary breakup in the atomization regime. Therefore, under decompression where atomization was never observed, it is possible to trigger it by using perturbing elements such as a fine net at the nozzle entrance in order to create internal flow disturbances (Tamaki et al. 1998; Hiroyasu 2000; Tamaki et al. 2001).

Parker et al. (1998) developed a diagnostic that, contrary to the phase doppler particle analyzer mentioned earlier, allows the drop-size distribution of atomization regime sprays to be measured near the nozzle exit. This diagnostic is a line-of-sight technique. It is a three-laser extinction measuring system that uses infrared wavelengths (0.633, 1.06 and 9.2 μm) whose penetration is better if the drop-sizes are not too large, and that analyses the attenuation of the beams by the spray. Parker et al. (1998) applied this technique to fuel sprays produced by a single diesel injector ($d = 0.17$ mm, $L/d = 3.6$) at an injection pressure of 20 MPa for three ambient conditions, namely: (1) atmospheric pressure and room temperature ($\rho_L/\rho_G = 640$), (2) high ambient pressure and room temperature (argon, $P_{amb} = 1.1$ MPa, $\rho_L/\rho_G = 43$) and (3) high ambient pressure (from 2.5 to 4 MPa) and high ambient temperature (from 700 to 900 K) corresponding to $\rho_L/\rho_G < 100$. Measurements were performed on the spray centerline at several distances from the nozzle ranging from 5 to 35 mm. One of the important results is that, whatever the operating conditions, drop-sizes could be measured as close as 5 mm from the nozzle tip. This finding is in favor of the absence of a continuous liquid column connected to the nozzle exit. Under atmospheric pressure and room temperature, the spray Sauter mean diameter ranged from 5.4 to 7.8 μm when the distance from the nozzle increased. Both ambient pressure and temperature increases induced a slight decrease of the mean spray diameter at any position. Parker et al. (1998) compared their results with Sauter mean diameter predictions found in the literature. These comparisons reported poor agreement except for the cases 2 and 3 for which Faeth's model based on Eq. (7) for the primary breakup Sauter mean diameter coupled with a secondary breakup model reported acceptable estimations. Furthermore, they noticed that, under atmospheric conditions (case 1), models based on aerodynamic primary breakup failed in reporting good predictions. Parker et al. (1998) concluded that, in agreement with Faeth and co-workers, when $\rho_L/\rho_G > 500$, aerodynamic forces are not the dominant mechanism in primary atomization.

Badock et al. (1999a) analyzed the behavior of real size transparent diesel injection nozzles. Sharp-edged inlet and round-inlet nozzles with diameter ranging from 0.164 to 0.214 mm were tested. Injections were performed under atmospheric condition and for an injection pressure ranging between 15 and 60 MPa. Shadowgraph images with a short

duration flashlight (<20 ns) were taken to visualize the internal flow as well as the spray at the nozzle exit. These visualizations were used to qualitatively describe the internal flow and to measure the spray angle. Badock et al. (1999a) observed that sharp-edged inlet nozzles promoted the development of cavitation that was barely seen in round nozzles. However, they noticed no impact of the cavitation on the spray angle: even when cavitation extended to the nozzle tip as for the super-cavitation reported Hiroyasu and co-workers, no sharp reduction of the spray angle was observed. This disagreement may come from the fact that, as explained by Dumont et al. (2000), wall flow detachment can result either from hydraulic flip or super-cavitation. In hydraulic flip, a gaseous layer at a pressure equal to the atmospheric pressure surrounds the detached liquid flow in the nozzle. The resulting issuing liquid jet is cavitation free and its interface is totally smooth which prevents atomization. This phenomenon is complex and unstable: as soon as the flow is perturbed upstream, hydraulic flip is not present anymore. Super-cavitation is characterized by the presence of a layer of vapor phase around the liquid flow in the nozzle. The pressure in this layer is equal to the liquid vapor pressure and an increase of the spray angle is observed at the nozzle exit revealing early atomization. Thus, the behavior reported by Hiroyasu and co-workers is likely to be hydraulic flip and the one observed by Badock et al. (1999a) might be super-cavitation. In a subsequent investigation, Badock et al. (1999b) visualized the internal flow for a wider set of real single-hole diesel injector nozzles ($d \in [0.18; 0.3\ \mu m]$, $L/d \in [3.3; 5.6]$) under an ambient pressure of 1.5 MPa. Visualizations were performed with shadowgraph and tomography images, the later being obtained thanks to the use of a laser sheet with a thickness <20 μm. The laser sheet technique was found very efficient to report details in the central flow region that could not be obtained from shadowgraph technique. In particular, it was observed that cavitation films and bubbles did not extend into the central part of the liquid flow and that the existence of cavitation foam or of many small bubbles inside the nozzle holes could be discounted. Even at injection pressure up to 60 MPa, the hole was filled with liquid surrounded by cavitation films, which led to the hypothesis that under diesel-like pressure conditions, an intact liquid core leaves the nozzle holes.

Yue et al. (2001) developed a diagnostic to investigate the jet structure near the nozzle tip. This technique is based on the absorption of monochromatic X-ray beam to measure the liquid volumetric fraction as a function of the position. The advantage of using X-rays is that they have low cross section when interacting with matter and multiple scattering is typically a negligible component in X-ray measurements. The beam spot size was 500 μm × 200 μm. The measuring technique they developed was highly quantitative and allowed liquid volumetric fraction to be measured. It was applied on a jet produced by a 0.187 mm diameter diesel injector at various injection pressures (20, 50 and 80 MPa). Measurements were conducted on the spray centerline and at several distances from the nozzle varying from 1 to 6 mm. Whatever the injection pressure, it was found that the liquid volumetric fraction at 1 mm from the injection was never >0.8. This value was reached at the beginning of the injection. Furthermore, as time went, the liquid volumetric fraction near the nozzle decreased down to a value of the order of 0.5. Yue et al. (2001) interpreted this result as an absence of intact liquid column at the nozzle exit.

Similar to Kim et al. (1997), Arcoumanis et al. (2001) performed visualizations of the internal diesel injector flow using transparent up-scaled injector models based on real injector design including the sac volume and several injection holes. The material used to build the nozzle and the test fluid had the same refractive index permitting uninterrupted optical access into the nozzle sac volume and hole irrespective of geometrical complexities. The Reynolds number of the issuing flow ranged from 15,000 and 44,000. The shadowgraph images obtained by Arcoumanis et al. (2001) revealed three different cavitation regimes when the injection pressure is increased. Initially, a bubbly flow structure was identified (incipient cavitation) followed by pre-film stage cavitation (consisting in a dense bubble cloud) and film type cavitation (complete flow separation that takes place at the nozzle hole inlets). Arcoumanis et al. (2001) observed also the presence of cavitation strings in the sac volume, which seemed to develop transiently and periodically between adjacent holes and then interacted with the cavitation films in the nozzle. These observations were also made on real size injector. Arcoumanis et al. (2001) concluded that interaction between geometrically induced hole cavitation (initiated at hole entrances) and dynamically induced cavitation strings or vortices represent a significant breakthrough in the understanding of cavitation in diesel engine injection nozzle.

Payri et al. (2004) investigated the jet produced by bi-orifice nozzles with sharp-edged inlet ($d = 0.131$ mm) or conical inlet ($d = 0.125$ mm). The injection pressure varied from 10 to 80 MPa and the ambient pressure ranged from 0.1 to 80 MPa. Shadowgraph images of the issuing jet were taken by using an electronic flash and a 12-bit color CCD camera. Payri et al. (2004) measured also the evolution of the total mass flow rate as a function of the injection pressure and ambient pressure in order to detect the presence of cavitation in the nozzle exit. In the absence of cavitation, the mass flow rate always increased with the injection pressure. However, when cavitation occurred, the mass flow rate saturated and was constant if the injection pressure was further increased. In this condition, the

velocity of the issuing liquid is equal to the Bernoulli's velocity but the effective section of the liquid flow continuously decreases leading to a constant mass flow rate. The results reported that cavitation never occurred in conical inlet nozzle. For sharp-edge inlet nozzles, cavitation appeared at an injection pressure that increased with the ambient pressure. Furthermore, in the absence of cavitation, both nozzle sets showed equivalent spray angle at the nozzle tip. However, when cavitation occurred in sharp-edged inlet nozzle, the spray angle reported a sharp increase. These observations agree with those reported by Karasawa et al. (1992).

In order to investigate the structure of diesel jets near the nozzle exit, Yon et al. (2003) performed visualizations of the liquid jets by coupling shadowgraph and laser sheet techniques. A 50 μm thickness laser sheet was positioned in the spray dense region just downstream the nozzle tip according to several inclinations with respect to the nozzle axis. At the same time, a short duration light source (10 ns) illuminated the jets from the back. The Mie scattering information provided by the laser light and the shadowgraph information provided by the flash light was recorded by a single CCD camera. The visualizations were analyzed by conducting ray-tracing simulations in order to identify the different structures in the images. Yon et al. (2003) argued that ray-tracing technique is the only theoretical tool that can be used to interpret the complex images recorded near the nozzle tip. This visualization technique and analysis were used for jets produced by a diesel injector ($d = 0.2$ mm, $L/d = 4$, $\Delta P_i \in [10; 80$ MPa]). Yon et al. (2003) observed that, near the injector, the jet was composed of a plain liquid core surrounded by a dispersed phase. They also noticed the presence of a cloud of very small cavitation bubbles in the liquid central part as well as long cylindrical gas cavities located in the periphery of the liquid core.

Li and Collicott (2006) performed shadowgraph images of the liquid flow inside cylindrical orifices of different geometrical characteristics ($d \in [0.206; 0.397$ mm], $L/d \in [5; 10]$ under several injection pressures ($\Delta P_i \in [46; 207$ MPa]). Furthermore, the cylindrical discharge hole showed a 14° tilt angle with the axis of the whole injector. They reported that three-dimensionality, such as hole-tilt or cross flow at the inlet, causes three different structures in the cavitation compared to axisymmetric inflow. The first cavitation structures were due to the three-dimensionality of the flow in the hole. Because of hole-tilt, a pair of counterrotating streamwise vortices was created at the nozzle entrance. When these vortices spin sufficiently fast, the pressure drops to vapor pressure and streamwise cavitation structures appeared. The second structure occurred as cavitation around the periphery of the flow. The onset of these structures was generally a circle normal to the axis of the hole and was not affected by hole-tilt. Badock et al. (1999a) observed similar cavitation circles. The third cavitation structures were created by surface roughness and develop along the wall. This type of structure was believed to be a major cause of difference of observation from one investigation to another.

Experimental diagnostics dedicated to the investigation of the primary breakup of jets such as those produced by diesel injector are still under development. One the most promising is probably the ballistic imaging technique which makes use of a new generation of laser light sources, the ultra-short laser pulse. Such a technique has been developed by Paciaroni et al. (2004, 2006) to image the near-field liquid core. It consists in illuminating the flow by an ultra-short laser pulse (80 fs) and to record the ballistic photons only. When used in a shadowgram arrangement, the ballistic photons, which have passed through the medium without scattering, can provide diffraction-limited imaging of the medium. Furthermore, because they travel the shortest path, ballistic photons also exit first and they are sorted thanks to the use of a temporal gate opened during the passage of these photons only. Images of a water jet issuing a 457 μm diameter hole at a velocity of 190 m/s have been taken at different positions from the nozzle. (Examples of images are shown in Fig. 8.) Important information is available from these images. Near the nozzle exit (Fig. 8a), a dense core is imaged with no evidence of breakup. The liquid core shows strong evidence for turbulent primary breakup. Spatially periodic structures are observed and the evolution of the liquid core is characterized by the growth of these structures with downstream position (see Fig. 8b, c).

Among other techniques specifically dedicated to the investigation of high-speed jet primary breakup are the development of image processing to analyze the drop-size and morphology distribution in the dense region (Blaisot and Yon 2005), the use of high rate imaging technique (Delacourt et al. 2005), the coupling of ballistic imaging and X-ray absorption imaging (Briggs et al. 2006) and the development of very high spatial resolution imaging technique (Nakagawa et al. 2006).

One of the main conclusions that can be drawn from these experimental investigations is that internal flow effects have paramount influence on the onset of primary atomization of jets in the second wind-induced and atomization regimes. Jets free of any internal perturbation such as laminar jets without boundary layers as those studied by Faeth and co-workers or liquid flows that experienced hydraulic flip do not atomize even in the range of high gaseous Weber number. Studying the behavior of cavitation free jets, Faeth and co-workers concluded that the presence of vorticity due to turbulence or to variations of mean velocity from viscous effects in the boundary layer

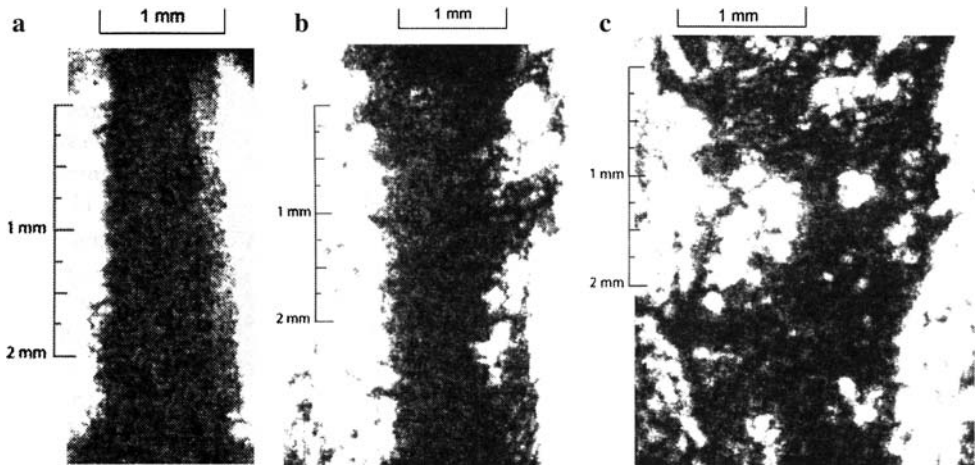

Fig. 8 Ballistic imaging of a high-speed jet ($Re_L = 102{,}000$, $We_L = 233{,}000$) **a** at the nozzle exit; **b** 19.5 mm from the nozzle exit; **c** 37.5 mm from the nozzle exit (from Paciaroni et al. 2006)

play a dominant role in primary breakup along the surface of liquid jets. They established that when $\rho_L/\rho_G > 500$ the effects of aerodynamic forces are unimportant in primary breakup but dominate the secondary breakup. However, when $\rho_L/\rho_G < 500$, aerodynamic forces help primary atomization. This limit in fluid density ratio was confirmed by the drop sizes measured near the nozzle exit by Parker et al. (1998) and that were found much smaller than those that would be produced by aerodynamic shear.

As far as the effects of liquid turbulence are concerned, Karasawa et al. (1992) and Tamaki et al. (1998) reported that the increase of turbulence in cavitation free jets did not particularly promote atomization, which is somewhat in contradiction with Faeth and co-workers conclusions. Note, however, that Faeth and co-workers examined large jets (above the millimeter range) at moderate velocity, whereas Karasawa et al. (1992) and Tamaki et al. (1998) considered small jets at very high velocity.

Liquid cavitation in the nozzle affects the behavior of jets in the second wind-induced and atomization regimes. The investigations reported above agree to say that the design of the discharge orifice is a dominant parameter for the onset of cavitation. Works due to Hiroyasu and co-workers, Ohrn et al. (1991a, b), Karasawa et al. (1992), Tamaki et al. (1998), Badock et al. (1999a) and Payri et al. (2004) all reported that round or conical inlet discharge nozzle prevents from the development of cavitation structures in the discharge orifice. On the other hand, sharp-edged inlet nozzles promote cavitation. However, whereas it is always reported that atomization is promoted when cavitation is present, the exact influence of cavitation on jet primary breakup is not fully identified and conclusions on this point differ from one investigation to another. Karasawa et al. (1992) and Payri et al. (2004) concluded that the main influence of cavitation was to increase the effective issuing velocity of the liquid jet. Tamaki et al. (1998) suggested that the presence of cavitation in the nozzle orifice induces the development of disturbance in the liquid flow. Hiroyasu (2000) noted that one of the effects of cavitation is to increase the turbulence in the liquid. In their review, Smallwood and Gülder (2000) identified two possible contributions of cavitation with the bursting and collapsing vapor cavities as soon as the liquid leaves the nozzle and with its propensity to increase the turbulence intensity in the liquid flow. However, they noticed a lack of quantitative information on these two possible phenomena. Dumont et al. (2000) pointed out that the production of droplets from the collapse of bubbles at the jet interface has never been clearly reported and that bubble bursts more probably produce surface perturbation. The ballistic images of high-Weber number atomizing jets reported by Paciaroni et al. (2004, 2006) did not show any small droplets produced by cavitation bubble collapsing. However, the presence of cavitation in their experiments was not demonstrated. Experiments conducted on real diesel injector design (Kim et al. 1997; Badock et al. 1999a, b; Arcoumanis et al. 2001; Yon et al. 2003) reported that liquid cavitation could have different origin (geometrically or dynamically induced) and could promote different structure in the issuing liquid flow. The influence of liquid cavitation on atomization might be a function of the origin and of the structure of cavitation. Anyway, the exact role of cavitation on the primary breakup mechanism requires more work to be fully identified and understood.

Another point of disagreement concerns the presence of a continuous liquid column at the nozzle exit in the atomization regime. As mentioned earlier this region of the spray is difficult to be experimentally investigated because of its high density. This has motivated the development of specific diagnostics to explore this region. However, these techniques report inconsistent information according to the measured quantity. For instance, Hiroyasu and co-workers always detected breakup lengths with an electrical resistance method and concluded to the presence of a continuous liquid

column at the nozzle exit. On the other hand, the drop-size measurements performed at the nozzle by Parker et al. (1998) with the three infrared laser extinction technique plead for the non-existence of this continuous liquid phase. The measurements of the liquid volumetric fraction at the nozzle performed by Yue et al. (2001) using a X-ray absorption technique lead to a similar conclusion. Sophisticated visualizations techniques and protocols such as those proposed by Yon et al. (2003) and Paciaroni et al. (2004, 2006) reveal that the issuing liquid stream is a multiphase flow with complex gaseous structures of different origins. As mentioned above these structures are strongly functions of the nozzle internal design and flow conditions. Finally, Kim et al. (1997) reported that the development of cavitation-column type in the sac volume could modify the spray plume to a hollow cone spray. Therefore, most of the discrepancies noticed between different experimental approaches are likely to be due to differences in nozzle internal designs and in internal flow details.

3 Flat liquid sheets

This section reports experimental investigations performed on the primary atomization process of flat liquid sheets evolving in a gaseous environment at rest. The most popular type of nozzle that produces flat liquid sheet is the fan nozzle. The orifice of this nozzle is formed by the intersection of a V groove with a hemispheric cavity communicating with a cylindrical liquid inlet (Lefebvre 1989). This design promotes impinging streamlines at the nozzle where a liquid sheet parallel to the major axis of the orifice develops. For a sufficient injection pressure, this sheet disintegrates into a narrow elliptical spray.

Flat liquid sheets can also be formed by the impingement of two cylindrical jets. The shape of the sheet is a function of the impingement angle made by the two jet axes. If this angle is equal to 180°, the liquid sheet is radial. An alternative to this technique consists of impinging a cylindrical liquid jet onto a solid surface. Here again the shape of the sheet is a function of the angle of impingement, a regular radial sheet being obtained when the liquid impact is normal to the surface.

One of the important characteristic features of the sheets produced by fan nozzle or by impingement is that they are decreasing in thickness in the streamwise direction. As it will be seen later this characteristic is a necessary condition to observe the disintegration of the liquid stream into a spray. Furthermore, the decreasing thickness of the sheet promotes the production of very small droplets and is a valuable aspect of this atomization process.

Compound injectors, often used in gasoline port-fuel engine, also produce flat liquid sheet. These injectors are made of a superposition of three circular disks with different circular orifices, the discharge orifice being not aligned with the upper-disk orifices. This internal design imposes drastic flow deflections and favors the development of a double-swirl at the nozzle exit. As soon as the liquid issues from the nozzle, this double-swirl induces a radial expansion of the flow that organizes as a sheet rather than as a cylindrical jet.

The experimental studies reviewed in this section concern flat sheets produced by fan nozzles, impingement and compound atomizers only. Conical liquid sheets such as water bells (Taylor 1959a) or those issuing from swirl atomizer (Lefebvre 1989) are not considered here.

One of the major scientific references on the behavior of flat liquid sheet is due to Squire (1953), who developed a linear stability theory for a liquid sheet of constant thickness evolving in a gaseous environment. Similar to the one due to Weber (1931) for cylindrical liquid jet, this approach assumed the temporal exponential growth of an initial perturbation. Squire (1953) considered that sinuous type of perturbation only where the two sheet interfaces are in phase. When the perturbation wavelength is greater than the thickness t_L of the sheet ($kt_L < 0.5$) and when the fluid density ratio ρ_G/ρ_L is of the order of 10^{-3}, Squire (1953) established the following condition of instability:

$$We_L = \frac{\rho_L U_L^2 t_L}{\sigma} > 2 \tag{9}$$

This condition shows that a minimum difference of velocity between the two fluids is required for an instability to develop. Such an aerodynamically driven instability is a Kelvin–Helmholtz instability. Furthermore, when $We_L > 20$ (We_L is given by Eq. (1) where t_L replaces d), Squire (1953) found that the characteristics of the optimum sinuous wave were:

$$\lambda_{opt} = \frac{4\pi t_L}{We_G} \quad k_{opt} t_L = \frac{We_G}{2} \quad \omega_{r\,max} = \frac{\rho_G U_L^2}{\sqrt{2 t_L \rho_L \sigma}} \tag{10}$$

where the gaseous Weber number We_G is also based on the sheet thickness. Hagerty and Shea (1955) demonstrated that only two modes of Kelvin–Helmholtz instability could develop on a flat liquid sheet, namely, the sinuous mode (where both interfaces oscillate in phase) and the dilational mode (where interfaces are in phase opposition). These two modes of instability, also called anti-symmetric and symmetric modes, respectively, can be distinguished by their temporal growth rate, the one of the sinuous mode being always greater. (A review of these theoretical approaches can be found in Sirignano and Mehring (2000).)

Dombrowski and co-workers have extensively investigated the behavior of flat liquid sheet produced by fan nozzles (Dombrowski et al. 1960; Fraser et al. 1962; Crapper et al. 1973; Clark and Dombrowski 1974;

Dombrowski and Foumeny 1998). The sheets issuing from fan nozzle are bordered by two thick edges. As a result of the surface tension, the edges of the sheet contract and a curved boundary is produced as the sheet develops downstream. At low injection pressure, edge contraction lasts until the edge of the sheet coalesce. During the contraction, drops are emitted from the edge of the sheet in a manner somewhat analogous to a cylindrical liquid jet. These drops follow the direction tangential to the sheet at the point where they are produced. When the sheet contraction is completed drops cross over from one side to the other. At higher injection pressure, contraction is less pronounced and the sheet eventually disintegrates before the two edges coalesce. Two sheet disintegration modes are reported. Under atmospheric pressure, a large wavelength sinuous wave grows and eventually leads to the sheet disintegration (Fig. 9). At sub-atmospheric pressure, perforation holes appear on the sheet and extend up to the disintegration of the whole sheet. (Sindayihebura and Dumouchel (2001) reported a similar perforating atomization process on a high viscous sheet produced by a swirl atomizer (Fig. 10).)

Dombrowski et al. (1960) provided a deep analysis of the flow in the sheet. They studied the flat sheet produced by a single fan nozzle. During their experiments, several liquids were tested ($\sigma \in [0.02;\ 0.073$ N/m], $\mu_L \in [10^{-3};\ 50 \times 10^{-3}$ kg/ms] and the injection pressure was varied from 0.06 to 0.34 MPa. By taking photographs of the sheet containing suspended aluminum particles, they observed that the sheet streamlines are straight and unaffected by the curved boundary. Therefore, the drops produced at the edge are emitted in a direction that is different from that of the local sheet streamline. By taking double exposure photographs, Dombrowski et al. (1960) also reported that the stream velocity is constant along the sheet and depends on the injection pressure only. This finding made them suggest that the energy absorbed in producing the larger surface area when the sheet expands is derived from the enthalpy of the liquid. This hypothesis cannot be easily confirmed since the predicted temperature drop along the sheet is too small for accurate measurement. (They estimated this temperature drop to be of the order of 0.01°C.) It is interesting to point out that Sirignano and Mehring (2000) evoked the compensation of surface energy evolution by temperature variation when analyzing the Rayleigh breakup mechanism of a cylindrical liquid jet.

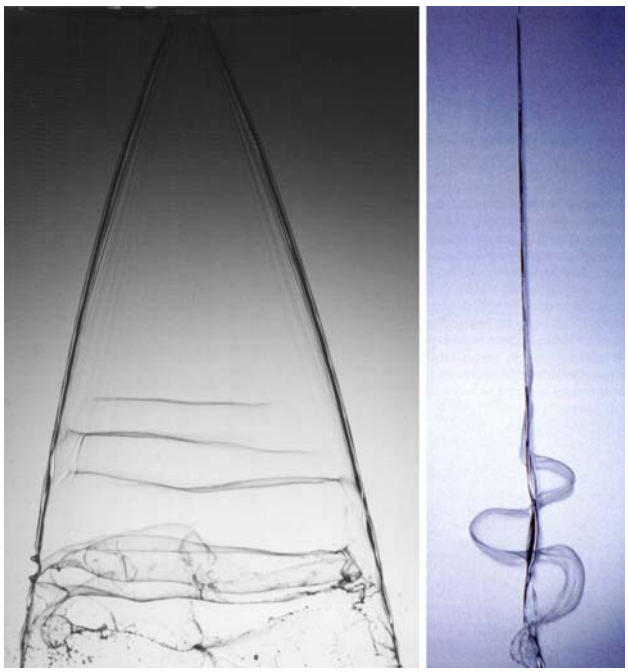

Fig. 9 Sinuous mode of disintegration of a fan-nozzle liquid sheet (*left* front view, *right* side view, from Dumouchel 2005)

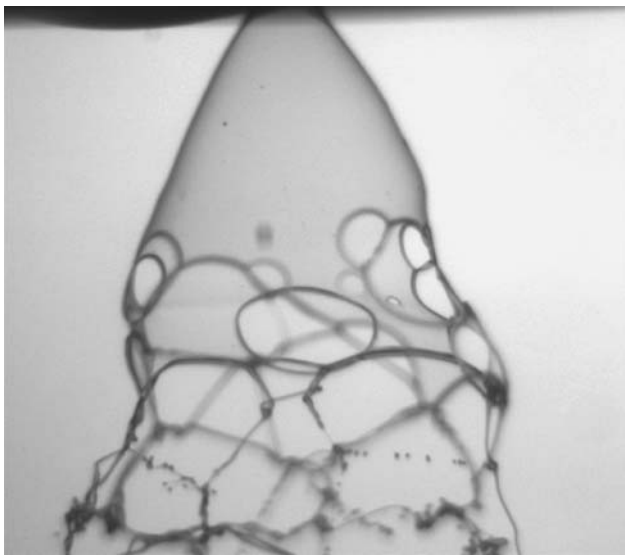

Fig. 10 Illustration of the perforating disintegration regime (case of a conical sheet, from Sindayihebura and Dumouchel 2001)

Dombrowski et al. (1960) also measured the sheet thickness as a function of the distance from the nozzle by applying a method based on light interference. The liquid sheet was illuminated with a monochromatic light beam that reflected on the front and back interfaces. These reflections interfered with each other because of the difference of their light paths. Images of the reflected light showed a succession of bright and dark fringes, two adjacent bright or dark fringes corresponding to a given sheet thickness variation that is a function of the refractive index, the angle of refraction of the light in the film and the wavelength of the monochromatic light. They found that the sheet thickness t_L varies with the distance x from the nozzle as $t_L(x) = K/x$, where K is called the sheet thickness parameter. When the injection pressure is >0.15 MPa, the thickness parameter is independent of the surface tension

coefficient and correlates with $(\Delta P_i \rho_L)^{1/2} \Big/ \mu_L$; K decreases when $(\Delta P_i \rho_L)^{1/2}/\mu_L$ increases. In this case, typical value of the thickness parameter K is 14×10^{-4} cm^2 for liquid viscosity <0.002 kg/ms. Thus, the nozzle they studied produced a sheet which is <5 μm thick 3 cm from the orifice. For smaller injection pressure, the thickness parameter decreases as the surface tension is increased. Using the parameter K, Dombrowski et al. (1960) succeeded in developing a model to predict the liquid sheet edge.

Fraser et al. (1962) examined the behavior of flat water sheets produced by a set of fan nozzles showing thickness parameters ranging from 10×10^{-4} to 31×10^{-4} cm^2. The injection pressure was set equal to 0.17, 0.67 and 5 MPa. The objective in using high injection pressures was to identify the possible influence of liquid turbulence on the sheet behavior. The surrounding ambient conditions were varied in order to investigate the influence of the aerodynamic forces on the sheet behavior. The air density covered a range from subatmospheric to atmospheric condition ($\rho_G \in [0.05;\ 1.2$ kg/m$^3]$). Visualizations of the liquid sheet were performed by flash photography with a rear illumination and specular illumination configuration. Furthermore, drops were captured on a cavity slide filled with oil. The collected drops were recorded on a photomicrograph at a magnification of 8× and the drop-size distributions were measured from the photographic negative, projected on a screen to give a total magnification of 100×. Under atmospheric pressure, the sinuous mode of disintegration was always observed. As the air density was reduced, the sheet breakup length increased and the mode of disintegration changed from the sinuous to the perforating mode. Thus, the perforating mode of disintegration always takes place at a larger distance from the orifice than the sinuous mode. These observations lead to the conclusion that, as described by Hagerty and Shea (1955) stability theory, aerodynamic forces dominate the development of the sinuous mode of breakup. At atmospheric pressure, the characteristic time of this mode is smaller than the one of the perforation mode and the sinuous mode controls the sheet development before the appearance of the perforation in the sheet. At sufficiently small sub-atmospheric pressure, the characteristic time of the sinuous mode becomes greater than the one of the perforation mode. Therefore, the perforation mode manifests first. Although the perforation mode was operated on a thinner sheet, Fraser et al. (1962) found that the droplets produced by this mode were greater than those produced by the sinuous mode. This comes from the fact that the perforation disintegration mode goes through the reorganization of the liquid as ligaments before producing droplets (see Fig. 10). Thus, the mode of disintegration takes no benefit of the small sheet thickness. When working at high injection pressures, Fraser et al. (1962) observed that the turbulence in the liquid sheet played only a minor role and did not appear to assist the atomization process to any significant extent either in vacuum or in atmosphere. Fraser et al. (1962) suggested a model of the breakup of the sinuous sheet that assumed that the most rapidly growing wave is detached at the leading edge in the form of a ribbon half a wavelength wide. This ribbon immediately contracts into a ligament, which subsequently disintegrates into drops of equal diameter following a Rayleigh mechanism. This model made use of the optimum wavelength derived by Squire (1953) for the sheet (Eq. 10) and by Rayleigh (1878) for the ligament (Eq. 5). It led to a drop diameter scaling a liquid Weber number, based on a characteristic length of the liquid sheet, at the power of −1/3.

Crapper et al. (1973) published shadowgraph images of fan-nozzle liquid sheets on which perturbations of controlled frequency and amplitude were induced by vibrating the nozzle normal to the plane of the sheet. Front and side visualizations showed that contrary to what is assumed by the 2D linear theory, the wave growth is critically dependent upon the sheet velocity and the distance from the nozzle. When the sheet velocity is high, the wave grows until breakdown occurs. However, at lower velocity, the rate of growth is at first large but then rapidly diminishes until a maximum amplitude is reached after which the amplitude may actually diminish. The cause of this behavior was attributed to the nature of the air flow pattern around the sheet. Consequently, streamlines adjacent to the sheet were visualized using smoke tracers and a flash stroboscope synchronized with the vibrating system. These visualizations reported boundary-layer separation and the formation of gaseous vortex upstream each liquid crest that rapidly grows in size. The extent to which the vortex grows depends upon the operating condition. At high growth rate, the sheet breaks down rapidly and vortex growth is minimal. This shows that the gas dynamic induced by the liquid sheet influences the behavior of the liquid sheet.

Clark and Dombrowski (1974) and Dombrowski and Foumeny (1998) investigated the influence of the surrounding gas temperature on the sinuous Kelvin–Helmholtz instability. Clark and Dombrowski (1974) examined water sheets produced at different injection pressures ($\Delta P_i \in [0.17;\ 0.62$ MPa] and ambient temperatures (between 20 and 380°C). Their work was based on the analysis of shadowgraph images. At room temperature, the sinuous wave controlled the sheet disintegration. When the temperature increased, the wave motion was less pronounced due to a reduction of the gas density, i.e., to less effective aerodynamic forces. At higher temperature, an additional higher frequency wave covered the great part of the sheet and the disintegration occurred as a result of aerodynamic sinuous wave and random perforations. When

the temperature was further increased, the aerodynamic sinuous wave appeared only if the liquid sheet velocity was high, but the perforation mode dominated the liquid disintegration. Above this, the high frequency waves that appeared to be dilational waves were more visible. On the basis of the visualizations, Clark and Dombrowski (1974) suggested that the perforation mode of disintegration is electrohydrodynamic in origin and results from the accumulation of negative charge at the liquid surface. Dombrowski and Foumeny (1998) experimentally demonstrated that this electrohydrodynamic mechanism of disintegration requires surface disturbances to be initiated. These investigations show to which extend primary atomization mechanisms can be modified in hot atmospheres. This point is important to be considered in the production of sprays dedicated to combustion.

Contrary to fan-nozzle liquid sheets, liquid sheets formed by a normal impingement of cylindrical liquid jets follow a radial expansion and are not bounded by thick rims due to surface tension edge effect. Therefore, contraction of the sheet is never observed, even for low liquid velocity. Taylor (1959b, c) conducted early experimental investigations on the behavior of such sheets. The behavior of radial liquid sheets is categorized by representing the radial position r_b at which breakup occurs as a function of the liquid Weber number. (This approach is similar to the plot of the stability curve for cylindrical jets). The liquid Weber number is based on the cylindrical jet diameter d and velocity U_L. An example of this curve is shown in Fig. 11 where r_b is divided by the jet radius ($d/2$). This curve delimits two main breakup regimes. For low-Weber number, the liquid sheet is smooth and liquid beads are formed along the circular periphery and eventually detach from the sheet. (An illustration of this regime is shown in Fig. 12a). In this first breakup regime, r_b varies linearly with We_L. Beads come from Rayleigh instability. For high liquid Weber numbers, a large amplitude sinuous Kelvin–Helmholtz instability grows on the liquid sheet and causes its disintegration (see Fig. 12b). This second atomization regime is similar to the one observed on flat nozzle liquid sheet with sufficiently high liquid Weber number to prevent contraction.

Huang (1970) examined the behavior of water radial liquid sheets formed by the impingement of two co-axial cylindrical jets. The diameter of the impacting jets varied from 1.59 to 4.76 mm and the experiments covered a large liquid Weber number range ($We_L \in [100; 30{,}000]$). Huang took photographs of the sheet with short exposure time (between 1 and 3 μs) in order to measure the radial position of sheet breakup. He also performed high-speed camera visualizations (up to 6,000 images/s) to measure the wave speed of the Kelvin–Helmholtz instability. From these experiments, Huang (1970) determined criteria based on liquid Weber number to categorize the sheet behavior. The first regime of atomization was associated to liquid Weber number <500 (see Fig. 11). By assuming that the inward radial and circumferential surface forces balance the inertia force exerted radially outward on the edge of the circular sheet, Huang demonstrated that the radial position of breakup r_b should be proportional to the liquid Weber number. His experimental results confirmed this dependence and reported:

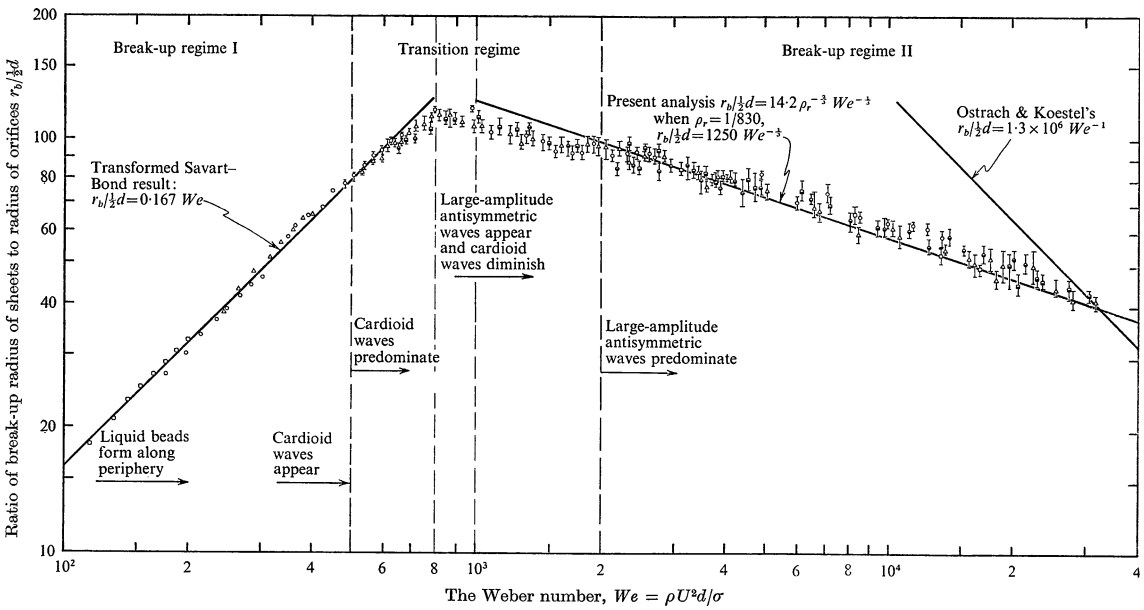

Fig. 11 Radial breakup position of a radial liquid sheet as a function of We_L (from Huang 1970)

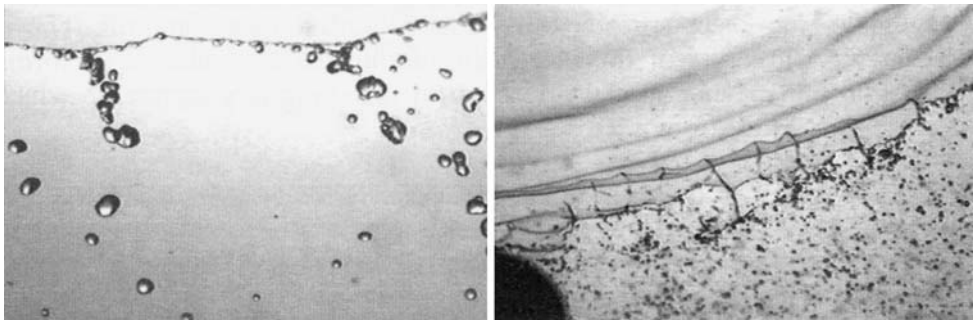

Fig. 12 Disintegration regimes of radial liquid sheet. *Left* smooth regime (regime 1), *right* flapping regime (regime 2) (from Clanet and Villermaux 2002)

$$\frac{r_b}{\frac{1}{2}d} = 0.167We_L \tag{11}$$

In this first atomization regime, the high-speed motion pictures revealed that the droplets are formed when the liquid beads merge to form larger beads, which eventually detach from the semi-cylindrical periphery. In the region of intermediate Weber numbers ($500 < We_L < 2{,}000$) Huang (1970) defined a transition regime (see Fig. 11) where Taylor's cardioid wave pattern appears in the first half of the region while the sheet begins to flap in the second half. Huang (1970) demonstrated that cardioid wave pattern was initiated by small amplitude disturbances at the impingement point. These waves modify the sheet periphery that becomes cusp-shaped. This, however, does not change significantly the drop production mechanism. In the transition regime, r_b shows a maximum at a critical liquid Weber number equal to 1,200. Kelvin–Helmholtz regime of instability was observed for liquid Weber number greater than 2,000. Huang proposed an analogy with the prediction of cylindrical jet breakup length (Eqs. 4, 5) to predict the sheet radial breakup position. By using the optimum wave characteristics obtained by Squire (1953) (Eq. 10), he found that the sheet radial breakup position should be proportional to $We_L{}^{-1/3}$. This correlation was confirmed by the measurements that reported:

$$\frac{r_b}{\frac{1}{2}d} = 1{,}250We_L^{-1/3} \tag{12}$$

By analyzing the high-speed visualizations, Huang (1970) reported an exponential growth of the wave amplitude along the radial direction and found wave propagation speed in agreement with the linear theory that accounts for the continuous decreasing thickness of the sheet in a limited range of Weber number only, namely, $We_L < 4{,}450$ only. Above this limit, non-linear effects are non-negligible.

Clanet and Villermaux (2002) and Villermaux and Clanet (2002) investigated the behavior of radial liquid sheet produced through the impact of a cylindrical liquid jet of diameter d on small circular disk. They used different disk diameters (from 3.8 to 20.8 mm) and jet diameters (from 0.8 to 5 mm) keeping constant the ratio between these two diameters (of the order of 4). Experiments were performed with water and ethanol and the all system of sheet formation could be immerged in a low-density ($\rho_G = 1.2$ kg/m^3) or a high-density ($\rho_G = 6$ kg/m^3) surrounding gas. The liquid Weber number varied from 80 to 30,000. Clanet and Villermaux performed visualizations of the liquid sheet with a short exposure photograph system and high-speed camera (up to 6,000 images/s). Clanet and Villermaux (2002) measured drop size from image analysis. They also reproduced Dombrowski et al. (1960) method based on light interference to measure the sheet thickness as a function of the radial distance from the impact, and determined the sheet velocity by following the motion of ash dusted on its surface. Villermaux and Clanet (2002) used a 2D laser-induced fluorescence (LIF) technique to investigate the shape of the liquid sheet along the radial direction. Clanet and Villermaux (2002) examined the behavior of the sheet in the first regime of atomization, whereas Villermaux and Clanet (2002) concentrated on the Kelvin–Helmholtz instability regime.

Measurements reported by Clanet and Villermaux (2002) showed that radial liquid sheets have similar characteristics as fan-nozzle sheets, namely, a constant velocity and a thickness $t_L(r)$ proportional to the inverse of the radial distance from the impact. They derived the following expression for the local thickness:

$$t_L(r) = \frac{d^2}{8r} \tag{13}$$

By measuring the value of r_b on mean images, they found that the first atomization regime is observed when $We_L < 1{,}200$. This value is of the order of the critical liquid Weber number reported by Huang (1970) as well as the sheet breakup radial position that was found to be

$$\frac{r_b}{\frac{1}{2}d} = 0.112We_L \tag{14}$$

The drop diameter was found to decrease as the liquid Weber number was increased and depended on the impacting jet diameter or not according to the situation: the

drop diameter scaled with the jet diameter d in the limit $d \ll (2\sigma/\rho_L g)^{1/2}$ or with $(2\sigma/\rho_L g)^{1/2}$ otherwise. Clanet and Villermaux (2002) explained that the beads at the origin of the drop formation grow and propagate on the periphery of the sheet. During their propagation, they are attached at the liquid film by capillary action and they are subject to both gravitational and centrifugal acceleration. When acceleration effect overcomes the attachment capillary force, drops detach. The thickness of the film that characterizes the strength of the attaching force imposes to the mean drop diameter a $We_L^{-1/3}$ dependence. In conclusion the drop diameter results from a local equilibrium between the local accelerations and the local attaching forces. This conclusion holds for any process involving drop production from smooth liquid sheet.

Villermaux and Clanet (2002) observed that the critical liquid Weber number to observe Kelvin–Helmholtz instability is a function of the surrounding density: for water sheet this number is equal to 1,000 when $\rho_G = 1.2$ kg/m^3 and decreases to 500 when $\rho_G = 6$ kg/m^3. In the first breakup regime, the evolution of the radial position of breakup with the liquid Weber number is independent of the gas density and follows Eq. (14). In the Kelvin–Helmholtz instability regime, whereas the decrease of the radial position of breakup begins for smaller liquid Weber number when the gas density is increased, it still scales with $We_L^{-1/3}$ as found by Huang (1970) (see Eq. 12).

By analyzing transverse cut of the liquid sheet using planar laser illumination, Villermaux and Clanet (2002) found that the amplitude growth of the most amplified wave was stronger than exponential because of continuous thinning of the liquid sheet. Furthermore, they measured the passage frequency of the wave crest and found it constant along the sheet. This frequency was found equal to $\left(\rho_G U_L^3/10\pi\sigma\right)$ when We_L ranged from 1,000 to 10,000. Another important finding reported by Villermaux and Clanet (2002) concerns the drop formation in the Kelvin–Helmholtz regime. Contrary to Fraser et al. (1962) suggestion, they observed that the liquid sheet does not break at each half wavelength to form ligaments, but drops are produced from the breakup of streamwise ligaments that develop at the sheet edge (see Fig. 12, right image). They analyzed these ligaments to result from Rayleigh–Taylor instability caused by the fact that the shear Kelvin–Helmholtz instability has a propagation velocity different than the liquid velocity and induces transient acceleration of the fluid particles. The wavelength of this instability scales with the surface tension and the resulting drop diameter is found proportional to We_L^{-1}. This dependence is different that the one reported by Fraser et al. (1962) who based their breakup model on a different mechanism.

The last type of liquid sheets presented in this section is that produced by compound nozzles commonly used in gasoline port-fuel injection (Zhao and Lai 1995). As explained above, these sheets result from the presence of a double swirl flow in the nozzle discharge orifice that promotes the expansion of the jet as a planar sheet. These sheets are not as thin as those produced by impaction or fan nozzles and report a different atomization process as shown in Fig. 13. As soon as the liquid issues from the nozzle, the sheet edges are perturbed by large wavelength disturbances as well as by much smaller ligaments. These ligaments that may produce very small drop near the nozzle exit, resemble to ligaments observed by Faeth and co-workers on turbulent jets (Fig. 5c). As going downstream, the liquid sheet deforms: first gulfs are created and second the sheet reorganizes as a ligament network prior to the disintegration. Many experimental and numerical investigations performed on the behavior of compound injector suggested that the liquid turbulence was the main factor controlling the atomization process (see the review due to Zhao and Lai 1995).

Dumouchel et al. (2005a) conducted an experimental investigation on a series of compound nozzles with a constant discharge orifice diameter ($d = 0.18$ mm) but different disk thicknesses and offsets of the discharge orifice. The experimental work consisted in taking shadowgraph images

Fig. 13 Disintegration process of liquid sheet produced by compound nozzle: water, $d = 180$ µm, $\Delta P_i = 0.35$ MPa, $We_G = 0.85$ (from Grout et al. 2007)

with a short duration light (11 ns) and a 6 Mpixels camera and to measure the drop-size distribution with a laser diffraction instrument. Furthermore, the internal flow was numerically simulated using a RNG k–ε model to calculate the turbulence. This work was performed with a substituting liquid whose physical properties are close to those of gasoline and with injection pressure ranging from 0.1 to 0.5 MPa. By measuring the issuing mean velocity as a function of the injection pressure, it was first noticed that the gaseous Weber numbers were always about <5. In this condition, the aerodynamic forces are expected to have no effect on the primary atomization process. Dumouchel et al. (2005a) found that the spray surface energy per unit liquid volume (σ/D_{32}) scaled with the sum of the non-axial and turbulent kinetic energies of the issuing flow and concluded to the importance of the double-swirl flow structure and of the turbulence on the atomization process. The double-swirl has two effects. As it increases, the radial expansion of the sheet increases and therefore its thickness is less, which promotes the production of small drops. At the same time, the turbulence intensity is increased due to an increase of the wall friction in the orifice nozzle. The increase of turbulence promotes a higher level of initial perturbation. When it is sufficiently high (for high injection pressure or low viscous liquid) the small ligaments near the nozzle exit are more numerous, smaller in size and may produce more small drops. But this early breakup mechanism always involves a very small amount of liquid. As going downstream, the liquid flow reorganization is controlled by surface tension forces as well as the disintegration of the ligament network. This scenario was confirmed by a fractal analysis of the atomizing liquid flow (Dumouchel 2005; Dumouchel et al. 2005b; Grout et al. 2007).

Shavit and Chigier (1995) were the first to apply a fractal analysis on atomizing liquid flow. They examined the case of co-axial cylindrical jets. Contrary to what is observed on low-velocity jets or smooth liquid sheets, there is no single dominant disturbance on the liquid surface: a wider range of perturbations, with different length-scales, deforms the interface that becomes very tortuous. The fractal analysis is a mean of quantifying this tortuosity. Dumouchel et al. (2005b) performed such an analysis on a high number of liquid flow images. They found that the local mean fractal dimension of the liquid interface correlated with the local interface length and observed that this fractal dimension increased with distance from the injector, reached a maximum and decreased. Shavit and Chigier (1995) reported a similar behavior. The maximum in fractal dimension was obtained where the flow reorganization occurred and indicated a decrease in the liquid interface caused by surface tension efforts. Grout et al. (2007) improved the fractal analysis by first determining the best appropriate method for their images. Then, they concentrated on two particular fractal dimensions: the textural fractal dimension of liquid sheet at the nozzle exit and the structural fractal dimension of the ligament network found in the final step of the primary atomization process. The textural dimension characterizes the interface tortuosity without accounting for the whole jet shape. This dimension was found to correlate with the Reynolds number of the issuing flow, confirming that the initial tortuosity of the liquid sheet is controlled by the liquid turbulence. The structural fractal dimension of the ligament network characterizes the shape of the whole flow. It was found that this dimension correlated with liquid Weber number of the flow confirming the dominant action of the surface tension forces in the flow reorganization. Furthermore, the smallest perturbation length-scale as a function of the distance from the nozzle can be also obtained from a fractal analysis. Grout et al. (2007) measured this scale as a function of the downstream distance and found that it correlated with a capillary characteristic length-scale. This shows that surface tension controls the disappearance of perturbations either by damping or breakup. Such an analysis is similar to the morphological analysis of jet breakup developed by Yon et al. (2004). It suggests that, as done for the modeling of turbulence, atomization could be described as a cascade of structures of different length-scales, the role of the viscosity in turbulence being played by surface tension in liquid atomization.

The investigations described in this section report several primary atomization processes of flat liquid sheets according to the way these sheets are produced. Liquid sheets produced by fan nozzle atomize thanks to the growth of Kelvin–Helmholtz instability provided that the sheet liquid Weber number is not too low. If this condition is not satisfied, the liquid sheet either contracts before atomizing if the difference of velocity with the surrounding gas is too low or disintegrates under perforations if the gas density is small (Dombrowski and co-workers). The minimum liquid Weber number, based on the sheet thickness, to trigger the Kelvin–Helmholtz instability is estimated to be equal to 2 by the linear theory (Eq. 9) but has not been quantified by experiments. Radial liquid sheets produced by jet impaction also report a primary atomization process triggered by Kelvin–Helmholtz instability. Here again, this type of instability is conditioned by a liquid Weber number, which is based this time on the diameter and velocity of the impacting jet(s). Under atmospheric condition, Huang (1970) and Clanet and Villermaux (2002) found that the minimum liquid Weber number to trigger Kelvin–Helmholtz instability is of the order of 1,000. If not, the liquid sheets disintegrate in large droplets at its periphery whose diameters are controlled by a balance between centrifugal

acceleration and surface tension forces (Clanet and Villermaux 2002). Villermaux and Clanet (2002) found, however, that the minimum liquid Weber number for the Kelvin–Helmholtz instability to develop is a function of the density of the surrounding gas: it decreases when the gas density increases. It appears therefore that a criterion for the onset of Kelvin–Helmholtz instability for flat sheets produced by fan nozzles or impaction should incorporate the gas density. By using the experimental results reported by Villermaux and Clanet (2002), the following criterion for the onset of Kelvin–Helmholtz instability can be derived for radial sheets:

$$We_L \left(\frac{\rho_G}{\rho_L}\right)^{0.5} > 42 \quad (15)$$

More experimental work should be conducted to confirm this suggestion that indicates that the onset of the Kelvin–Helmholtz instability depends on both fluid densities.

Beside the Kelvin–Helmholtz instability disintegration process, flat sheets produced by fan nozzles or by impaction present other similarities. They are initially smooth, have a constant velocity in the streamwise direction and a thickness inversely proportional to the distance from the nozzle or the impacting point (Dombrowski et al. 1960; Clanet and Villermaux 2002). This is likely due to the fact that these sheets result from a similar way of production. Indeed, the smooth sheet produced at the exit of a fan nozzle results from the impaction of streamlines at the nozzle orifice caused by its specific design. The impaction of streamlines in the nozzle orifice is not fundamentally different than the impaction of two jets or of one jet on a solid surface.

Two points of disagreement between the reported studies should be mentioned. One concerns the growth of the Kelvin–Helmholtz instability. Crapper et al. (1973) observed the rate of growth is at first large but then rapidly diminishes until a maximum amplitude is reached after which the amplitude may diminish. This was observed on a low liquid velocity. Huang (1970) reported that the rate of growth of the instability is exponential in time as predicted by the linear theory. On the other hand, Villermaux and Clanet (2002) found an amplitude wave growth stronger than exponential. Crapper et al. (1973) attributed their observations to the development and growth of vortex in the gas next to the sheet. Villermaux and Clanet (2002) explained that the strong growth is a consequence of the continuously thinning sheet. This interpretation is consistent with Eq. (10) that shows that the growth rate of the optimum perturbation could increase continuously when the sheet thickness decreases. On the other hand, one may wonder whether Crapper et al. (1973) observation could not be attributed to sheet contraction. Indeed, the decrease of the wave amplitude was observed on small velocity sheets only for which contraction could be suspected before the Kelvin–Helmholtz instability atomization is completed.

A second point of disagreement concerns the disintegration process and drop formation. Fraser et al. (1962) suggested that the sheet breaks at each half wavelength and produces ligaments that disintegrate under Rayleigh instability. However, Villermaux and Clanet (2002) observed that drops are produced from the disintegration of streamwise ligaments resulting from Rayleigh–Taylor instability. It has to be noticed that whereas Villermaux and Clanet (2002) images clearly show the presence of the streamwise ligaments during the drop production phase, the scenario proposed by Fraser et al. (1962) has never been clearly visualized.

Liquid sheets produced by the presence of a high transverse flow component in the nozzle discharge orifice show totally different behavior than the liquid sheet evoked so far. These sheets are not smooth and not as thin as those produced by fan nozzles or impacting jets. The atomization of these sheets does not require aerodynamic forces. The onset of the atomization is dominated by the intensity of the non-axial flow component and the turbulence intensity in the issuing liquid flow. The action of the surface tension forces dominates the evolution of the liquid system shape as well as the liquid flow disintegration. The interesting aspect here is that rather good atomization efficiencies can be reached even at low injection pressure. The difficult point, however, is that the atomization process is not as organized as for smooth liquid sheets and is characterized by ranges of perturbation length and time scales. Furthermore, the prediction of such process would require the internal flow to be characterized in detail, which is not an easy task. The coupling between simulations of the internal flow and shape analysis of the liquid flow using a fractal approach seems to be a promising direction to follow.

4 Air-assisted cylindrical jets

This section is dedicated to the behavior of a cylindrical liquid jet surrounded by an annular gaseous stream. In the literature, these jets are often called coaxial jets. The liquid jet issues from a cylindrical orifice (defined by a diameter d_L) and the air stream issues from a coaxial annular slit (defined by an internal outer diameter d_G). External mixing injector designs are considered only: both stream exits are co-planar and the gas and liquid flows enter in interaction with each other when leaving their respective nozzle. Each stream is characterized by its own average velocity noted U_L and U_G from the liquid and the gas, respectively. Furthermore, this section is also restricted to cases where both fluids are flowing in the same direction with no swirl component of velocity in the gas stream. (The effect of a swirl gas flow in

coaxial injection is detailed in Lasheras and Hopfinger (2000) and Dunand et al. (2005).)

Besides the non-dimensional numbers introduced for the liquid jet (see Eq. 1), other appropriate numbers can be defined namely, the gaseous Reynolds number Re_G, the effective Reynolds number Re_{eff}, the momentum flux mass ratio per unit volume M, the area ratio A', the mass flux ratio m and the relative gaseous Weber number We_R. Following Lasheras et al.'s notations (Lasheras et al. 1998), these numbers are given by

$$\begin{cases} \mathrm{Re}_G = \frac{\rho_G U_G d_G}{\mu_G} & \mathrm{Re}_{eff} = \mathrm{Re}_G\left[1 - \frac{d_L^2}{d_G^2} + \frac{d_L^2}{M d_G^2}\right] & M = \frac{\rho_G U_G^2}{\rho_L U_L^2} \\ A' = \frac{A_G}{A_L} & m = \frac{\rho_L U_L A_L}{\rho_G U_G A_G} & We_R = \frac{\rho_G (U_G - U_L)^2 d_L}{\sigma} \end{cases} \quad (16)$$

where ρ_G is the gas density; μ_G, the gas dynamic viscosity; A_L and A_G, the area of the liquid and gas flow outlets, respectively. The effective Reynolds number Re_{eff} characterizes the total flow (gas + liquid) in the jet (Lasheras et al. 1998).

Chigier and co-workers reported a series of experimental investigations on the behavior of coaxial air–water jets (Farago and Chigier 1990, 1992; Eroglu et al. 1991; Eroglu and Chigier 1991a, b). The liquid flow nozzle diameter was of the order of 1 mm and its length was equal to 55 mm. The internal outer diameter of the surrounding airflow was of the order of 10 mm. Their experimental arrangement covered the following ranges of non-dimensional numbers: $Re_L \in [200; 20{,}000]$, $Re_G \in [13{,}000; 104{,}000]$, $We_R \in [0.001; 600]$). Shadowgraph images were taken with a 0.5 μs light source. From an analysis of over 1,000 images, Farago and Chigier (1992) proposed a morphological classification of disintegrating coaxial air–water jets. Three atomization regimes were identified: the Rayleigh-type breakup, the membrane-type breakup and the fiber-type breakup.

The Rayleigh-type breakup is identified when drops are produced without any liquid membrane or ligament shedding from the liquid flow. Drop diameters are of the order of the jet diameter. This regime can be divided in two subregimes called axisymmetric and non-axisymmetric. In the axisymmetric subregime ($We_R < 15$) the gas flow accelerates the liquid jet that shows shorter breakup length than in still gaseous environment and drops result from the growth of an axisymmetric sinusoidal wave. In the non-axisymmetric subregime ($15 < We_R < 25$), the gas flow reduces the liquid jet diameter and drops are still produced by the breakup of the flow as a whole. At low We_R, the liquid jet can show a hook-like shape as illustrated in Fig. 14a. For higher We_R, the liquid jet is straighter.

The membrane-type breakup ($25 < We_R < 70$, Fig. 14b) is characterized by the development of thin liquid sheets, which form Kelvin–Helmholtz waves and break into droplets of much smaller diameter than in the previous regime. The morphology of the jet becomes similar to that of a thin liquid sheet.

The fiber-type regime ($100 < We_R < 500$, Fig. 14c) is identified as the formation of thin liquid fibers that peel off the jet and disintegrate by a non-axisymmetric Rayleigh-type breakup. Farther downstream, the main liquid core becomes wavy and breaks into ligaments from which new fibers are peeled off. The diameters of the drops are very small and generally increase with the downstream distance. In this mode, most of the liquid proportion is atomized in the second atomization region. Farago and Chigier (1992) divided this regime in two sub-modes: pulsating and superpulsating modes. The pulsating mode is the normal mode of atomization whereas the superpulsating mode ($150 < We_R < 500$) is connected to an extremely high periodical change between low and high-density regions in the sprays. An illustration of this sub-mode is given in Fig. 14d. Farago and Chigier (1992) observed a dominance of the superpulsating mode when

$$\mathrm{Re}_L / We_R^{0.5} < 100 \quad (17)$$

Farago and Chigier (1992) succeeded in classifying these breakup regimes in a We_R–Re_L map.

The most commonly quantified coaxial jet characteristic is the liquid core length L_C. In the Rayleigh breakup regime, this length is equivalent of the breakup length of atomizing cylindrical jets. In the membrane-type regime, the liquid core length is equivalent in the liquid jet intact length. In the fiber-type regime, two characteristic lengths are defined (Porcheron et al. 2002). In the near-field region, the liquid flow is divided in two regions; the potential liquid core and the liquid core. Attached to the nozzle, the potential liquid core is a continuous liquid structure without gas inclusions. The length of the potential liquid core is noted as L_{PC}. Farther downstream, the liquid core is composed of liquid structures with gas inclusions. Its length is noted as L_C.

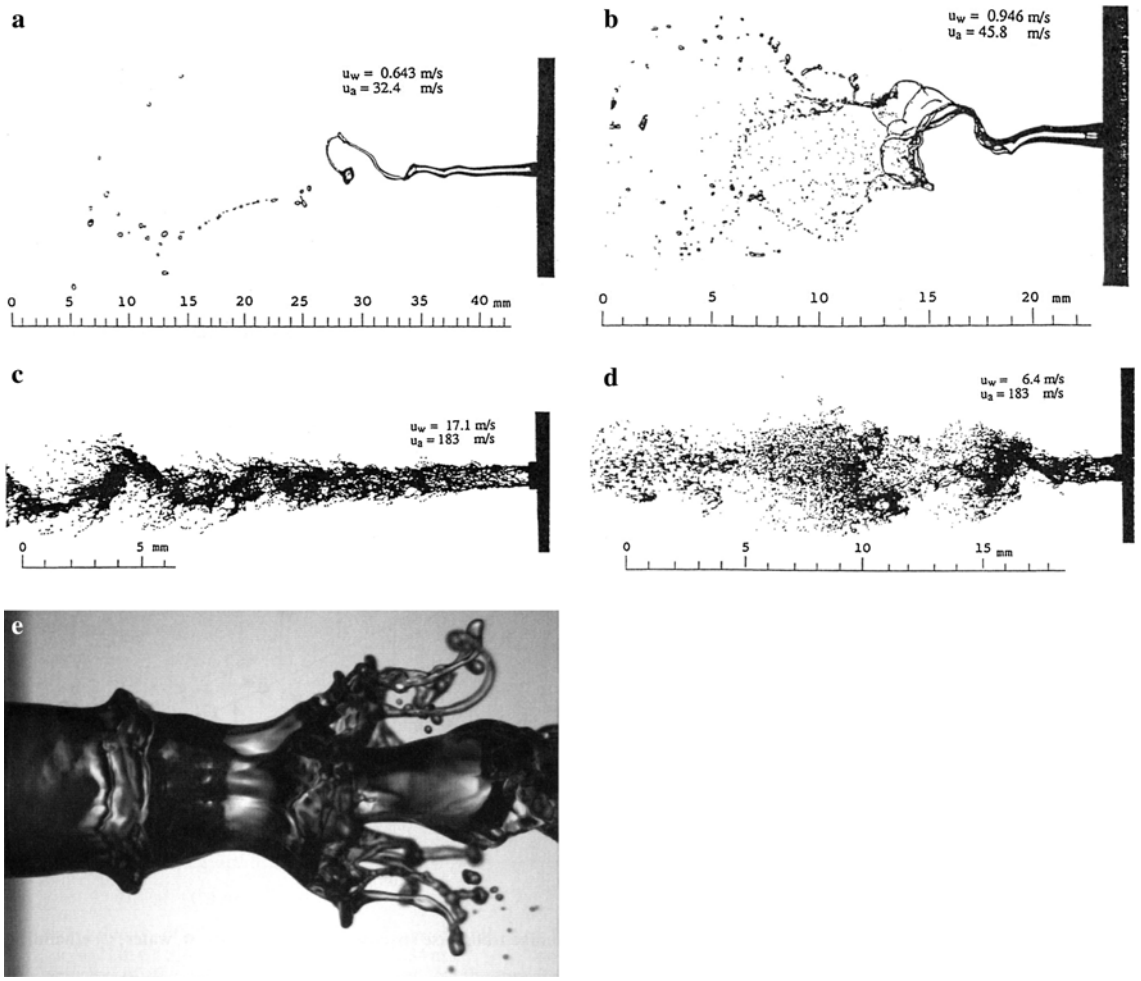

Fig. 14 Air-assisted cylindrical jet atomization regimes. **a** Non-axisymmetric Rayleigh regime, **b** membrane-type regime, **c** fiber-type regime, **d** superpulsating submode, **e** digitations regime (**a–d** from Farago and Chigier (1992), **e** from Marmottant and Villermaux (2004))

Eroglu et al. (1991) measured the liquid jet intact length on the instantaneous shadowgraph images used for the classification: the length they measured was likely the liquid core length. Their measurements were performed in the membrane-type and fiber-type regimes. For each operating conditions, four to seven photographs were analyzed and average lengths were calculated. More than 1,500 photographs were analyzed to yield the correlation given in Table 2. This correlation shows a continuously decreasing liquid core length when the gaseous relative Weber number increases or when the liquid Reynolds number decreases.

In subsequent studies, Eroglu and Chigier (1991a, b) measured the perturbation wavelength on the liquid–gas interface as well as the wave frequencies. The wavelengths were measured in the visualizations. Wave frequencies were measured by a laser beam attenuation technique. This technique consists in positioning a collimated laser beam near the liquid–gas interface and perpendicular to the jet axis and to record the temporal beam attenuation due to the liquid flow undulation. Frequency of the jet undulation is obtained by performing a FFT of the temporal signal. The measurements were conducted for coaxial jets showing the three possible atomization regimes ($Re_L \in [1.4;\ 17{,}650]$, $We_R \in [13;\ 267]$). The liquid flow transition from laminar to turbulent occurred when $5{,}000 < Re_L < 10{,}000$ and the airflow test conditions corresponded only to turbulent flows. Eroglu and Chigier (1991a, b) observed two wave types. At low liquid velocities, the dominant wave was sinuous and became dilational at high liquid velocities. For

Table 2 Correlations for the characteristic length of air-assisted liquid jets

Eroglu et al. (1991)	$\frac{L_C}{d_L} = 0.66 We_R^{-0.4} Re_L^{0.6}$
Woodward et al. (1994)	$\frac{L_C}{d_L} = 0.095 \left(\frac{\rho_G}{\rho_L}\right)^{-0.36/Z} We_R^{-0.22/Z} Re_L^{0.68}$
Lasheras et al. (1998)	$\frac{L_{PC}}{d_L} = \frac{6}{\sqrt{M}}$
Porcheron et al. (2002)	$\frac{L_C}{d_L} = 2.85 \left(\frac{\rho_G}{\rho_L}\right)^{-0.38} Oh^{0.34} M^{-0.13}$
Leroux et al. (2007)	$\frac{L_C}{d_L} = \frac{10}{M^{0.3}}$

L_C liquid core length, L_{PC} potential core length

intermediate liquid velocities, the initial disturbances were of the dilational type and sinuous wave formation started further downstream. They noted that the wavelength increased with the downstream distance and analyzed spatially averaged wavelength. This mean wavelength increased with the gas velocity. For an increasing liquid velocity, it first increased, reached a maximum and then decreased towards a constant value when the liquid flow is fully turbulent. Furthermore these wavelengths were found smaller than the jet perimeter. Eroglu and Chigier (1991a, b) concluded that the onset of these perturbations is controlled by the liquid turbulence and that their growth is dominated by the aerodynamic interaction. Frequencies appeared independent of the axial location and the frequency band increased with the liquid velocity. Furthermore, the average frequency was found to increase with both the liquid and the gas velocities. However, having performed spatial average for the wavelength and frequency, the reported behavior is global and not easily analyzable.

Woodward et al. (1994) investigated the behavior of water jets surrounded by an annulus gas flow. The diameter d_L of the inner flow was equal to 4.8 mm and the nozzle area ratio was $A' = 2.5$. The gas used for the annular flow was either nitrogen or helium and the ambient pressure varied from 0.1 to 2.1 MPa. The operating conditions covered two liquid Reynolds numbers (95,000 and 160,000) and relative gaseous Weber number ranging from 14 to 32,000. Woodward et al. (1994) used a line-of-sight technique based on the analysis of X-ray transmitted intensity through the issuing two-phase flow in the near-filed region to measure the jet liquid core length. Images of the optical signal were recorded with a CCD camera at a rate of 60 images/s. The liquid core lengths were measured from image processing. Woodward et al. (1994) found that the liquid core lengths were functions of the ambient pressure, the gas density and both liquid and gas velocities. Unexpected behavior was observed. For $Re_L = 95{,}000$ and $P_{amb} = 0.1$ MPa, very short liquid core lengths were measured and were independent of the gaseous flow velocity. Furthermore, when the ambient pressure was increased, the liquid core increased, reached a maximum and then decreased. The maximum was found for an ambient pressure of 0.5 MPa whatever the gas velocity. For $Re_L = 160{,}000$, a similar behavior was obtained except that the liquid core length was found to increase from $P_{amb} \approx 1$ MPa only. For smaller ambient pressures, the liquid core length was short and independent of both the ambient pressure and the gas velocity. These results show that at low ambient pressures, aerodynamic forces were not the dominant factor to trigger the primary atomization. Woodward et al. (1994) suggested that the difference in the injector internal flow conditions associated with low versus high ambient pressures were responsible for this behavior and that cavitation occurred inside the injector at low P_{amb} and caused large disturbances in the liquid jet. They concluded in the presence of two jet breakup mechanisms whose relative effects depend on the ambient conditions, namely, cavitation-induced turbulence and aerodynamic shear, the first effect being dominant at low ambient pressure. Woodward et al. (1994) derived a correlation for the liquid core length (Table 2). In this correlation, the parameter Z integrates the ratio of the fluid specific heats and the gas-specific constant. This parameter is essentially the ratio of the acoustic velocity of the liquid to that of nitrogen and implies a Mach number effect on coaxial jet breakup. Although the correlation proposed by Woodward et al. (1994) was obtained for different operating conditions than the one obtained by Eroglu et al. (1991), note the similar dependence in Re_L.

Attempts of other types of analysis have been carried out on atomizing coaxial jet. Shavit and Chigier (1995) applied a fractal analysis on the liquid jet. The injector and fluids were the same as used by Farago and Chigier (1990, 1992), Eroglu et al. (1991) and Eroglu and Chigier (1991a, b). Their working conditions covered the ranges $Re_L \in [1{,}120; 6{,}000]$ and $We_R \in [12; 120]$. This was the first attempt in analyzing the liquid primary atomization process using the concept of morphological characterization. As explained in the previous section, a fractal analysis is a mean of quantifying the interface tortuosity caused by perturbations covering a wide range of characteristic length-scales. This description does not attribute a single characteristic length-scale to a poly-perturbed system. Such an approach requires accurate visualizations with a rather high magnification. The shadowgraph images taken by Shavit and Chigier (1995) covered a 3.1×2.3 mm^2 area with a spatial resolution of 4.81 μm/pixel. The visualization area was translated from the nozzle exit to a downstream position where the atomization process was completed. At each position, a fractal dimension could be obtained. Shavit and Chigier (1995) related the fractal nature of the atomization process to the major impact of the turbulent airflow. The fractal dimension increased with the downstream position, reached a maximum and then decreased, illustrating an increase of the liquid tortuosity followed by a reorganization of the flow where tortuosity progressively disappears. Shavit and Chigier noticed that the position at which the fractal dimension was a maximum corresponded to the region where breakup became effective. A fractal analysis can also give information on the spectrum of length-scales characterizing the system. Shavit and Chigier (1995) showed that the spray drop-size distribution range was bounded within the spectrum of length-scales before

breakup. They suggested that a possible course of analysis would be to predict the shape and dynamics of the liquid–gas interface and subsequently to predict the drop size and velocity. Their work offers an interesting alternative to quantify and, maybe, categorize liquid atomization processes.

Lasheras et al. (1998) investigated the behavior of water jets assisted by coaxial annular air stream. The nozzle diameter of the liquid jet was $d_L = 3.8$ mm, and its length was equal to 110 mm. The outer internal nozzle diameter of the annular air jet was $d_G = 5.6$ mm and its length was equal to 28 mm. The operating conditions covered the following ranges: $Re_L \in [570; 5{,}700]$ and $We_R \in [16; 4{,}000]$. In these conditions, the airflow was always turbulent and the liquid flow could be laminar or turbulent. Several experimental diagnostics were used to investigate the near-field region. The liquid shedding frequency was measured one diameter d_L downstream of the nozzle using an attenuation beam technique similar to the one used by Eroglu and Chigier (1991a, b). Instantaneous shadowgraph images were taken at a framing rate of 1/30 s and a shutter speed $<10^{-4}$ s. High-speed films (1,000–6,000 frames/s) were also captured in this region to measure the acceleration of the liquid by the gas flow. Lasheras et al. (1998) mainly concentrated on the behavior of coaxial jets in the membrane-type and fiber-type regimes. They observed the fiber-type breakup regime for $We_R > 200$ which is greater than the limit reported by Farago and Chigier (1992). Furthermore, Lasheras et al. (1998) reported a breakup regime that was not described by Farago and Chigier (1992), namely, the digitations-type breakup regime. This regime, also reported by other studies (Lasheras and Hopfinger 2000; Marmottant and Villermaux 2004), shows the development of digitations (ligaments) on the crests of an axisymmetric perturbation and the subsequent disintegration of these ligaments by a non-axisymmetric Rayleigh-type regime (it is illustrated in Fig. 14e). According to Lasheras and Hopfinger (2000), the digitations-type breakup regime lies in the membrane-type breakup regime of Farago and Chigier's classification. Lasheras et al. (1998) observed this digitations-type breakup regime for turbulent gaseous flow and laminar liquid flow. Farago and Chigier (1992) worked in such operating conditions but their injector design showed two major differences compared to the one used by Lasheras et al. (1998). First, the diameter of the liquid orifice was less ($d_L = 1$ mm) compared to the one used by Lasheras et al. ($d_L = 3.8$ mm). Second, the gas to liquid diameter ratio that was of the order of 10 for Farago and Chigier (1992) and <1.5 for Lasheras et al. (1998). It seems therefore that geometrical details of the injector design influence the atomization regimes and their classification.

Lasheras et al. (1998) found that the shedding frequency of the initial shear instability increased with the gas velocity but at a rate that depended on the liquid velocity. This behavior was demonstrated to be due to the nature of the liquid flow: when the liquid flow was laminar, the frequency scaled as the square of the gas velocity and when the liquid flow was turbulent, the frequency was directly proportional to the gas velocity. This shows an influence of the nature of the liquid flow on the dynamic of the initial shear instability. Other investigations led to a similar conclusion (Eroglu and Chigier 1991a, b; Mayer and Branam 2004).

Lasheras et al. (1998) produced a correlation for the liquid potential core length based on a model that accounted for the domination of the annular flow in the near-field region as evidenced by previous investigations (Dahm et al. 1992; Rehab et al. 1997). Although these two experimental investigations concerned single-phase coaxial jets, it is worth to mention them at this stage. The near-field flow is of paramount importance for the onset of instability and primary breakup of coaxial air–liquid jets. However, no experimental investigation has provided clear visualizations of this region. Dahm et al. (1992) and Rehab et al. (1997) performed visualizations of single-phase coaxial water jets in order to provide qualitative information on the structure of the near-field flow. Both groups used LIF tomography visualization. Dahm et al. (1992) used a two-color planar LIF to follow the two interfaces each stream being seeded by a different dye. Still and 60 image/s visualizations were performed. The nozzle was profiled with convergent for both inner and outer flows in order to avoid development of Görter vortices in the boundary layers and to promote the injection of laminar flows. Rehab et al. (1997) used a single color planar LIF and the inner and outer flows were alternatively seeded. A CCD 50 frames/s camera was used and a spatial resolution of 300 μm/pixel was achieved. As in Dahm et al. (1992), convergent parts were profiled in the nozzle for the inner and outer flow. The images in these references are of very good quality and show important qualitative information. They show that the boundary layer in the inner flow and the two boundary layers in the outer flow (one along the internal wall, one along the external wall) give rise to the development of two mixing layers at the nozzle exit, one between the two flows and a second one between the outer flow and the surrounding medium. Dahm et al. (1992) observed a wide variety of near-field vortex patterns with different interaction dynamics, which depend both on the velocity ratio and on the absolute velocities of the two streams. In addition, the boundary-layer thicknesses and wake defect in each layer must be accounted for understanding the complex near-field flow structures and dynamics that control the potential core length of the liquid flow. Rehab et al. (1997) reported

that the annular jet dominates the near-field structure. The outer mixing layer pinches the central jet at the end of the inner potential core whose length decreases when the ratio U_G/U_L increases (U_G stands here for the annular flow velocity). Furthermore, beyond a certain value of U_G/U_L the outer jet fluid begins to penetrate upstream on the inner jet axis. This recirculation flow truncates the inner flow and oscillates at a low frequency (proportional to U_G) and with large amplitude. This demonstrated the dominance of the outer flow on the inner flow length. In two-phase condition, Lasheras et al. (1998) explained the truncation of the inner flow by the outer flow as follows. The high-velocity airflow caused local reduced pressures and induced a recirculation in the central region. This recirculation may still occur when the liquid flow rate is less than the rate at which the air stream can entrain water. In this condition, the liquid flow is truncated by a gas cavity, the oscillation of which leads to the superpulsating mode. If the liquid flow rate is high enough to fill the cavity, the external mixing layer pinches the liquid flow farther downstream. They concluded that the length of the liquid flow is mainly controlled by the momentum flux ratio M and derived the correlation given in Table 2 for the potential core length L_{PC} of the jet. Above a critical value of M, of the order of 35, the liquid flow is chopped off and the superpulsating mode is reached. This momentum flux ratio critical value can be compared with Farago and Chigier (1992) criteria for the onset of the superpulsating mode (Eq. 17). Farago and Chigier (1992) worked with water and a liquid nozzle diameter equal to 1 mm. Furthermore, considering that in the superpulsating mode $U_L \ll U_G$, Eq. (17) can be rewritten as $M > 7$. This value is smaller than the one reported by Lasheras et al. (1998). This might be a consequence of the differences in the nozzle design between these two investigations as mentioned earlier.

The experimental investigation of Hardalupas et al. (1998) reported liquid core length measurements of air–water coaxial jets produced by nozzles with different orifice diameters ($d_L = 1.2$ and 2.3 mm; $d_G = 9$, 15 and 23 mm). The flow conditions covered a range of relative gaseous Weber number from 3 to 2,300, liquid Reynolds number from 3,500 to 45,000 and momentum flux ratio from 0.1 to 10. Shadowgraph images were taken with a high-speed camera (1,000 frames/s). No images were presented in the paper but Hardalupas et al. (1998) explained that the jet broke up into liquid clusters produced at a near-uniform frequency. This description seems to correspond to the pulsating and superpulsating modes of the fiber-type regime. A mean liquid core length was measured over 2,000 photographs for each flow condition. These measurements showed that the liquid core length L_C was always proportional to $(1 + M^{-0.5})$. This dependence is very similar to the one suggested by Lasheras et al. (1998) and one of the conclusions of Hardalupas et al. (1998) is that the momentum flux ratio is the appropriate parameter to characterize the liquid core length. Furthermore, their experimental results revealed that the coefficient of proportionality between L_C and $(1 + M^{-0.5})$ was a function of the diameters d_G and d_L with a greater dependence with the latter.

In a review article dedicated to liquid jet instability in coaxial gas stream, Lasheras and Hopfinger (2000) pointed out that the classification of coaxial jet atomization regimes could not be based on the relative gaseous Weber number and the liquid Reynolds number only as attempted by Farago and Chigier (1992) but should also consider the momentum flux ratio. However, they deplored a lack of experimental data to give precise location of the different regime boundaries. As far as the near-field region is concerned, Lasheras and Hopfinger (2000) emphasized the role of the boundary layers present in the two-phase flow on the onset of primary breakup mechanism in the membrane-type and fiber-type regimes. (As mentioned earlier, qualitative visualizations of these boundary layers are available in Dahm et al. (1992) and Rehab et al. (1997).) Lasheras and Hopfinger (2000) explained that the gas vorticity is responsible for the development on the liquid interface of an instability characterized by a long wavelength that scales with the gaseous boundary-layer thickness. For larger gas velocities, a second instability, with shorter wavelength and driven by the liquid vorticity layer, co-exists. In the membrane-breakup regime, the liquid is drawn out into sheets when the interfacial waves are amplified and the development of these sheets may be accompanied by spanwise perturbations at the sheet rims. Atomization of these structures occurs when the surface tension forces become of the order of the aerodynamic forces. Thus, in the membrane-type regime, the surface tension is not accounted in the onset of instability but is taken into account in the drop formation. However, in the fiber-type regime, surface tension is believed to be unimportant on the instability onset as well as on the primary drop diameter. The size of the fibers may scale with the streamwise vortices of the interfacial gas shear layer. Lasheras and Hopfinger (2000) pointed out experimental results from the literature that evidenced the existence of these two regimes in terms of primary droplet sizes.

The investigation of the breakup regimes at low We_R (Rayleigh-type and lower part of membrane-type) has not aroused a noticeable interest compared to the membrane-type and the fiber-type regimes. One should, however, mention the experimental investigation due to Shavit (2001), which concentrated on the Rayleigh-type regime addressing the question of whether the breakup occurs due

to convective or absolute instability. Shavit (2001) defined these two types of instability according to the role of air turbulence on the liquid jet motion. For Shavit (2001) absolute instability is characterized by a dominant role of the dynamic motion of the gas flow structures on the liquid jet motion and breakup. On the other hand, when the air turbulence has a limited influence on the liquid jet behavior, the instability is convective and the initial disturbance may prove to be important. Shavit (2001) used an injector allowing the air turbulence to be controlled independently of the mean gas velocity or the gas Reynolds number. No details on the coaxial injector were given. Air and water were used and the flow conditions were $U_L = 1$ m/s and $U_G = 27$ m/s and an air turbulence intensity that varied from 10 to 24%. Shavit (2001) reported shadowgraph images of the jet and seeded the air stream by 3 μm particles in order to investigate the gas velocity field thanks to the use of a two-component laser Doppler velocimeter. It was observed that the sole increase in gas turbulence emphasized the lateral motion of the liquid jet and could favor the passage from axisymmetric Rayleigh-type to non-axisymmetric Rayleigh-type regime with overturning of the liquid jet. However, it was found that the low-density gas flow did not impose its dynamics on the liquid jet. In the breakup region, the motion of the liquid jet dominated temporal interactions between the liquid and the air. The liquid flow served as a major source for air turbulence, caused drastic increase in the air integral time scales and broke the self-similarity of the free turbulent airflow. Thus, the airflow in the breakup region was influenced by the liquid flow much more than the liquid flow was influenced by the airflow. Shavit (2001) concluded that the major influence of air turbulence was to generate an initial disturbance at the nozzle exit and that this initial disturbance increased with the air turbulence intensity. However, in the breakup zone, the liquid jet behavior is not very sensitive to the degree of air turbulence. This shows that in this low-Weber regime, the liquid breakup is not due to absolute instability according to Shavit's (2001) definition.

Porcheron et al. (2002) conducted an experimental investigation on the structure of the flow in the near-field region using an optical fiber probe measurement technique. An optical fiber probe leads the photodiode-modulated infrared light to its sapphire tip that has a sensitive cross-sectional area of 90 μm in diameter. At the tip, the light is either reflected internally or refracted outside according to the refractive index of the fluid in contact with the sensitive part of the probe. The resulting temporal signal shows two levels corresponding to the detection of liquid or gas. The analysis of this signal reports the liquid presence probability (LPP). The interesting aspect of this diagnostic is that it allows the potential liquid core length L_{PC} and the liquid core length L_C to be measured. L_{PC} is defined by the farthest downstream position where LPP = 1, and L_C is defined as the distance at which LPP = 0.5. Furthermore, considering the small section of the probe, local measurements can be performed and LPP map can be plotted. Porcheron et al. (2002) conducted measurements on liquid oxygen jets ($d_L = 5$ mm, $U_L = 2$ m/s) assisted by helium ($We_R = 14{,}000$), nitrogen ($We_R = 12{,}000$) or argon ($We_R = 12{,}300$) annular flow ($d_G = 16$ mm) and on water jets assisted by air or argon ($d_L = 2.1$ mm, $d_G = 7$ mm, $We_R = 730$). The injection conditions placed the jets in the fiber-type breakup regime. The results showed that the liquid core length was not dependent on the parameter M only but was also a function of the gaseous density. At constant U_L and M, they reported an intensification of the primary breakup mechanism identified by a reduction of L_C in both the radial and axial directions when the gas density increased. By performing PDPA measurements in the gaseous phase, they found that the axial velocity decrease along the jet axis was steeper when the gas density diminishes. Furthermore, for a given liquid velocity, the gas velocity near the liquid phase in the bottom part of the liquid core was constant whatever the initial gas velocity. The correlation obtained from these results for L_C (Table 2) shows a dependence in ρ_G similar to the one proposed by Lasheras et al. (1998) but a far less influence of the gas velocity. Furthermore, Porcheron et al. (2002) correlation suggests a weak influence of the surface tension on the length of the liquid core even in the fiber-type regime.

Mayer and Branam (2004) conducted an experimental investigation on ethanol liquid jet assisted by an annular nitrogen flow. The geometrical characteristics of the injector were $d_L = 2.2$ mm and $d_G = 10$ mm, and both fluid channels showed a constant section over 90 mm. Operating conditions covered three liquid Reynolds numbers, namely, 3,000, 7,500 and 30,000. The ambient pressure varied from 0.1 to 6.5 MPa and the relative gaseous Weber number ranged from 0 to 69,000. Mayer and Branam (2004) took shadowgraph images with 20 ns flashlight. For each operating condition, 30–60 images were analyzed to determine the amplitude and the wavelength that developed on the liquid–gas interface. The field of visualization was limited and did not permit the measurement of liquid core length. As far the jet breakup mechanisms were concerned, Mayer and Branam (2004) observed the atomization regimes identified by Farago and Chigier (1992). They found a criterion for the superpulsating regime identical to the one established by Farago and Chigier (1992) (Eq. 17) but with an exponent for the relative gaseous Weber number equal to −0.4 instead of −0.5. Furthermore, they pointed out that, contrary to

Farago and Chigier's observations, the fiber-type regime could be observed at very small We_R provided that the liquid Reynolds number is high enough (>20,000). They explained that Farago and Chigier did not observe this because they did not explore Reynolds number >20,000. A look at Mayer and Branam's visualizations indicates, however, a confusion in the definition of the atomization regime. What they identified as fiber-type regime at low We_R was the atomization regime of non air-assisted cylindrical liquid jets (region E in Figs. 1, 5c). In the coaxial jets breakup mechanism classification reported by Lasheras and Hopfinger (2000), this regime is clearly identified as the atomization regime and not as fiber-type regime, this latter being related to the production of fiber in the streamwise direction due to high interactions between the liquid and the gas. Mayer and Branam (2004) investigated the influence of the liquid velocity, the relative velocity and the ambient pressure independently. In their analysis, they systematically associated the role of the liquid velocity to the one of liquid turbulence and the role of the relative velocity and ambient pressure to the one of aerodynamic forces. Thus, the evolution of the wavelength and amplitude of the interface perturbation as a function of these three parameters led them to conclude that, while aerodynamic forces (relative velocity and ambient pressure) definitely have a significant effect on the jet surface disturbances, initiation tends to be caused by the internal liquid flow structures. Mayer and Branam (2004) also observed that the jet behavior depended on the sign of the relative velocity between the liquid and the gas and not on the absolute value of this velocity difference only. For instance, for a constant We_R, they noticed a reduction of the spray angle if $(U_G - U_L) > 0$ compared to the case where this difference is negative. From this observation, Mayer and Branam (2004) concluded that injector performances could not simply be described by scalar geometrical and operational injection parameters (such as We_R, Re_L or Oh) but should include injection direction of the fluid flows with each other. A different conclusion could be drawn from this point: it emphasizes the importance of the momentum flux ratio M in the behavior of coaxial jets. Mayer and Branam (2004) did not take this parameter into account in their analysis.

Marmottant and Villermaux (2004) conducted an experimental investigation on the digitations-type breakup regime (Fig. 14e). The characteristics of the nozzle were $d_L = 7.8$ mm and $d_G = 11.2$ mm. Furthermore, both gas and liquid nozzles were profiled in order to reduce as much as possible turbulence in the flows. Several liquids were used, namely, water, ethanol and mixture of water–glycerol, and the annular co-flowing gas was air. The velocity-profile of the airflow was measured with standard hot-wire anemometry in order to measure the boundary-layer thickness in the gas stream. Liquid and gas mean velocities were varied from 0.45 and 1.69 m/s and from 2.1 to 90 m/s, respectively. Shadowgraph images were taken by two techniques. For length and displacement measurements, a high-resolution camera was mounted in combination with a couple of 5 μs flash lamps. To follow the entire evolution of the motion, a high-speed camera (4,500 images/s) was used. Wavelengths of the liquid jet undulations and droplet sizes were measured on the still images. Finally, frequency of the jet undulation was also measured using a beam attenuation technique already mentioned in previous investigations (Eroglu and Chigier 1991a, b; Lasheras et al. 1998). The anemometry measurements reported that the air boundary-layer thickness, defined as the vorticity thickness δ, scaled as the inverse of the square root of a gaseous Reynolds number based on the width of the annular gaseous flow. When the gas velocity was <20 m/s, the visualizations reported the growth of an axisymmetric instability whose wavelength was a function of the air velocity; it is therefore distinct than the capillary instability. The frequency of this instability (measured at 1 d_L from the nozzle) scaled with $U_G^{3/2}$. (This dependence is different than the one reported by Lasheras et al. (1998).) Above a critical gas velocity ($U_G > 20$ m/s), the undulations were no longer axisymmetric and displayed transverse azimuthal modulations. These modulations grew in amplitude, formed ligaments that eventually disintegrated. The number of transverse undulations was found to increase with the air velocity. By examining the axial velocity of the initial shear instability, the evolution of the length and diameter of the ligaments and the resulting drop sizes, Marmottant and Villermaux (2004) detailed the digitations-type breakup regime as follows.

The formation of the initial axisymmetric wave on the liquid is due to shear instability of the Kelvin–Helmholtz type. The optimum wave number of this instability depends on whether the gaseous vorticity layer is thin or thick. Marmottant and Villermaux established a criterion to segregate these two situations. It is based on the value of relative Weber number $We_{R\delta}$ based on the vorticity thickness. They derived the following expression for the optimum wave number:

$$\begin{cases} \text{Thin vorticity layer: } We_{R\delta} < \left(\frac{\rho_G}{\rho_L}\right)^{1/2} \Rightarrow k_{opt} = \frac{2\rho_G U_G^2}{3\sigma} \\ \text{Thick vorticity layer: } We_{R\delta} > \left(\frac{\rho_G}{\rho_L}\right)^{1/2} \Rightarrow k_{opt} \approx 1.5\left(\frac{\rho_G}{\rho_L}\right)^{1/2}\delta \end{cases} \quad (18)$$

The experiments conducted by Marmottant and Villermaux (2004) all corresponded to the thick vorticity layer description. Rayleigh–Taylor instability is then triggered

at the wave crest of Kelvin–Helmholtz instability producing liquid ligaments which further stretch in the air stream and break into droplets. The wavelength λ of this instability scales with $We_{R\delta}$ as follows:

$$\lambda \approx 2.8 We_{R\delta}^{-1/3} \left(\frac{\rho_G}{\rho_L}\right)^{-1/3} \quad (19)$$

The onset of Rayleigh–Taylor instability is due to the fact that the acceleration of the interface is oscillatory, in phase opposition with the interface displacement. When the acceleration is orientated towards the heavier phase, the system is unstable in the sense of Rayleigh–Taylor. This condition for instability is reached at a liquid crest. This behavior is similar to the one described on the edge of radial flapping sheets (Villermaux and Clanet 2002). The experiments reported by Marmottant and Villermaux (2004) corresponded to the thick vorticity layer situation thus the surface tension was unimportant in the onset and growth of the initial shear instability but did affect the ligament production and breakup. However, their analysis reports that the liquid surface tension could have a non-negligible influence on the initial shear instability if the vorticity layer is thin.

Stepowski and Werquin (2004) measured the local near-field liquid volume fraction of a coaxial jet using planar LIF in the liquid phase. A 0.3-mm thick pulsed-laser sheet passed through the axis of the jet and extended to 6 cm downstream. The water was seeded and a CCD camera captured the fluorescence emission. Each pixel recorded a signal proportional to the amount of liquid contained in the elementary volume defined by the sheet thickness, the pixel size and the optical setup. These 2D images were then interpreted as map of liquid volume fraction. The characteristic diameters of the injector were $d_L = 1.8$ mm and $d_G = 3.4$ mm. The operating conditions covered the following ranges: $Re_L \in [840; 8{,}120]$, $We_G \in [136; 1{,}225]$, $M \in [2.5; 26]$. These operating conditions corresponded to the fiber-type regime breakup as categorized by Farago and Chigier (1992). The 2D map of liquid volume fraction provided a measurement of the liquid potential core L_{PC}: this length was defined as the farthest position from the injector where the liquid volume fraction is equal to 1. The length L_{PC} reported a linear dependence with $M^{-1/2}$ in agreement with Lasheras et al. (1998) (see Table 2). However, Stepowski and Werquin (2004) observed this dependence for $M < 10$ only. Furthermore, the slope of this growth depended in a non-monotonic way on the relative gaseous Weber number. The authors suggested therefore that the initial relative gaseous Weber number was not the single parameter to classify breakup regimes.

Stepowski and Werquin (2004) conducted an original analysis of their measurements. It consisted in determining local probability density function of the liquid volume fraction using a cumulative procedure. Performing an appropriate change of variable, it was found that the probability density function has a canonical form and, applying an analogy with statistical physics, local spray temperature and degree of freedom were introduced. This degree of freedom varied from 2 in the near-field region to 3 in the spray region where the liquid is fully atomized. This statistical approach is interesting and offers new alternative analysis of atomization processes.

Leroux et al. (2007) investigated the behavior of co-axial liquid jets produced by nine different nozzles. The nozzles differed by the liquid and gas outlet diameters that could be independently varied. The liquid nozzle diameter was equal to 0.4, 1 and 2 mm and the gas nozzle diameter was equal to 3.5, 6 and 8 mm. They used air and five different liquids (water, water–glycerol mixtures, propanol and a mixture of water–propanol). Their operating conditions covered the following ranges of non-dimensional numbers: $Re_L \in [50; 1{,}000]$, $We_R \in [10; 1{,}000]$, $M \in [0.2; 50]$. The experimental investigation conducted by Leroux et al. (2007) was based on shadowgraph image analysis using a very short light pulse (5 ns). The liquid core length was averaged over 100 images for each working conditions. One of the main objectives of this work was to establish criteria for jet disintegration mechanisms. They determined the minimum momentum flux ratio at which the superpulsating mode was reached as well as the maximum momentum flux ratio under which the Rayleigh regime could be observed. They found that Rayleigh-type regime was observed for $M < 7 \times 10^6/Re_G^{1.9}$ and the superpulsating sub-mode was observed for $M > 2 \times 10^5/Re_G^{1.1}$. Between these two limits, the jet broke up in the membrane or fiber-type regimes. Subsequently, Leroux et al. (2007) suggested categorizing the primary breakup mechanism in a M–Re_G map. This suggestion was found appropriate to dissociate the Rayleigh-type regime and the superpulsating mode, but could not dissociate the membrane-type and fiber-type regimes. This classification, however, suggests that the gas turbulence, characterized by Re_G, influence the Rayleigh-type regime. On the basis of their measurements, Leroux et al. (2007) suggested a correlation for the liquid core length. This correlation, shown in Table 2, has a similar form as Lasheras et al. (1998) proposition but reports greater liquid core length. This difference is acceptable since Lasheras et al. (1998) modeled the potential liquid core length L_{PC} whereas Leroux et al. (2007) measured more certainly the liquid core length L_C, which is greater than L_{PC}.

The first conclusion that can be drawn from the experimental investigations reported in this section is that a definite and universal way of categorizing the coaxial jet atomization regimes has not been established so far. A first attempt due to Farago and Chigier (1992) suggested a classification as a function of the liquid Reynolds number

and the relative gaseous Weber number. The limitations between the different regimes were found inappropriate to categorize other experimental observations. For instance, Lasheras et al. (1998) reported that the minimum relative gaseous Weber number to trigger the fiber-type regime was twice greater than the one identified by Farago and Chigier (1992). Furthermore, Lasheras et al. (1998) identified a breakup regime not reported by Farago and Chigier (1992): the digitations-type breakup regime. It should be noted that the injector used by Farago and Chigier (1992) and by Lasheras et al. (1998) showed geometrical differences in terms of liquid diameter (1 mm for Farago and Chigier and 2.9 mm for Lasheras et al.) and of gas to liquid diameter ratio (10 and 1.5, respectively). The effects of these differences should be explored to see their real impact of the jet atomization regimes. Lasheras and Hopfinger (2000) pointed out that a categorization of the coaxial jet disintegration regimes should be based at least on the liquid Reynolds number, the relative gaseous Weber number and the momentum flux ratio. However, they deplored a lack of experimental results to establish a complete jet atomization regime classification. Further works are therefore still required on this point.

To fulfill a complete coaxial jet atomization regime classification requires a complete identification of the parameters that have an influence on the jet behavior. Valuable information can be drawn on this point from the experimental investigations described in this section. Measurements of perturbation wavelength reported by Eroglu and Chigier (1991a, b) suggested that the liquid turbulence influenced the initial jet perturbation. Lasheras et al. (1998) found that the dependence of the initial shear instability frequency with the gaseous velocity was different for laminar and turbulent liquid flow. Mayer and Branam (2004) emphasized also the importance of the liquid turbulence on the initial jet perturbation, and in agreement with Eroglu and Chigier (1991a, b) suggested that the perturbation growth is dominated by aerodynamic interaction. These results reveal that internal liquid flow details are important and must be taken into account.

Other results lead to similar conclusions as far as the gas flow is concerned. For instance, Lasheras et al. (1998) and Marmottant and Villermaux (2004) reported a different dependence between the initial shear instability frequency and the gaseous velocity. The main difference between the operating conditions of these two investigations concerns the gas flow: Lasheras et al. (1998) worked with turbulent gas flows whereas Marmottant and Villermaux (2004) kept this flow laminar. Furthermore, working with laminar gas and liquid flows, Marmottant and Villermaux (2004) demonstrated that the wave number of the initial axisymmetric Kelvin–Helmholtz instability scaled with different parameters according to the thickness of the gaseous vorticity layer (Eq. 18). This shows the extent to which gas flow details are important.

The measurements of the liquid core or potential liquid core length and the subsequent correlations as those reported in Table 2 are also an indicator of the parameters that are important in coaxial jet primary atomization. It is difficult to recommend one of these correlations compared to the other since they all reported an appropriate agreement with the experimental results they were deduced from. From a general point of view, it can be seen that, although it is not always explicit, the momentum flux ratio M is an important parameter. This result was confirmed by other investigations (Hardalupas et al. 1998; Mayer and Branam 2004; Stepowski and Werquin 2004). Hardalupas et al. (1998) noticed that the expression of the liquid core length should also include both the diameters of the liquid and gas flows, and Stepowski and Werquin (2004) observed that the dependence of the potential liquid core length with the momentum flux ratio was a complex function of the relative gaseous Weber number. Finally, the correlation reported by Woodward et al. (1994) (Table 2) emphasizes the importance of the liquid cavitation on the liquid core length and therefore on the atomization regime. All these results show that a complete understanding and description of the coaxial jet behavior should include details of injector geometry as well as of the flows such as the vorticity layer thicknesses, the turbulence intensities and the presence of cavitation.

Most of the results reported in this section were obtained from visualizations and image analyses. One should mention the emergence of different diagnostics such as the measurement of LPP by optical fiber probe (Porcheron et al. 2002) or the measurement of 2D liquid volume fraction by LIF (Stepowski and Werquin 2004) as well as attempts of performing different analysis such as fractal analysis (Shavit and Chigier 1995) or the application of statistical physics (Stepowski and Werquin 2004). Such approaches should be encouraged as they could provide complementary information and open new ways of apprehending the physics of atomization.

5 Air-assisted flat liquid sheets

This section is dedicated to the behavior of liquid sheets bordered by two gas flows. It is limited to the case of flat liquid sheets and does not consider the case of annular liquid flows assisted by inner and outer gas flows. (The behavior of such systems is described in Carvalho and Heitor (1998).) Furthermore, in the investigations summarized in this section, both gas flows are identical (same geometry, same velocity). Investigations on the behavior of

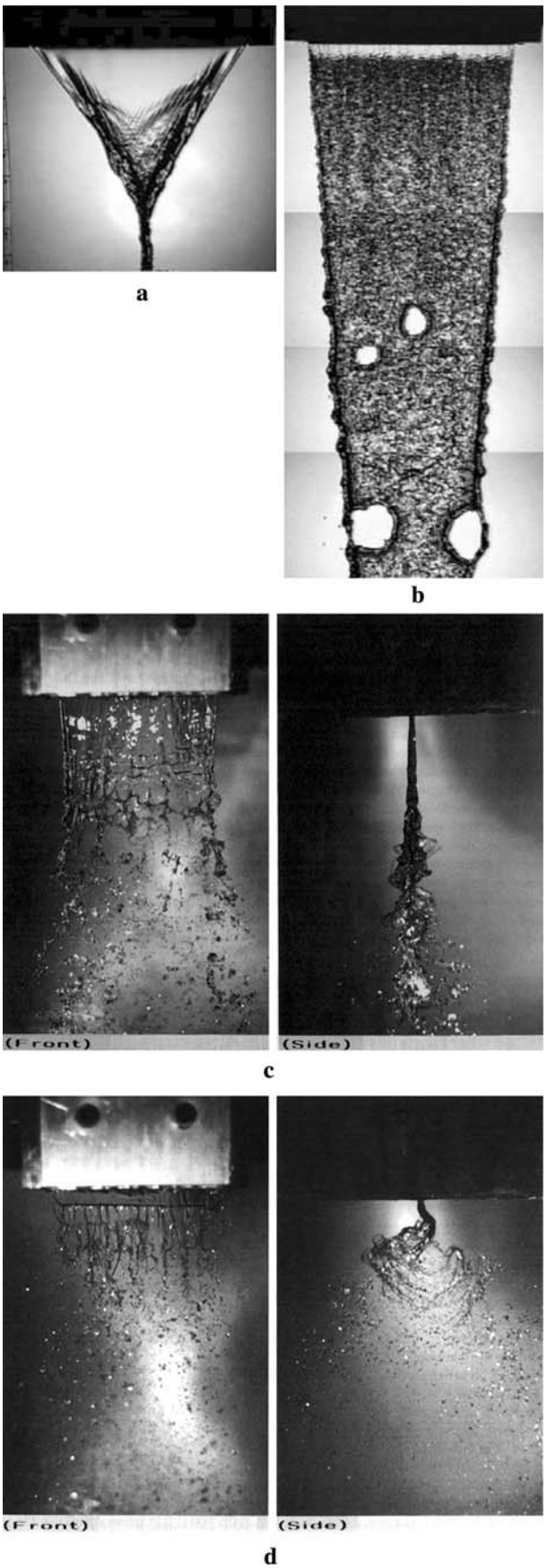

Fig. 15 Air-assisted flat sheet atomization regimes. **a**, **b** Liquid sheet contraction, **c** cellular breakup regime, **d** streamwise ligament breakup regime [**a**, **b** from Carvalho et al. (2002), **c**, **d** from Lozano et al. (1996)] ▶

flat liquid flows bordered by different gas flows can be found in the literature (Yule et al. 1998, for instance).

Two-dimensional atomizers produce air-assisted flat liquid sheets considered here. The liquid sheet emerges from a central rectangular slit and is sandwiched by two sheets of high-speed air. The liquid and gas flow have the same width but different thicknesses (noted t_L and t_G for the liquid and gas, respectively). According to the internal design of the atomizer, the gas streams can be perfectly parallel to the liquid flow or impinge on it at a given angle. The role of this angle is important. When it is steep, the liquid is shattered almost instantaneously into drops of various sizes. Lefebvre (1992) identified this disintegration regime and named it prompt atomization. The present review considers the cases where liquid and gas flows are mostly parallel. The non-dimensional numbers used in the literature to characterize the two-phase flow are identical to those defined for coaxial jets (Eq. 16) where the liquid and gas flow thicknesses replace the diameters d_L and d_G. The liquid slit aspect ratio (width/thickness) is also used to characterize the nozzle geometry. (Typical values of this ratio range from 80 to 500.)

Shadowgraph images taken in both directions (parallel and perpendicular to the atomizer width) reported several atomization processes of the liquid sheet according to the operating conditions. Using the observations returned by several investigations (Rizk and Lefebvre 1980; Stapper and Samuelsen 1990; Mansour and Chigier 1990, 1991; Stapper et al. 1992; Vich et al. 1996; Lozano et al. 1996; Carvalho et al. 2002; Park et al. 2004), these atomization processes can be described as follows.

In the absence of air stream ($U_G = 0$), the liquid sheet converges down to a point where the two rims developing on the sheet edges coalesce (Fig. 15a). This behavior is similar to the one of low-velocity fan liquid sheets except that in the present situation the sheet has a triangular shape. Two forces act on the sheet rims. Surface tension force pulls the rims toward the axis whereas inertial force acts in the axial direction. At low liquid velocity, the central part of the sheet is kept smooth and small amplitude waves emanate from the rims with no apparent consequence of the global sheet convergence. For higher liquid velocities, small distortions, indicative of the transition to turbulence, develop on the sheet surfaces. But the turbulence dissipates quickly without initiating any disintegration process. For further increased liquid velocity, perforations appear and grow on the sheet but this behavior is not accompanied by any drop production (Fig. 15b).

When a high-speed gas stream is added, it develops a significant shear at the interfaces of the low-velocity liquid sheet particular in the nozzle vicinity. Instabilities are triggered and cause the formation of longitudinal and transverse waves on the liquid sheet. The amplitude of these waves quickly grows resulting in the sheet disintegration. The literature reports three breakup regimes according to the ratio U_G/U_L.

At low U_G/U_L, the sheet oscillates in a mixture of sinusoidal and dilational waves with low amplitude growth. The liquid sheet penetration is high and the spray angle is small. The disintegration of the sheet is due to the growth of both spanwise and streamwise ligaments giving rise to liquid cellular structures (Fig. 15c). This type of mechanism is referred to as cellular breakup regime (Stapper and Samuelsen 1990).

When the relative velocity increases (higher U_G/U_L) streamwise vorticity becomes much more important and ligaments are formed in the flow direction and predominate over the formation of spanwise ligaments. Above this, the liquid flow is subject to a strong lateral sinusoidal oscillation. The strong amplitude growth of this sinusoidal oscillation induces a high spray angle, the sheet breakup length is short and the stretching of streamwise ligaments mainly produces the droplets (Fig. 15d). This breakup mechanism is the stretched streamwise ligament breakup regime (Stapper and Samuelsen 1990). The 'flag-effect' regime identified by Vich et al. (1996) and characterized by the development of large liquid membrane caused by the sinuous undulation prior to the formation of the streamwise ligaments is likely to be a sub-mode of the stretched streamwise ligament breakup regime corresponding to lower gas velocity. The cellular and stretched streamwise ligament breakup regimes are not affected under reasonable changes in viscosity or surface tension. These liquid properties modify the characteristic time and length-scales, influencing therefore the drop sizes, but not the general structure of the breakup mechanisms. (Stapper et al. 1992).

For further increased U_G/U_L ratio, the streamwise ligaments recede to the nozzle tip. No intact liquid sheet length is visible and breakup in longitudinal ligaments occurs at the nozzle exit. This regime could be likened to the dripping regime of liquid jet. As explained by Lin and Reitz (1998) for the case of cylindrical jets, the non-formability of liquid sheets observed at high U_G/U_L could be the manifestation of absolute instability. An increase of liquid viscosity favors this breakup regime (Rizk and Lefebvre 1980).

Arai and Hashimoto (1985) investigated the behavior of flat water-sheets ($t_L = 0.4$ or 1 mm) with a constant width equal to 200 mm (aspect ratio between 200 and 500) placed in the center of an airflow (300×300 mm^2). The liquid velocity ranged from 0.5 and 2 m/s and the gas velocity from 23 to 67 m/s. These operating conditions correspond to a relative gaseous Weber number We_R ranging from 1 to 80. Arai and Hashimoto (1985) measured average breakup length from many shadowgraph images. Front and side views of the liquid sheet were taken. They also measured the breakup frequency with a stroboscope as well as the liquid sheet vibrating frequency by analyzing a laser light beam reflected by the liquid sheet with a photomultiplier. The three breakup regimes described above were observed. From the breakup length measurements, Arai and Hashimoto (1985) derived the correlation presented in Table 3 (in which t_L must be expressed in meter). It is interesting to note the analogy between this correlation and the one reported by Eroglu et al. (1991) for coaxial jets (see Table 2). Arai and Hashimoto (1985) reported that the breakup frequency was equal to the liquid sheet vibration frequency meaning that the vibration of the liquid sheet strongly governs the disintegration phenomena. They derived the correlation shown in Table 4 for the sheet vibrating frequency (in which t_L must be expressed in meter).

Chigier and co-workers published a series of articles on the behavior of air-assisted liquid sheet produced by a slit atomizer with the following geometrical characteristics: $t_L = 0.254$ mm, aspect ratio = 120, $t_G = 1.45$ mm. The fluids used were air and water and the following ranges of velocity were covered: $U_G \in [0; 145$ m/s], $U_L \in [1.5; 8$ m/s]. Mansour and Chigier (1990) performed shadowgraph images of the liquid sheet. Front and side views were taken. In the absence of airflow, their measurements showed that the sheet convergence length was proportional to the liquid velocity. In the presence of airflow, they noticed that the

Table 3 Correlations for breakup length of air-assisted liquid sheets

Arai and Hashimoto (1985)[a]	$\frac{L_{BU}}{t_L} = 0.055 t_L^{-0.5} We_R^{-0.5} Re_L^{0.6}$
Carvalho et al. (2002)	$\frac{L_{BU}}{t_L} = \frac{6.51}{M^{0.68}}$
Park et al. (2004)	$\frac{L_{BU}}{t_L} = C \frac{\rho_L U_L}{\rho_G (U_G - U_L)} We_R^{-0.5}$

[a] t_L must be expressed in meter

Table 4 Correlations for the frequency and the wavelength of the sinuous wave of air-assisted liquid sheets

Arai and Hashimoto (1985)[a]	$\frac{f t_L}{U_L} = We_L^{-0.5} \left[0.85 t_L^{0.5} We_R^{0.5} Re_L^{0.15} + 0.06\right]$
Lozano et al. (2001)	$\frac{f t_L}{(U_G - U_{min})} = 0.01$
Carvalho et al. (2002)	$\frac{f t_L}{U_L} = 0.13 M^{0.38}$
Lozano et al. (2005)	$\frac{f\sqrt{t_G t_L}}{(U_G - U_{min})} = F\left(\frac{\rho_G U_G^2 t_G}{\rho_L U_L^2 t_L}\right)$
	$\frac{\lambda}{\sqrt{t_L t_G}} = \frac{20.39}{\sqrt{\frac{\rho_G U_G^2 t_G}{\rho_L U_L^2 t_L}}}$

[a] t_L must be expressed in meter

edges of the sheet showed a mechanical breakup regime similar to the Rayleigh instability observed on small Weber cylindrical liquid jet. At the same time, the liquid sheet atomizes due to aerodynamic effects caused by air friction. Mansour and Chigier (1990) also measured the spray angle in the breakup region on liquid sheet side views. This angle was measured by following the crests of the major perturbation, ignoring the surrounding droplets. Measurements in the dripping regime that is when the breakup length recedes to the nozzle exit were difficult to perform. It was found that the spray angle decreased as the liquid velocity increased or as the air velocity decreased. Mansour and Chigier (1990) concluded that the effect of increasing the specific energy of air per unit volume of liquid resulted in a substantial increase in the amplitude of the liquid sheet oscillation. The initial perturbations were amplified at a much faster rate and the liquid sheet became highly unstable.

Mansour and Chigier (1991) observed that the type of the dominant wave that governs the sheet deformation was a function of the breakup regime. In the cellular breakup regime (low U_G/U_L) the wave that predominates was identified of the dilational type. In the stretched streamwise ligament breakup regimes (intermediate U_G/U_L) the dilational wave could be initially established at the nozzle exit and a sinusoidal mode generated a little farther downstream grew faster and masked the dilational wave. The sinusoidal mode dominated only when enough energy was transferred to the liquid sheet due to air shear. If the velocity ratio was furthermore increased, the sinusoidal mode dominated right at the nozzle exit. Considering Mansour and Chigier (1990) measurements, it can be seen that as the sinusoidal mode becomes more and more dominant, the spray angle increases. Mansour and Chigier (1991) concluded that the sinusoidal mode was the energy-consuming mode that therefore required sufficient energy (provided here by the air flow) to develop. They pointed out that this was in agreement with previous theories (Hagerty and Shea 1950), which stated that the growth rate of the sinusoidal mode was greater than the growth of the dilational mode.

Mansour and Chigier (1991) performed sheet breakup length measurements from many photographs. They found that this length increased with a decrease of the velocity ratio U_G/U_L that is when the dominant mode evolved from sinusoidal to dilational. Note that Arai and Hashimoto (1985) reported a similar dependence between L_{BU} and U_G/U_L (Table 3). Furthermore, Mansour and Chigier (1991) found that the breakup length was proportional to the liquid velocity for sufficiently high gas velocity (in the dominating sinusoidal mode region).

Mansour and Chigier (1991) also measured the frequency of the sheet undulation with a laser light attenuation technique identical to the one used for coaxial jets. The collimated laser beam passes through the liquid sheet in the transverse direction (direction parallel to the sheet width) and the FFT of the temporal laser beam oscillation gives information on the frequency of the lateral motion of the sheet. Mansour and Chigier (1991) positioned the laser beam 2 mm upstream of the breakup region. The oscillation frequency as a function of the liquid velocity for different air velocities reported three distinct regions separated by jumps in frequency. These three regions correspond to the three breakup regimes of the sheet. In the dripping and stretched streamwise ligament breakup regimes, the frequency of the liquid sheet is highly stable and shows a very narrow width. In these regimes, the sheet frequency increased linearly with the gas velocity and moderately depended on the liquid velocity. Note that, for a given gas velocity, a local maximum in the frequency could be identified when the liquid velocity increased. In the cellular breakup regime the reproducibility of frequency measurement was low. Secondary modes appeared and the bandwidth of frequency oscillations widened. The passage from the stretched streamwise ligament breakup to the cellular regimes showed a sudden increase of the dominant frequency that still increased with the gas velocity and did not dependent on the liquid velocity.

Finally, Mansour and Chigier (1991) reconsidered the spray angle measurements they performed in the investigation mentioned above (Mansour and Chigier 1990). This time, in the dripping regime of breakup, the droplet cloud was globally considered for spray angle measurement. The results they obtained were different. For each tested air velocity, the spray angle underwent an increase followed by a decrease as the liquid velocity was increased. Furthermore, when the air velocity increased, the maximum in spray angle decreased and was obtained for a greater liquid velocity. By comparing the undulation frequency and the spray angle, they pointed out that the maximum in spray angle corresponded to the local maximum in the frequency measured in the stretched streamwise ligament breakup regime.

Eroglu and Chigier (1991c) completed Mansour and Chigier's investigations by measuring the wavelength of the lateral sheet oscillation. They performed these measurements on shadowgraph images in a way similar to the one used for coaxial jet analysis (Eroglu and Chigier 1991a, b). The wavelength was measured on both sides of the liquid sheet as a function of the distance from the nozzle and spatial averaged wavelengths were analyzed. These averaged wavelengths decreased when both the liquid and the gas velocities increased. This behavior is in disagreement with linear theory that predicts a decrease of the wavelength with an increasing relative velocity, namely, an increasing gas velocity or/and a decreasing liquid velocity (Chigier and Dumouchel 1996). However, the linear theory applied by

Chigier and Dumouchel (1996) calculated the characteristics of the sinuous optimum perturbation. For high air velocities, when this mode of perturbation is dominant, the predictions agreed with the measurements. As mentioned earlier, the sinuous mode of perturbation is not always dominant and especially when the liquid velocity increases. Eroglu and Chigier (1991c) suggested that when the liquid velocity increased, the dilational wave development was accompanied by turbulent fluctuations in the sheet. At high liquid mass flow, they suspected the small-scale turbulent structures inside the liquid sheet to control the initial phase of the wave development and cause short wavelength surface disturbances to develop. Finally, by testing several liquids, Eroglu and Chigier (1991c) showed that the frequency decreased when the liquid viscosity increased but was globally insensitive to surface tension variations.

Lozano et al. (1996) investigated the behavior of flat water-sheet sandwiched by two co-flowing identical airflows. The liquid sheet thickness was equal to 0.95 mm and its aspect ratio was 84. The internal geometry of the atomizer was designed in order to damp turbulence in the liquid flow. The thickness of the gas flows was equal to 10 mm. The liquid and gas velocities varied from 0.2 to 2.45 m/s and from 8 to 65 m/s, respectively. The airflows were characterized by a two-component LDV system. For that purpose, the air was seeded with water–glycerol droplets. The airflows were found parallel, non-turbulent and with thin boundary layer at the nozzle exit. Shadowgraph images were taken with a 1 μs flash lamp. Spray angle and streamwise ligament spacing were measured on these images. Furthermore, a laser attenuation technique similar to the one used by Mansour and Chigier (1991) was used to measure the sheet undulation frequency. Lozano et al. (1996) observed the three disintegration regimes. The evolutions of the frequency and of the spray angle as a function of the liquid and gas velocities confirmed the results reported by Mansour and Chigier (1991). Although the technique of streamwise ligament spacing was not accurate, they noticed that the ligament spacing decreased as the gas velocity increased and was far less influenced by the liquid velocity. Furthermore, they found that a decrease of the filament spacing was accompanied by a production of thinner streamwise ligaments. They subsequently developed a 3D vortex dynamics model (Lozano et al. 1996, 1998) in order to predict the onset of streamwise ligaments. The model was based on the assumption that the liquid–gas surface behaves as inviscid vortex sheet. The results suggested that streamwise ligaments are due to 2D Kelvin–Helmholtz instability mechanism. However, this model has not received a quantitative experimental validation so far.

Lozano et al. (2001) investigated the behavior of a water sheet surrounded by two co-flowing air streams. The internal liquid and gas channels were contoured in order to ensure laminar flows. At the nozzle outlet, the flows were perfectly parallel. The thickness of the water slit was 0.35 mm and the aspect ratio was equal to 230. The gas flow thickness was equal to 3.45 mm. The liquid and gas velocities were varied from 0.6 to 6 m/s and from 15 to 75 m/s, respectively. Besides frequency measurements performed with a laser light attenuation technique, Lozano et al. (2001) measured wavelengths and amplitude oscillation growth rate on planar LIF images. The water sheet was seeded and visualized by a 500 μm laser sheet positioned in the middle of the liquid sheet and perpendicular to it. Wavelengths were measured on instantaneous images and the oscillation amplitude growth rates were determined on average images.

Frequencies, measured as a function of the liquid and gas velocities, showed similar behavior as those found by previous investigations: they increase linearly with U_G and were weakly dependent on U_L. Furthermore, whatever the air velocity, the local maximum frequency identified by Mansour and Chigier (1991) was reached at a constant momentum flux ratio M equal to 0.5. Lozano et al. (2001) found that the sheet frequency could be associated to a constant Strouhal number $(ft_L/(U_G - U_{min})$ where U_{min} is the minimum gas velocity to initiate a detectable sinusoidal oscillation in the liquid sheet) equal to 0.01 whatever the momentum flux ratio (see Table 4). For Mansour and Chigier (1991) and Lozano et al. (1996) experiments, this Strouhal number is equal to 0.0067 and 0.007, respectively. Lozano et al. (2001) attributed the small discrepancy among the Strouhal numbers (0.01, 0.007, 0.0067) to the fact that their experiments were the only ones where air and water flows were perfectly parallel whereas in Mansour and Chigier (1991) and Lozano et al. (1996) air was impinging onto the liquid at a small angle. The existence of these constant Strouhal numbers led Lozano et al. (2001) to suggest that, similarly to Karman vortex street (Strouhal = 0.21), the mechanism that triggers the initial longitudinal perturbation is believed to be due to vortex shedding. The low Strouhal numbers found for flat liquid sheet could be due to the fact that the vortex shedding is influenced by the inertia of the liquid sheet whose displacement might modify pressure and velocity in the air. This would explain the strong influence of the liquid sheet thickness on the frequency (see Table 4).

Lozano et al. (2001) also presented a linear theory analysis of a viscous liquid sheet sandwiched between two identical semi-infinite viscous air streams taking into account the air boundary-layer thickness. This numerical work showed that the air boundary-layer thickness had an influence on the optimum wave: when this thickness is increased, the growth rate, wave number and frequency of the optimum wave decrease. Comparison between measured and calculated frequencies reported good qualitative

agreements. Above all, Lozano et al. (2001) noted that viscous linear theory reported closer results than the inviscid theory and concluded to the importance of both fluid viscosities on the characteristics of the dominant undulation.

The analysis of instantaneous LIF images reported that the wavelength decreased with an increase of the relative velocity. This evolution agrees with the trend predicted by the linear theory. However, it was found that the sinuous wave wavelength at the nozzle exit did not vary if the momentum flux ratio M was constant. At higher velocities, transverse structures appeared on the liquid sheet. These structures were believed to be the most probable cause of longitudinal filament formation. Lozano et al. (2001) measured the longitudinal filament spacing and found it to decrease when the gas velocity increased and rather insensitive to liquid velocity variation. These results agreed with Lozano et al.'s (1996) observations.

The oscillation amplitude growth rate measured on average LIF images confirmed that the initial instability development followed an exponential growth as suggested by the linear theory. However, the region of exponential growth is limited and the growth rate decreases at some distance from the nozzle.

Lozano and Barreras (2001) investigated the influence of the liquid flow inertia on the surrounding gas flows. They performed visualizations of both the liquid and the gas flows when the liquid sheet is disintegrating in the stretched streamwise ligament breakup regime. (The atomizer was the same as Lozano et al. (2001).) The liquid sheet was visualized by Mie scattering and planar LIF was performed in the gas phase using the same laser sheet as Lozano et al. (2001). Air was seeded by acetone vapor. At moderate liquid velocity (high spray angle, high frequency) the visualizations reported that the sheet oscillation caused air boundary-layer separation with detachment of small vortical structures. The air boundary-layer separation created a low-pressure region in the wave trough with higher relative pressures in the opposite side of the sheet. This unbalance pushed the sheet to oscillate back contributing to the enhancement of the flapping motion. Therefore, when the pressure field induced by the air vortices can effectively displace the water sheet, flapping is initiated and amplification of the sinusoidal wave is very efficient. For higher liquid velocity, it was noticed that the air stream convected the air vortices down without interacting with the liquid sheet. In agreement with Lozano et al. (2001) experimental results, this study confirmed that the presence of the massive liquid sheet substantially reduces the vortex shedding frequency at the nozzle exit. Furthermore, it emphasized the complex interaction between the liquid and the gas flows in the primary disintegration mechanism dominated by the air vorticity layer and the liquid total momentum.

Carvalho et al. (2002) investigated the behavior of a 0.7 mm thick water sheet bordered by two 7 mm thick gas flows. The aspect ratio of the liquid section was equal to 114. Liquid and air velocities were varied from 0.6 to 6.4 m/s and from 0 to 40 m/s, respectively. The liquid sheet was illuminated by a laser light sheet or by a strobe light. The laser sheet was perpendicular to the liquid sheet and was used to take Mie scattering images. Shadowgraph images with the strobe light were performed in both front and side directions. The images were used to measure breakup lengths and spray angles. Furthermore, the sheet breakup frequency was determined by matching the strobe light frequency with that of the flow. The sheet undulation frequency was also determined from a laser beam attenuation technique. These measurements were performed in the breakup region identified on the strobe light images.

Carvalho et al. (2002) first measured the contraction length of the converging liquid sheet when it is not assisted by airflows ($U_G = 0$). They reported observations in agreement with Mansour and Chigier (1990) and demonstrated that the convergence length to sheet thickness ratio scales with the liquid Reynolds number Re_L.

When gas flows were added, Carvalho et al. (2002) defined the breakup length as the distance at which the liquid sheet starts to break up. The measurements were performed on strobe light images. The general evolutions of the breakup length with the liquid and gas velocities agreed well with those reported by Mansour and Chigier (1991). From these measurements, Carvalho et al. (2002) derived the correlation shown in Table 3.

As reported by Arai and Hashimoto (1985), Carvalho et al. (2002) found that the breakup frequency was equal to the wave undulation frequency. As observed by Mansour and Chigier (1991) they found that the determination of a dominant frequency in the cellular breakup regime was difficult because of the widening of frequency power spectra. The analysis of the wave undulation frequency was therefore limited to the dripping and stretched streamwise ligament breakup regimes. They found that this frequency increased with the liquid velocity as well as with the gas velocity. However, contrary to Lozano et al. (1996, 2001), the evolution of the frequency with the gas velocity was not linear but depended on the liquid velocity as shown by the correlation given in Table 4.

Carvalho et al. (2002) emphasized the importance of the technique used to measure spray angle. They found that the laser sheet images reported higher spray angles than those measured on the shadowgraph images. This difference is due to the fact that laser sheet images visualize the droplet mist that surrounds the liquid sheet because of the high intensity of the light it scattered. This mist is not visible on shadowgraph images and the angle measured on these images is more a quantification of the sheet amplitude and

should be called a sheet angle. The spray angle measured from laser light sheet visualizations reported a similar behavior as those found by Mansour and Chigier (1991) and Lozano et al. (1996). For a given gas velocity, this angle increased with the liquid velocity reached a maximum and then decreased. When the gas velocity increased, the maximum spray angle decreased and was reached for a greater liquid velocity. Carvalho et al. (2002) found that the maximum spray angle was reached when the momentum flux ratio M was equal to 0.5. This value coincides with Mansour and Chigier (1991) and Lozano et al. (2001). Lozano et al. (2001) found that this value of the momentum flux ratio corresponded to the local maximum wave undulation frequency and Mansour and Chigier (1991) reported that the local maximum of frequency corresponded to the maximum spray angle.

Park et al. (2004) investigated the cellular breakup regime of a water sheet sandwiched between two airflows. The operating conditions were: $t_L = 0.354$ mm, $t_G = 1.397$ mm, $U_L \in [2; 9.8$ m/s] and $U_G \in [13.3; 93.1$ m/s]. Shadowgraph images were performed with a high-speed CCD imaging system. These images were used to measure average cell sizes, breakup length and spatial growth rates. Park et al. (2004) observed that the lateral motion of the liquid sheet in the cellular breakup regime is caused by the superposition and the combination of several sinuous and dilational waves. Therefore, they concluded that the laser beam attenuation technique used by previous workers was not adapted to investigate this regime for which the measurement of a unique frequency of the lateral sheet motion might not be physically representative. Park et al. (2004) reported that the average cell size scaled as the inverse of the square of the relative velocity and that was not dependent on the liquid turbulence. Furthermore, by performing simulations of the gas flow at the nozzle exit, they pointed out that the gas flow reattached on the liquid surface at a distance that was of the same order of magnitude as the distance at which the liquid sheet started to be disturbed. From these results, they concluded that the turbulent air stream seemed the most influential source of initial perturbations for cellular breakup. Park et al. (2004) defined the breakup length as the distance from the nozzle to the first rupturing point of a liquid sheet. Their measurements led to the correlation shown in Table 3. This correlation is different from those reported by Arai and Hashimoto (1985) and by Carvalho et al. (2002) but one has to keep in mind that Park et al. (2004) mainly investigated the cellular break regime. In this regime we can note that the influence of the liquid velocity is more important. Finally, Park et al. (2004) reported wave amplitude spatial growth rates from their visualizations. As observed by Lozano et al. (2001), they found that the initial wave growth was exponential as suggested by linear theories. They also noticed that the distance along which the wave amplitude growth was exponentially decreased as the velocity ratio U_G/U_L increased.

Lozano et al. (2005) investigated the influence of both liquid and gas stream thicknesses on the stretched streamwise ligament breakup regime. The liquid channel thickness varied from 0.5 to 1.9 mm corresponding to a maximum liquid velocity equal to 4.44–1.17 m/s, respectively. The gas stream channel thickness ranged from 3.43 to 35 mm and the maximum gas velocity was 75 m/s. In this study, they improved the laser attenuation technique by using two laser beams to simultaneously measure the frequency and the wavelength of the sinuous oscillation of the sheet. Their analysis reported that the most convenient parameter to categorize the sheet behavior was not the momentum flux ratio M but the total momentum ratio defined by $\left(\frac{\rho_G U_G^2 t_G}{\rho_L U_L^2 t_L}\right)$. They obtained correlations for the wave frequency and for the wavelength λ based on this number (see Table 4). As far as the frequency is concerned, they pointed out, however, that the Strouhal numbers $\frac{f\sqrt{t_G t_L}}{(U_G - U_{min})}$ were dependent on the gas stream thickness and concluded that this characteristic scale was not appropriate to account for the air dependence unless it was weighed by some additional factor. The wavelength was found to increase linearly with the liquid velocity and the inverse of the gas velocity. As pointed out by Lozano et al. (2005) this result is in discrepancy with the inviscid linear theory that predicts a dependence on velocity squared. Lozano et al. (2001) demonstrated that this erroneous prediction is due to neglecting the gas viscosity.

All the experimental investigations reported in this section agree with the fact that a liquid stream issuing from a rectangular slit with a rather high aspect ratio requires the assistance of co-flowing gas stream to disintegrate. In the presence of air streams, three breakup mechanisms can be seen, namely, the dripping regime (high U_G/U_L), the ligament breakup regime (intermediate U_G/U_L) and the cellular breakup regime (low U_G/U_L). It must be noted that no attempt of categorizing these regimes has been found in the literature. However, one should mention that if the transition from the stretched streamwise ligament breakup regime to the cellular breakup regime is defined at the sharp spray angle decrease, this transition occurs for a momentum flux ratio M equal to 0.5 (Lozano et al. 2001; Carvalho et al. 2002).

The stretched streamwise ligament breakup regime has the best atomization performances (Lozano et al. 2001). Many studies reported that the spray angle reaches a maximum in this regime (Mansour and Chigier 1991; Lozano et al. 1996, 2001; Carvalho et al. 2002) due to a sharp growth of a longitudinal sinusoidal undulation. This sinusoidal perturbation wave is also observed in the dripping regime but its growth is far less. In the cellular

breakup regime, this perturbation wave does not exist (Park et al. 2004). Thus, the laser attenuation technique used to measure the sinusoidal wave frequency is appropriate in the dripping and ligament stretched breakup regimes only because single, dominant and reproducible frequency exists. Lozano et al. (2001) associated this frequency to a constant Strouhal number (Table 4) and argued that, such as in a von Karman-vortex street, this was the mark of the dominance of vortex shedding to initiate longitudinal perturbation. Carvalho et al. (2002) found that this frequency correlated to the momentum flux ratio M (Table 4). Note that this correlation expresses an almost constant Strouhal number based on the gas velocity and agrees quite well with Lozano et al. (2001) correlation. Considering Lasheras et al.'s model (1998) for coaxial jets, the influence of M could illustrate the importance of the vorticity layer on the onset of the shear instability in the near-field region. By visualizing the air stream next to the liquid flow, Lozano and Barreras (2001) reported experimental evidences of the importance of the gaseous vorticity layer on the instability onset. They also pointed out that the massive liquid sheet substantially influenced the vortex shedding frequency at the nozzle exit. The correlations due to Lozano et al. (2005) (Table 4) are expected to be more reliable since more parameters were varied in their experiments. They show that the important parameter to be considered is not the momentum flux ratio but the total momentum ratio. Lozano et al. (2005), however, mentioned that the correlation for the frequency did not correctly account for the gas stream thickness. All these results illustrate that the air vorticity layer and the total liquid momentum are of first order of importance in the sinusoidal wave onset. Thus, the appropriate gas characteristic length-scale could be the vorticity layer thickness. This point would require further investigation.

When the liquid velocity is increased, the liquid sheet eventually disintegrates under the cellular breakup regime. A strongly growing sinusoidal perturbation is not visible anymore and the spray angle reduces strongly. Park et al. (2004) noted that the sheet is perturbed by a superposition of several undulation waves and that frequency and wavelength measurements from the side of the sheet are physically irrelevant. Frequency measurements performed in this regime must be considered as indicative. Mansour and Chigier (1991) attributed the small wavelengths measured in this regime to the fact that the onset of initial perturbation is due to liquid turbulence. Lozano and Barreras (2001) observed that when the liquid velocity is high, the air vortices appear to be convected down by the airflow without interacting with the liquid sheet. Lozano et al. (2001) reported that the streamwise ligament spacing depended on the gas velocity but not on the liquid velocity. Park et al. (2004) noted that the liquid sheet started to be disturbed at a distance where the gas stream reattached the liquid flow. Furthermore, they found that the size of the cells was independent of the liquid turbulence and suggested that the onset of the liquid sheet perturbation was mainly controlled by the turbulent airflow. Contrary to what happens in the other regimes, in the cellular breakup regime the total gas momentum is too small compare to the total liquid momentum to initiate a lateral sinusoidal wave that promotes atomization. It appears from these results that the onset of the cellular breakup regime is dominated by the gas flow but the exact role of vorticity layer and gas turbulence has not been quantified so far. Furthermore, liquid velocity and turbulence in the liquid flow seem to be less important parameters. Further experimental investigations, accounting for instance for the fluid physical properties, should be conducted to confirm these results. Indeed, almost all experimental investigations conducted on the behavior of air-assisted liquid sheets have dealt with air and water.

We should note that the exact mechanism that conducts to the development of streamwise ligaments in the three breakup regimes has not been fully established so far. It is clear that the onset of these ligaments results from air interaction since they never appear when $U_G = 0$. Lozano et al. (1996, 1998) emitted the idea that 2D Kelvin–Helmholtz instability mechanism was at the origin of streamwise ligaments but this has not been qualitatively validated so far. When the liquid velocity decreases, the recession of these ligaments towards the nozzle tip, leading to the dripping regime, has not been explained either. This behavior must result from a strong interaction between the liquid and the gas very near the nozzle exit. As shown by Park et al. (2004) simulations, the gas and the liquid flows do not interact with each other as soon as they leave the nozzle. A distance of reattachment is identified. In the cellular breakup regime this distance is of the order of the minimum distance required to see perturbations on the liquid sheet. Park et al. (2004) also reported a gaseous recirculation zone above the point of reattachment. One should wonder whether this recirculation zone, which depends on the atomizer design and gas velocity, is not dominant in the onset of the dripping mode. The influence of this specific zone located right at the nozzle exit has not been explored so far and should be investigated.

6 Summary and concluding remarks

Visualizations of liquid streams evolving in a gaseous atmosphere have been extensively published over the years and used to identify and categorize liquid stream primary atomization regimes. Shadowgraph arrangement, where the light source, the liquid stream and the camera are aligned,

is the most commonly encountered configuration for this purpose. Despite this, no universal categorization of liquid stream atomization regimes is available so far and this remark stands for any type of liquid flow. Liquid stream atomization regimes are categorized by attributing each regime a domain of non-dimensional numbers. One of the reasons that explain the absence of a universal atomization regime categorization is that some parameters, which have an important contribution on the stream behavior, are not taken into account in non-dimensional groups.

For cylindrical liquid jets evolving in a gas at rest, atomization regimes were identified from the evolution of the liquid jet breakup length with the jet velocity and regime delineations have been based on typical values of liquid or gaseous Weber numbers, Ohnesorge number, density ratio or Taylor number (see Table 1). As shown in this table, the passage from the Rayleigh regime to the first wind-induced regime, which corresponds to a maximum in the stability curve, has been commonly associated to a typical gaseous Weber number thanks to Weber's linear theory (1931). Such a criterion suggests that the reduction of the jet breakup length in the first wind-induced regime is the effect of aerodynamic forces. However, many experimental investigations reported jets for which the maximum in the stability curve was independent of the surrounding gas density (Grant and Middleman 1966; Fenn and Middleman 1969; Leroux et al. 1996, 1997). For such jets, the passage from the Rayleigh to the first wind-induced regimes cannot be associated to a specific gaseous Weber number. The onset of the first wind-induced regime for these jets (denominated regime 1 jets by Leroux et al. (1996)) is not fully understood. Several explanations have been proposed. Fenn and Middleman (1969) suggested that the reduction of breakup length for regime 1 jets in the first wind-induced regime is due to shear stress effects, Phinney (1972) and Mansour and Chigier (1994) evoked a sharp increase of the initial disturbance amplitude and Sterling and Sleicher (1975) suspected the effect of jet velocity-profile relaxation. A low-Ohnesorge number is a characteristic feature of regime 1 jets. High-Ohnesorge jets show a Rayleigh to the first wind-induced regimes transition that is controlled by aerodynamic forces and is therefore associated to the critical gaseous Weber reported by Sterling and Sleicher (1975) (Table 1). (Leroux et al. (1996) dominated these jets as regime 3 jets.) A criterion to determine a jet regime has not been established so far. Leroux et al. (1996) introduced a jet parameter $\rho_G{}^*$ for this purpose. The value of this parameter can be approximated from the jet Ohnesorge number (Fig. 3) and the ratio $\rho_G{}^*/\rho_G$ indicates whether the jet is likely to behave as a regime 1 ($\rho_G{}^*/\rho_G > 1$) or a regime 3 jet ($\rho_G{}^*/\rho_G \ll 1$) but the physical significance of $\rho_G{}^*$ has not been established. One point can be ascertained from the different experimental results, behavior of regime 1 jets in the Rayleigh to the first wind-induced regime transition is controlled by the liquid flow showing the importance of the internal flow details of low-Ohnesorge jets. These details as well as their impact on the jet behavior are still to be identified in order to propose more complete atomization regime criteria.

The investigations evoked in the previous paragraph were based on breakup length measurements only performed on liquid jet visualizations. Other experimental investigations were dedicated to the measurement of the spatial or temporal evolutions of the jet diameter by using either a high-speed camera coupled with an asymmetric magnification imaging technique (Blaisot and Adeline 2000a, b, 2003) or a laser extinction technique (Amagai and Arai 1997; Arai and Amagai 1999; Godelle et al. 2000a, b; Ruiz 2002). These equipments allowed frequency, wavelength amplitude and propagation speed to be measured. The main conclusions reported by these investigations are the following. In the Rayleigh regime, experimental evidences show that several waves perturb the cylindrical jets (Amagai and Arai, Godelle et al.). The frequencies of these waves are in harmonic or not according to the jet diameter. Furthermore, in the breakup region the waves have similar amplitudes showing that the drop production is highly non-linear. Temporal and spatial jet diameter evolutions revealed also the existence of a neutral region along the jet in the Rayleigh regime where no disturbance growth can be detected. These findings show to which extent the description provided by the classical linear theory is limited. Furthermore, Godelle et al. and Blaisot and Adeline reported the disappearance of the neutral region for regime 1 jet in the first wind-induced regime explaining the sharp reduction of the breakup length. Indeed, as soon as the jet issued from the nozzle, growing perturbations are detectable. This confirms the importance of the internal flow details on the behavior of regime 1 jet in the first wind-induced regime and gives less credit to the action of the jet velocity-profile relaxation that would require a minimum distance to be perceptible and to influence the jet behavior.

The second wind-induced and atomization regimes of a cylindrical jet have been also related to specific values of a gaseous Weber number (see Table 1). These two breakup regimes show the production of small drops with interface peeling off as soon as the liquid issues from the nozzle. The experimental investigation due to Faeth and co-workers demonstrated that a high-Weber number is not a sufficient condition to reach these regimes. Indeed, they reported that high gaseous Weber number cylindrical laminar jets free of any boundary layer do not show interfacial drop peeling off. On the other hand, this primary breakup process is triggered in the presence of boundary layer or for turbulent jets. Thus, a criterion solely based on a gaseous Weber

number to delimitate the second wind-induced regime appears insufficient and that, once again, details of the internal liquid flow should be accounted.

This conclusion also stands for jets in the atomization regime as those commonly encountered in diesel application. These jets have a very high average velocity and a small diameter. The experimental investigation of the liquid jet atomization regime is difficult because of the very high jet velocity, the sudden atomization at the nozzle exit and the presence of a very high-density spray around the liquid jets. Thus, shadowgraph images, which have been widely performed to measure spray angle, are not appropriate anymore to catch details of the jet structure in the primary atomization zone and new diagnostics have been developed. Among them one should mention the electrical resistance method to measure the breakup length (Hiroyasu and co-workers), three-laser infrared extinction system to measure the drop-size distribution in the near-field region (Parker et al. 1998), absorption of monochromatic X-ray beam to measure the liquid volumetric fraction (Yue et al. 2001), coupling of tomography and shadowgraph images (Yon et al. 2003) and ballistic imaging technique (Paciaroni et al. 2004, 2006). Early investigations due to Reitz and Bracco (1982) and to Hiroyasu and co-workers emphasized the influence of the nozzle internal design on the jet primary atomization. This motivated the visualization of transparent nozzle internal liquid flow using either shadowgraph or tomographic techniques. Although all the experimental investigations confirm the dominant role of the nozzle design on the presence of cavitation in the liquid flow, the exact role of liquid cavitation is still not fully identified and several interpretations can be found in the literature, such as, to increase the effective jet velocity (Karasawa et al. 1992; Payri et al. 2004), to induce the development of disturbance in the liquid flow (Tamaki et al. 1998), to increase the turbulence in the liquid flow (Hiroyasu 2000; Smallwood and Gülder 2000), to produce small drops at the nozzle exit by bursting and collapsing of vapor cavity (Smallwood and Gülder 2000). Other authors (Kim et al. 1997; Badock et al. 1999a, b; Arcoumanis et al. 2001; Yon et al. 2003) reported that liquid cavitation structures have different origins (geometrically or dynamically induced) and therefore different shapes and influence at the nozzle exit. The cavitation structure characteristics are functions of the nozzle diameter, length, inlet condition, orientation and position with respect to the sac volume, the needle lift, etc. For instance, Kim et al. (1997) pointed out that the structure on the jet at the nozzle exit changed from spray plume to hollow cone due to column type of cavitation that appeared in the sac volume. The differences in nozzle geometry from one investigation to another are believed to be the main factor that explains some of the discrepancies reported such as for instance the presence of a continuous liquid flow at the nozzle exit: Hiroyasu and co-workers concluded to the presence of continuous liquid column at the nozzle exit whereas Parker et al. (1998) and Yue et al. (2001) reported fully atomized liquid at this location. Note that contrary to Hiroyasu and co-workers, Parker et al. (1998) and Yue et al. (2001) worked with real diesel injectors. Therefore, categorization of cylindrical jet primary breakup in the atomization regime must account for nozzle internal design and flow details. This is the purpose of the spray angle parameter A introduced by Reitz and Bracco (1982) (Table 1). This parameter that must be determined from experiments integrates the influence of the internal nozzle and flow details.

The experimental investigations dedicated to liquid sheet primary breakup show that the atomization regimes depend on the sheet production. Fan nozzles and impacting jets produce smooth liquid sheet continuously thinning and with constant velocity along the streamlines (Dombrowski et al. 1960; Clanet and Villermaux 2002). Using light interference technique, Dombrowski et al. (1960) and Clanet and Villermaux (2002) demonstrated that the local sheet thickness is always inversely proportional to the distance from the nozzle or from the impaction point. For sheet produced by impaction, the proportionality coefficient scales with the impacting jet section area. For fan nozzles, the proportionality coefficient scales with a parameter (K) that is a function of the injector design and of the liquid viscosity (Dombrowski et al. 1960). However, the relationship between the nozzle design, the liquid properties and the liquid sheet thickness parameter has not been established. As noticed earlier, the similarities between the sheets produced by fan nozzles or by impaction are likely due to the fact they result from a similar way of production, sheet emanating from fan nozzles resulting from the impaction of streamlines at the nozzle exit.

Smooth liquid sheets produced by fan nozzles or by jet impaction disintegrate by the growth of a Kelvin–Helmholtz provided that the liquid Weber number is high enough. If not, the liquid sheet produced by fan-nozzles contracts under the action of surface tension forces (Fraser et al. 1962). Note that the minimum liquid Weber number to avoid this contraction has not been quantified. These two primary breakup regimes are not assisted by liquid turbulence (Fraser et al. 1962). Under atmospheric conditions, the minimum liquid Weber number to initiate the Kelvin–Helmholtz instability on a liquid sheet produced by impacting jets has been evaluated to 1,000 by Huang (1970) and Villermaux and Clanet (2002). (This liquid Weber number is based on the diameter of the impacting jet.) Below this limit, the liquid sheet is kept smooth and liquid beads form along the circular periphery and detach from the sheet.

The Kelvin–Helmholtz instability onset is a function of the gaseous environment. Under subatmospheric condition, Fraser et al. (1962) reported that the sinuous mode of disintegration was no longer observed and the liquid sheet disintegrated under perforation. No criterion segregating the perforating from the sinuous mode of disintegration has been established. The perforating disintegration mode has not been reported for liquid sheets produced by impaction since no experiments were performed under subatmospheric pressure. However, Villermaux and Clanet (2002) found that the minimum liquid Weber number for the Kelvin–Helmholtz instability onset was function of the gas density. (An estimation of this dependence is given by Eq. (15).) Thus, the categorization of smooth liquid sheet primary breakup mechanisms requires additional experimental work to be completed.

As far as the growth of the Kelvin–Helmholtz instability is concerned, different observations were made. By analyzing high-speed visualizations, Huang (1970) reported an exponential growth of the instability when the liquid Weber number is <4,450. By analyzing 2D laser-induced high-speed visualizations, Villermaux and Clanet (2002) noticed that the growth was greater than exponential. They attributed this behavior to the fact the liquid sheet is continuously thinning. Crapper et al. (1973) observed on shadowgraph images that after a sharp increase, the amplitude of the sinuous wave that evolves on a fan-nozzle sheet may actually decrease. This behavior was reported when the liquid velocity was low. The limit in liquid velocity to see this behavior has not been established. By visualizing the surrounding gas medium, Crapper et al. (1973) attributed this phenomenon to the development and growth of vortex in the gas next to the sheet. However, this behavior has not been observed on circular sheets produced by impaction. One may wonder whether the behavior reported by Crapper et al. (1973) is not related to liquid sheet contraction that never happens on circular liquid sheet and that could be effective on fan-nozzle sheets when the velocity is low.

Finally, Fraser et al. (1962) and Villermaux and Clanet (2002) suggested a different description of the final stage of the primary breakup of liquid sheet. According to Fraser et al. (1962) the sheets breaks at each half wavelength to produce ligaments that disintegrate under a Rayleigh instability whereas Villermaux and Clanet (2002) observed that drops are produced from the disintegration of streamwise ligaments resulting from Rayleigh–Taylor instability. We should note that the description reported by Villermaux and Clanet (2002) has been clearly observed on visualizations which are not the case for the suggestion made by Fraser et al. (1962).

Liquid sheets emanating from compound nozzles show a totally different primary breakup mechanism. The production of these sheets results from the presence of a double swirl in the nozzle, the radial aperture of the sheet being related to the double swirl intensity. The disintegration of these sheets does not require aerodynamic force assistance to be effective. The onset of atomization is dominated by the intensity of the non-axial flow as well as by the liquid turbulence intensity and liquid surface tension forces control the liquid flow evolution and breakup. The interesting aspect of this atomization mechanism is that good atomization efficiency can be reached even at low injection pressure. Details of the internal flow here are of paramount importance. This complicates the investigation of this atomization mechanism since it is almost impossible to perform quantitative measurements of the flow characteristics at the nozzle exit. Furthermore, as the liquid turbulence is a key factor, the atomization mechanism is not as organized as for smooth liquid sheet and a single characteristic length-scale cannot describe the sheet evolution. The studies reported by Dumouchel and co-workers suggest the application of fractal analysis to describe the atomization process. Although the first results are very encouraging, further investigations are required to find how such approach could provide a better comprehension of the mechanisms as well as primary atomization models.

A universal classification of air-assisted cylindrical jet atomization mechanisms is not available so far. The first morphological classification due to Farago and Chigier (1992) suggested an organization of the three main breakup regimes (Rayleigh-type, membrane-type and fiber-type) in the We_R–Re_L plane. However, Lasheras et al. (1998) found that this classification did not suit their experimental observations. They attributed this difference to the fact that their liquid orifice diameter was almost four times greater than the one of Farago and Chigier (1992). Furthermore, the gas to liquid diameter ratio of these injectors was very different. This suggests that coaxial jet atomization regime classification should include more nozzle geometrical details than the sole liquid diameter included in the relative gaseous Weber number and in the liquid Reynolds number. In a subsequent investigation, Lasheras and Hopfinger (2000) pointed out that the classification of coaxial jet regimes should be based on three numbers at least, namely, the relative Weber number We_R, the liquid Reynolds number Re_L and the momentum flux ratio M. However, they deplored a lack of experimental data to give precise location of the regime boundaries.

The importance of the parameter M in coaxial jet behavior is evidenced by numerous measurements of jet liquid core or potential core length, L_C and L_{PC}, respectively. This characteristic is difficult to measure, especially in the fiber-type regime. Several diagnostics have been used for this purpose, namely, shadowgraph images (Eroglu and Chigier 1991a, b; Hardalupas et al. 1998; Leroux

et al. 2007), X-ray transmitted intensity technique (Woodward et al. 1994), optical fiber probe technique (Porcheron et al. 2002), planar LIF images (Stepowski and Werquin 2004). Most of the experiments reported that the liquid core length depends on the momentum flux ratio M as illustrated by the correlations presented in Table 2. Furthermore, Farago and Chigier (1992) and Lasheras et al. (1998) found that the superpulsating mode could be related to a critical momentum flux ratio equal to 7 and 35, respectively.

Although they present some similarities, the correlations for the liquid core length (Table 2) show non-negligible differences. Three main reasons are believed to be responsible for these differences. First, as noticed above, measurements were performed with different diagnostics. Second, the experimental investigations explored different domain of operating conditions. For instance, Eroglu et al. (1991) varied the water and air velocities only; Woodward et al. (1994) added the influence of the ambient pressure and of the gas; Porcheron et al. (2004) used liquid oxygen and varied the gas and liquid flow diameters; and Leroux et al. (2007) varied the injector diameters and the liquid physical properties. Third, the characteristics of coaxial jet breakup mechanisms depend on internal injector design. Woodward et al. (1994) found that at low ambient pressure the jet breakup mechanism was controlled by cavitation-induced turbulence rather than by aerodynamic shear. As evidenced by high-Weber number cylindrical jet behavior, the nozzle internal design influences liquid cavitation. Other coaxial jet breakup mechanism characteristics also report dependence with details of the internal flows. Eroglu and Chigier (1991a, b) and Mayer and Branam (2004) pointed out the importance of the liquid turbulence on the initial jet perturbation. Dahm et al. (1992), Rehab et al. (1997), Lasheras et al. (1998), Lasheras and Hopfinger (2000) and Marmottant and Villermaux (2004) showed that the initial interfacial instability is dominated by the gas vorticity layer characteristics. Measurements of instability frequencies performed with a laser attenuation technique (Eroglu and Chigier 1991a, b; Lasheras et al. 1998; Marmottant and Villermaux 2004) reported different behavior according to the degree of turbulence in both liquid and air flows. These examples illustrate the importance in accounting for liquid and gas flow details to categorize coaxial jet primary atomization mechanisms. For this purpose it should be recommended to couple experimental approaches with injector internal flow simulations to reach a more complete description and analysis of the mechanisms.

As far as air-assisted liquid sheets are concerned, no attempt of categorizing the three breakup regimes (dripping regime, stretched streamwise ligament breakup regime and cellular breakup regime) has been found in the literature. The characteristics of the liquid sheet behavior such as the liquid sheet breakup length measured on shadowgraph images (Arai and Hashimoto 1985; Mansour and Chigier 1990, 1991; Park et al. 2004) or on 2D laser sheet visualizations (Carvalho et al. 2002), the sheet undulation wavelength measured on shadowgraph images (Eroglu and Chigier 1991c; Park et al. 2004), on LIF images (Lozano et al. 2001) or with a double laser beam attenuation technique (Lozano et al. 2005), and the liquid sheet undulation frequency measured with a laser beam attenuation technique (Arai and Hashimoto 1985; Mansour and Chigier 1991; Lozano et al. 1996, 2001, 2005; Carvalho et al. 2002) are mainly dependent on the relative gaseous Weber number We_R, the liquid Reynolds number Re_L and the momentum flux ratio M. This is illustrated by the correlations presented in Tables 3 and 4. Except Park et al.'s result (2004) that was obtained for the cellular breakup regime, the correlations shown in these tables were derived for air-assisted liquid sheet in the dripping and ligament stretched breakup regimes. Considering Lasheras et al.'s model (1998) for coaxial jets, the influence of the number M illustrates the importance of the vorticity layer on the onset of the initial shear instability. Table 4 shows that the longitudinal wave oscillation frequency is always associated to a specific Strouhal number. According to Lozano et al. (2001) this is the mark of the dominance of vortex shedding to initiate longitudinal perturbation and Lozano and Barreras (2001) reported experimental evidences of the importance of the gaseous vorticity layer on the instability onset.

As far as the influence of the liquid flow is concerned, many experiments conducted in the stretched streamwise ligament breakup regime reported that the sinusoidal wave frequency moderately depended on the liquid velocity (Mansour and Chigier 1991; Lozano et al. 1996, 2001; Carvalho et al. 2002). No influence of the liquid turbulence has been reported on the sinusoidal wave frequency undulation. Furthermore, liquid velocity and turbulence have been found to have a negligible influence of the streamwise ligament spacing both in the stretched streamwise ligament breakup regime and cellular breakup regime (Lozano et al. 1996, 2001; Park et al. 2004). However, it has been demonstrated that the liquid sheet inertia reduces the vortex shedding frequency (Lozano et al. 2001; Lozano and Barreras 2001). In a subsequent investigation, Lozano et al. (2005) found that the best parameter to be considered to categorize air-assisted liquid sheet behavior is the total momentum ratio rather than the flux momentum ratio. It appears from these results that details of the liquid flow are less important than those of the gas flow.

It has been noticed from the experimental investigations performed on air-assisted liquid sheet that the exact origin of the streamwise ligaments that are present in each breakup regime has not received a clear explanation. Furthermore, the recession of these ligaments towards the nozzle tip when the liquid velocity is small (dripping regime) has not been neither explained nor characterized so far. As suggested above, one may wonder whether the recirculating zone in the gas, located between the nozzle exit and the point of flow reattachment and identified by Park et al. (2004), is not an important element to be considered to better describe and understand the near-field air-assisted liquid sheet behavior in the dripping regime.

These results suggest that, besides the parameters included in the correlations found in the literature (Tables 3, 4), the categorization of air-assisted liquid sheet primary atomization breakup should account for the total liquid momentum, the gas vortex layer characteristics, the turbulence in the gas flow, the flow reattachment distance from the nozzle and the gas recirculation zone at the nozzle exit.

The numerous experimental investigations reviewed in this paper show the wide variety of powerful diagnostics available now to investigate liquid stream primary breakup mechanisms. Among the recent developed techniques one should mention the ballistic imaging technique to perform accurate visualizations of high-velocity liquid jets, the X-ray extinction technique to quantify local liquid volumetric fraction in dense regions, the optical probe technique to determine local LPP in dense regions, the infrared laser extinction technique to measure drop-size distribution in dense sprays. Furthermore, one should emphasize attempts of using analyzing methods rarely applied in liquid atomization investigations such as the non-linear dynamic theory, the morphological and fractal analyses, and the statistical physics. Such developments must be encouraged as they provide new possibilities to investigate and characterize liquid stream atomization mechanisms.

References

Amagai K, Arai M (1997) Frequency analysis of disintegrating liquid column. In: Proceedings of ICLASS'97, Seoul, Korea, 18–22 August 1997, pp 361–368

Arai M, Amagai K (1999) Surface wave transition before breakup on a laminar liquid jet. Int J Heat Fluid Flow 20:507–512

Arai T, Hashimoto H (1985) Disintegration of a thin liquid sheet in a cocurrent gas stream. In: Proceedings of ICLASS'85, London, UK, 8–10 July 1985, paper VIB/1

Arai M, Shimizu M, Hiroyasu H (1985) Break-up length and spray angle of high speed jet. In: Proceedings of ICLASS'85, London, UK, 8–10 July 1985, paper IB/4

Arai M, Shimizu M, Hiroyasu H (1988) Break-up length and spray formation mechanism of high speed liquid jet. In: Proceedings of ICLASS'88, Sendai, Japan, 22–24 August 1988, paper A/4, pp 177–184

Arcoumanis C, Gavaises M, Flora H, Roth H (2001) Visualisation of cavitation in diesel engine injectors. Mec Ind 2:375–381

Bachalo WD (2000) Spray diagnostics for the twenty-first century. At Sprays 10:439–474

Badock C, Wirth R, Tropea C (1999a) The influence of hydro grinding on cavitation inside a diesel injection nozzle and primary break-up under unsteady pressure conditions. In: Proceedings of ILASS-Europe'99, Toulouse, France, 5–7 July 1999

Badock C, Wirth R, Fath A, Leipertz A (1999b) Investigation of cavitation in real size diesel injection nozzles. Int J Heat Fluid Flow 20:518–544

Bayvel L, Orzechowski Z (1993) Liquid atomization. Taylor and Francis, Washington, DC

Blaisot JB, Adeline S (2000a) Determination of local properties of the instabilities on a capillary jet. In: Proceedings of ICLASS'2000, Pasadena, CA, USA, 16–20 July 2000

Blaisot JB, Adeline S (2000b) Determination of the growth rate of instability of low velocity free falling jets. Exp Fluids 29:247–256

Blaisot JB, Adeline S (2003) Instabilities on a free falling jet under an internal flow breakup mode regime. Int J Multiph Flow 29:629–653

Blaisot JB, Yon J (2005) Droplet size and morphology characterization for dense sprays by image processing: application to diesel spray. Exp Fluids 39:977–994

Briggs TE, Malave A, Farrell PV (2006) Dual-wavelength absorption imaging of diesel sprays. In: Proceedings of ICLASS 2006, Kyoto, Japan, 27 August–1 September 2006, paper 135

Carvalho IS, Heitor MV (1998) Liquid film break-up in a model of a prefilming airblast nozzle. Exp Fluids 24:408–415

Carvalho IS, Heitor MV, Santos D (2002) Liquid film disintegration regimes and proposed correlations. Int J Multiph Flow 28:773–789

Chigier N (2005) The future of atomization and sprays. In: Proceedings of ILASS-Europe 2005, Orléans, France, 5–7 September 2005

Chigier N, Dumouchel C (1996) Atomization of liquid sheets. In: Kuo KK (ed) Recent advances in spray combustion: spray atomization and drop burning phenomena. Progress in astronautics and aeronautics, vol I, 166, chap 10. American Institute of Aeronautics and Astronautics, pp 241–259

Chigier N, Reitz RD (1996) Regimes of jet breakup and breakup mechanisms (physical aspects). In: Kuo KK (ed) Recent advances in spray combustion: spray atomization and drop burning phenomena. Progress in Astronautics and Aeronautics, vol I, chap 4, 166. American Institute of Aeronautics and Astronautics, pp 109–135

Clanet C, Villermaux E (2002) Life of a smooth liquid sheet. JFM 462:307–340

Clark CJ, Dombrowski N (1974) An experimental study of the flow of thin liquid sheets in hot atmospheres. JFM 64:167–175

Crapper GD, Dombrowski N, Jepson WP, Pyott GAD (1973) A note of the growth of Kelvin–Helmholtz waves on thin liquid sheets. JFM 57:671–672

Dahm WJA, Frieler CE, Tryggvason G (1992) Vortex structure and dynamics in the near field of a coaxial jet. JFM 241:371–402

Dan T, Yamamoto T, Senda J, Fujimoto H (1997) Effect of nozzle configurations for characteristics of non-reacting diesel fuel sprays. SAE technical paper 970355

Delacourt E, Desmet B, Besson B (2005) Characterisation of very high pressure diesel sprays using digital imaging techniques. Fuel 84:859–867

Dombrowski N, Foumeny EA (1998) On the stability of liquid sheets in hot atmospheres. At Sprays 8:235–240

Dombrowski N, Hasson D, Ward DE (1960) Some aspects of liquid flow through fan spray nozzles. Chem Eng Sci 12:35–50
Dumont N, Simonin O, Habchi C (2000) Cavitating flow in diesel injectors and atomization: a bibliographical review. In: Proceedings of ICLASS 2000, Pasadena, CA, USA, 16–20 July 2000
Dumouchel C (2001) Measurements of breakup length of cylindrical liquid jets. Application to low-pressure car injector. At Sprays 11:201–226
Dumouchel C (2005) Experimental analysis of a liquid atomization process at low Weber number. In: Proceedings of international symposium on heat and mass transfer in spray systems, Antalya, Turkey, 5–10 June 2005
Dumouchel C, Cousin J, Triballier K (2005a) On the role of the liquid flow characteristics on low-Weber-number atomization processes. Exp Fluids 38:637–647
Dumouchel C, Cousin J, Triballier K (2005b) Experimental analysis of liquid–gas interface at low Weber number: interface length and fractal dimension. Exp Fluids 39:651–666
Dunand A, Carreau JL, Roger F (2005) Liquid jet breakup and atomization by annular swirling gas jet. At Sprays 15:223–247
Eroglu H, Chigier N (1991a) Liquid jet instability in coaxial air flow. In: Proceedings of ICLASS'91, Gaithersburg, MD, USA, 15–18 July 1991, paper 78, pp 703–710
Eroglu H, Chigier N (1991b) Wave characteristics of liquid jets from airblast coaxial atomizers. At Sprays 1:349–366
Eroglu H, Chigier N (1991c) Liquid sheet instability in a coflowing airstream. In: Proceedings of ICLASS'91, Gaithersburg, MD, USA, 15–18 July 1991, paper 75, pp 679–686
Eroglu H, Chigier N, Farago Z (1991) Caoaxial atomizer liquid intact lengths. Phys Fluids 3:303–308
Faeth GM, Hsiang LP, Wu PK (1995) Structure and breakup properties of sprays. Int J Multiph Flow 21:99–127
Farago Z, Chigier N (1990) Parametric experiments on coaxial airblast jet atomization. In: ASME 35th international gas turbine conference, Brussels, Belgium, June 1990, paper 90-GT-81
Farago Z, Chigier N (1992) Morphological classification of disintegration of round liquid jets in a coaxial air stream. At Sprays 2:137–153
Fenn RW, Middleman S (1969) Newtonian jet stability: the role of air resistance. AIChE J 15:379–383
Fraser RP, Eisenklam P, Dombrowski N, Hasson D (1962) Drop formation from rapidly moving liquid sheets. AIChE J 8:672–680
Frohn A, Roth N (2000) Dynamics of droplets. Springer, Heidelberg
Funada T, Joseph DD, Yamashita S (2004) Stability of a liquid jet into incompressible gases and liquids. Int J Multiph Flow 30:1279–1310
Godelle J (1999) Caractérisation de systèmes dynamiques complexes: instabilités de jet. Ph.D. thesis, University of Paris VII, France
Godelle J, Letellier C, Dumouchel C (2000a) Velocity profile effect and phase intermittency in low velocity cylindrical liquid jets. In: Proceedings of ICLASS'2000, Pasadena, CA, USA, 16–20 July 2000
Godelle J, Letellier C, Dumouchel C (2000b) Phase intermittency versus stochastic dynamics in low velocity cylindrical liquid jets. In: Proceedings of ILASS-Europe 2000, Darmstadt, Germany, 11–13 September 2000
Godelle J, Letellier C (2000) Symbolic statistical analysis for free liquid jets. Phys Rev E 62:7973–7981
Grant RP, Middleman S (1966) Newtonian jet stability. AIChE J 12:669–678
Grout S, Dumouchel C, Cousin J, Nugglish H (2007) Fractal analysis of atomizing liquid flows. Int J Multiph Flow 33:1023–1044
Hagerty WW, Shea JF (1955) A study of the stability of plane fluid sheets. J Appl Mech 22:509–514
Hardalupas Y, Tsai RF, Whitelaw JH (1998) Primary breakup of coaxial airblast atomizers. In: Proceedings of ILASS-Europe'98, Manchester, UK, 6–8 July 1998, pp 42–47
Hiroyasu H (2000) Spray breakup mechanism from the hole-type nozzle and its applications. At Sprays 10:511–527
Hiroyasu H, Arai M, Shimizu M (1991) Break-up length of a liquid jet and internal flow in a nozzle. In: Proceedings of ICLASS'91, Gaithersburgh, MD, USA, 15–18 July 1991, paper 26, pp 275–282
Huang JCP (1970) The break-up of axisymmetric liquid sheets. JFM 43:305–319
Ibrahim EA, Marshall SO (2000) Instability of a liquid jet of parabolic velocity profile. Chem Eng J 76:17–21
Karasawa T, Tanaka M, Abe K, Shiga S, Kurabayashi T (1992) Effect of nozzle configuration on the atomization of a steady spray. At Sprays 2:411–426
Keller JB, Rubinow SI, Tu YO (1973) Spatial instability of a jet. Phys Fluids 16:2052–2055
Kitamura Y, Takahashi T (1978) Influence of the nozzle length on breakup of a liquid jet. In: Proceedings of ICLASS 78, paper 1.1, pp 1–7
Kim JK, Nishida K, Hiroyasu H (1997) Characteristics of the internal flow in a diesel injection nozzle. In: Proceedings of ICLASS'97, Seoul, Korea, 18–22 August 1997, pp 175–182
Lasheras JC, Hopfinger EJ (2000) Liquid jet instability and atomization in a coaxial gas stream. Annu Rev Fluid Mech 32:275–308
Lasheras JC, Villermaux E, Hopfinger EJ (1998) Break-up and atomization of a round water jet by a high-speed annular air jet. JFM 357:351–379
Lefebvre AH (1989) Atomization and sprays. Hemisphere Publishing Corporation, New York
Lefebvre AH (1992) Energy considerations in twin-fluid atomization. ASME J Eng Gas Turbine Power 114:207–212
Leib SJ, Goldstein ME (1986a) Convective and absolute instability of a viscous liquid jet. Phys Fluids 29:952–954
Leib SJ, Goldstein ME (1986b) The generation of capillary instability on a liquid jet. JFM 168:479–500
Leroux B, Delabroy O, Lacas F (2007) Experimental study of coaxial atomizers scaling. Part I: Dense core zone. At Sprays 17:381–407
Leroux S (1996) Stabilité d'un jet liquide cylindrique. Influence de fortes pressions ambiantes. Ph.D. thesis, Université of Rouen, France
Leroux S, Dumouchel C, Ledoux M (1996) The stability curve of Newtonian liquid jets. At Sprays 6:623–647
Leroux S, Dumouchel C, Ledoux M (1997) The breakup length of laminar cylindrical liquid jets. Modification of Weber's theory. In: Proceedings of ICLASS'97, Seoul, Korea, 18–22 August 1997, pp 353–360
Li H, Collicott SH (2006) Visualisation of cavitation in high-pressure diesel fuel injector orifices. At Sprays 16:875–886
Lin SP (2003) Breakup of liquid sheets and jets. Cambridge University Press, London
Lin SP, Creighton B (1990) Energy budget in atomization. J Aero Sci Technol 12:630–636
Lin SP, Lian ZW (1989) Absolute instability in a gas. Phys Fluids A1:490–493
Lin SP, Lian ZW (1990) Mechanics of the breakup of liquid jets. AIAA J 28:120–126
Lin SP, Reitz RD (1998) Drop and spray formation from a liquid jet. Annu Rev Fluid Mech 30:85–105
Lozano A, Barreras F (2001) Experimental study of the gas flow in an air-blasted liquid sheet. Exp Fluids 31:367–376
Lozano A, Call CJ, Dopazo C, Gacia-Olivares A (1996) Experimental and numerical study of the atomization of a planar liquid sheet. At Sprays 6:77–94

Lozano A, Gacia-Olivares A, Dopazo C (1998) The instability growth leading to a liquid sheet breakup. Phys Fluids 10:2188–2197
Lozano A, Barreras F, Hauke G, Dopazo C (2001) Longitudinal instabilities in an air-blasted liquid sheet. JFM 437:143–173
Lozano A, Barreras F, Siegler C, Löw D (2005) The effects of sheet thickness on the oscillation of an air-blasted liquid sheet. Exp Fluids 39:127–139
Malot H, Blaisot JB, Dumouchel C (2000) Droplet size distribution of sprays produced by Newtonian liquid jets. In: Proceedings of ICLASS'2000, Pasadena, CA, USA, 16–20 July 2000
Malot H, Dumouchel C (2001) Experimental investigation of the drop size distribution of sprays produced by a low-velocity Newtonian cylindrical liquid jet. At Sprays 11:227–254
Mansour A, Chigier N (1990) Disintegration of liquid sheets. Phys Fluids 2:706–719
Mansour A, Chigier N (1991) Dynamic behavior of liquid sheets. Phys Fluids 3:2971–2980
Mansour A, Chigier N (1994) Effect of turbulence on the stability of liquid jets and the resulting droplet size distributions. At Sprays 4:583–604
Marmottant PH, Villermaux E (2004) On spray formation. JFM 498:73–111
Mayer WOH, Branam R (2004) Atomization characteristics on the surface of a round liquid jet. Exp Fluids 36:528–539
Mc Carthy MJ, Molloy NA (1974) Review of stability of liquid jets and the influence of nozzle design. Chem Eng J 7:1–20
Miesse CC (1955) Correlation of experimental data on the disintegration of liquid jets. Ind Eng Chem 47:1690–1695
Nakagawa H, Kamata S, Hori T, Okumura N, Senda J, Fujimoto HG (2006) Novel photographic imaging method for diesel spray structure with new lens and large sized film system. In: Proceedings of ICLASS 2006, Kyoto, Japan, 27 August–1 September 2006, paper 119
Ohrn TR, Senser DW, Lefebvre AH (1991a) Geometrical effects on discharge coefficients for plain-orifice atomizers. At Sprays 1:137–153
Ohrn TR, Senser DW, Lefebvre AH (1991b) Geometrical effects on spray angle for plain-orifice atomizers. At Sprays 1:253–268
Paciaroni M, Linne M, Hall T, Delplanque JP, Praker T (2004) Ballistic imaging for the liquid core of an atomizing spray. In: Proceedings of ILASS-Europe 2004, Nottingham, UK, 6–8 September 2004, pp 94–99
Paciaroni M, Linne M, Hall T, Delplanque JP, Praker T (2006) Single-shot two-dimensional ballistic imaging of the liquid core in an atomizing spray. At Sprays 16:51–69
Park J, Huh KY, Li X, Renksizbulut M (2004) Experimental investigation on cellular breakup of a planar liquid sheet from an air-blast nozzle. Phys Fluids 16:625–632
Parker TE, Raimaldi LR, Rawlins WT (1998) A comparative study of room-temperature and combustion fuel sprays near the injector tip using infrared laser diagnostics. At Sprays 8:565–600
Payri F, Bermudez V, Payri R, Salvador FJ (2004) The influence of cavitation on the internal flow and the spray characteristics in diesel injection nozzles. Fuel 83:419–431
Phinney RE (1972) Stability of a laminar viscous jet. The influence of the initial disturbance level. AIChE J 18:432–434
Porcheron E, Carreau JL, Prevost L, Le Visage D, Roger F (2002) Effect of injection gas density on coaxial liquid jet atomization. At Sprays 12:209–227
Rayleigh L (1878) On the instability of jets. Proc Lond Math Soc 10:4–13
Ranz WE (1956) On sprays and spraying. Dep. Eng. Res., Penn State Univ. Bull 65
Rehab H, Villermaux E, Hopfinger EJ (1997) Flow regimes of large-velocity-ratio coaxial jets. JFM 345:357–381
Reitz R (1978) Atomization and other breakup regimes of a liquid Jet. Ph.D. thesis, Princeton University, Princeton
Reitz R, Bracco FV (1982) Mechanism of atomization of a liquid jet. Phys Fluids 25:1730–1742
Rizk NK, Lefebvre AH (1980) Influence of liquid film thickness on airblast atomization. Trans ASME J Eng Power 102:706–710
Ruiz F (2002) Small waves on the jet "intact length": results using a new experimental technique. At Sprays 12:709–720
Sallam KA, Dai Z, Faeth GM (1999) Drop formation at the surface of plane turbulent liquid jets in still gases. Int J Multiph Flow 25:1161–1180
Sallam KA, Dai Z, Faeth GM (2002) Liquid breakup at the surface of turbulent round liquid jets in still gases. Int J Multiph Flow 28:427–449
Savart F (1833) Mémoire sur la constitution des veines liquides lancées par des orifices circulaires en mince paroi. Ann Chem 53:337–386
Shavit U (2001) Gas–liquid interaction in the liquid breakup region of two-fluid atomization. Exp Fluids 31:550–557
Shavit U, Chigier N (1995) Fractal dimensions of liquid jet interface under breakup. At Sprays 5:525–543
Sindayihebura D, Dumouchel C (2001) Pressure atomizer: hole break-up of the sheet. J Vis 4:5
Sirignano WA, Mehring C (2000) Review of theory of distortion and disintegration of liquid streams. Prog Energy Combust Sci 26:609–655
Smallwood GJ, Gülder OL (2000) Views on the structure of transient diesel sprays. At Sprays 10:355–386
Sowa WA (1992) Interpreting mean drop diameters using distribution moments. At Sprays 2:1–15
Stapper BE, Samuelsen GS (1990) An experimental study of the breakup of a two-dimensional liquid sheet in the presence of co-flow air shear. AIAA Paper 90-22730
Stapper BE, Sowa WA, Samuelsen GS (1992) An experimental study of the effects of liquid properties on the breakup of two-dimensional liquid sheet. Trans ASME Eng Gas Turbine Power 114:39–45
Stepowski D, Werquin O (2004) Measurement of the liquid volume fraction and its statistical distribution in the near development field of a spray. At Sprays 14:243–264
Sterling AM, Sleicher CA (1975) The instability of capillary jets. JFM 68:477–495
Squire HB (1953) Investigation on the instability of a moving liquid film. Br J Appl Phys 4:167–169
Tamaki N, Shimizu M, Hiroyasu H (2001) Enhancement of the atomization of a liquid jet by cavitation in a nozzle hole. At Sprays 11:125–137
Tamaki N, Shimizu M, Nishida K, Hiroyasu H (1998) Effects of cavitation and internal flow on atomization of a liquid jet. At Sprays 8:179–197
Taylor GI (1940) Generation of ripples by wind blowing over a viscous fluid. Collected work of G.I. Taylor, vol 3
Taylor GI (1959a) The dynamics of thin sheets of fluids. I—Water bells. Proc R Soc Lond A 253:289–295
Taylor GI (1959b) The dynamics of thin sheets of fluids. II—Waves in fluid sheets. Proc R Soc Lond A 253:296–312
Taylor GI (1959c) The dynamics of thin sheets of fluids. III—Disintegration of fluid sheets. Proc R Soc Lond A 253:313–321
Tropea C, Yarin AL, Foss JF (2007) Springer handbook of experimental fluid mechanics. Springer, Heidelberg
Vich G, Dumouchel C, Ledoux M (1996) Mechanisms of disintegration of flat liquid sheets. In: Proceedings of ILASS-Europe'96, Lund, Sweden, 19–21 June 1996, pp 121–126
Villermaux E, Clanet C (2002) Life of a flapping liquid sheet. JFM 462:341–363

Weber C (1931) Zum Zerfall eines Flussigkeitstrahles. Z Angew Math Mech 11:136–159

Woodward RD, Burch RL, Kuo KK, Cheung FB (1994) Correlation of intact-liquid core length for coaxial injectors. In: Proceedings of ICLASS'94, Rouen, France, 18–22 July 1994, paper VI-11, pp 105–112

Wu PK, Faeth GM (1993) Aerodynamic effects on primary breakup of turbulent liquids. At Sprays 3:265–289

Wu PK, Faeth GM (1995) Onset and end of drop formation along the surface of turbulent liquid jets in still gases. Phys Fluids 7:2915–2917

Wu PK, Miranda RF, Faeth GM (1995) Effects of initial flow conditions on primary breakup of nonturbulent and turbulent round liquid jets. At Sprays 5:175–196

Wu PK, Tseng LK, Faeth GM (1992) Primary breakup in gas/liquid mixing layers for turbulent liquids. At Sprays 2:295–317

Yon J, Blaisot JB, Ledoux M (2003) Unusual laser-sheet tomography coupled with backlight imaging configurations to study the diesel jet structure at the nozzle outlet for high injection pressures. J Flow Vis Image Process 9:1–20

Yon J, Lalizel G, Blaisot JB (2004) A statistical morphological determination of the growth rate of the interfacial disturbance of an excited Rayleigh jet. J Flow Vis Image Process 11:1–17

Yue Y, Powell CF, Poola R, Wang J, Schaller JK (2001) Quantitative measurements of diesel fuel spray characteristics in the near-nozzle region using X-ray absorption. At Sprays 2001:471–490

Yule AJ, Vamvakoglou K, Shrimpton JS (1998) Break-up of a thin flat sheet adjacent to a wide high velocity air stream. In: Proceedings of ILASS-Europe'98, Manchester, UK, 6–8 July 1998, pp 18–23

Zhao FQ, Lai MC (1995) The spray characteristics of automotive port fuel injection. A critical review. SAE technical paper ser. 950506